

Fotokatalytisk drivstoff-produksjon gjennom fotoreforming av hydrokarboner

Ida Lien Bjørnstad

Industriell kjemi og bioteknologi

Oppgaven levert: Juni 2011

Hovedveileder: Magnus Rønning, IKP

Biveileder(e): Nina Hammer, IKP
Charitha Udani, IKP
Asmira Delic, IKP



MASTER THESIS 2011

Title: Photocatalytic fuel production through photoreforming of hydrocarbons	Subject (3-4 words): Photocatalysis, photoreforming, hydrogen production
Author: Ida Lien Bjørnstad	Carried out through: 14.01.2011 – 10.06.2011
Advisor: Magnus Rønning	Number of pages: 138
Co-advisor: Nina Hammer	Main report: 67
External advisor:	Appendices: 71
ABSTRACT <p>The purpose of this study is to investigate the photoreforming of methanol for hydrogen production with CuO loaded TiO₂. The photocatalysts were characterized with TPO, TPR, BET, XRD, UV/vis spectrophotometry and chemisorption analysis. The photoactivity measurements were conducted in a specially designed photoreactor with internal UV radiation, continuous inert gas throughput and magnetic stirring.</p> <p>Goal of work (key words)</p> <p>The goal of this study was to investigate the impact of photocatalyst preparation, surface area, CuO loading and TiO₂ phase content on the photoactivity.</p> <p>Conclusions and recommendations (key words):</p> <p>The photoactivity measurements showed photocatalytic hydrogen evolution, but the evolution rate was too low for calculations. An improvement in the photoreforming setup is required for a proper investigation of the photocatalytic activity of the photocatalysts. Activity measurements should be conducted to find which parameters affect the photoactivity and which preparation method gives the most active photocatalysts.</p>	
I declare that this is an independent work according to the exam regulations of the Norwegian University of Science and Technology	
<p style="text-align: center;">Date and signature:</p>	

Preface

This study was done as a master thesis at the Norwegian University of Science and Technology during the spring of 2011. Supervisors were Magnus Rønning and Nina Hammer.

I chose this project because I find the field of environmentally friendly energy sources very interesting. I thought I could save the world, but I found out the hard way that research work includes mostly disappointments and waiting. This study therefore contains mostly reflections on how the experiments could be improved, and I did not get any answers to the questions I really wanted to investigate. I learned that all though I have gone through all my life thinking I was a patient, calm person, I'm really not. I did find this field very interesting and I have learned a lot. It was fun playing scientist for a while, but also frustrating.

I would like to thank my supervisors for all the help and understanding of my frustration. I also have to thank all those closest to me for keeping me sane and allowing me to be self-absorbed and antisocial during the roughest parts.

Ida Lien Bjørnstad

Abstract

The purpose of this study is to investigate the photoreforming of methanol for hydrogen production. Since the photocatalysis field needs a cheaper efficient photocatalyst than the more common Pt loaded TiO₂, CuO loaded TiO₂ was the chosen photocatalyst in this study.

This study investigated the impact of preparation methods on the photocatalysts. Incipient wetness impregnation, deposition precipitation and sol-gel preparation was studied. The impact of CuO loading, surface area and the phase content of TiO₂ on photoactivity were also supposed to be investigated.

The prepared photocatalysts were characterized with temperature programmed oxidation and reduction, X-Ray Diffraction, UV/vis spectrophotometry, SEM, EDS, BET surface area measurements and chemisorption measurements.

The incipient wetness impregnation (IWI) preparation decreased the surface area of the photocatalyst more than the deposition precipitation (DP) preparation, since the CuO particles deposited more in the pores with the IWI method. The DP prepared photocatalyst was more easily reduced and contained lower amount of amorphous phase in the photocatalyst than IWI photocatalysts.

The results from the UV/vis spectrophotometry showed the band gap of the photocatalyst decreased with increasing CuO loading, and that pure P25 had slightly higher band gap than anatase. There was not found any band gap dependency on surface area or crystallite size. The XRD results showed CuO dispersion increased with increasing surface area, and P25 contains more amorphous phase than the anatase and rutile photocatalysts.

The photoactivity measurements showed photocatalytic hydrogen evolution, but the evolution rate was too low for calculations. An improvement in the photoreforming setup is required for a proper investigation of the photocatalytic activity of the photocatalysts. Activity measurements should be conducted to find which parameters affect the photoactivity and which preparation method gives the most active photocatalysts.

Table of contents

Preface	2
Abstract.....	3
Table of contents	4
List of symbols and abbreviations.....	6
1. Background.....	8
2. Theory.....	10
2.1 The principle of photocatalysis	10
2.1.1 Photoreforming	12
2.2 Photocatalyst	13
2.2.1 TiO ₂ photocatalyst.....	13
2.2.2 CuO loaded TiO ₂ photocatalyst for photoreforming.....	14
2.3 Photocatalyst preparation.....	16
2.3.1 Incipient wetness impregnation method.....	16
2.3.2 Sol-gel method	17
2.3.3 Deposition precipitation method.....	17
2.3.4 Calcination	17
2.4 Methods used for characterization of the photocatalysts.....	17
2.4.1 Surface area measurements.....	17
2.4.2 UV-visible spectrophotometry.....	18
2.4.3 Temperature Programmed Reduction and Oxidation.....	19
2.4.4 X-Ray Diffraction	20
2.4.5 Scanning Electron Microscopy	22
2.4.6 Energy-Dispersive X-ray Spectrometry	22
2.4.7 Chemisorption analysis	23
2.5 Photocatalytic activity	25
2.5.1 Deactivation of the photocatalyst.....	27
3. Experimental	28
3.1 Catalyst preparation.....	28
3.1.1 Incipient wetness impregnation preparation.....	28
3.1.2 Sol-gel preparation	28
3.1.3 Deposition precipitation preparation.....	28

3.1.4	Overview of photocatalysts and preparation parameters.....	29
3.2	Catalyst characterization.....	29
3.2.1	BET surface area measurement.....	29
3.2.2	UV-visible spectrophotometry.....	29
3.2.3	Temperature programmed analysis	29
3.2.4	X-Ray Diffraction	30
3.2.5	SEM and EDS.....	30
3.2.6	Chemisorption analysis for dispersion measurements	30
3.2	Activity measurements	30
4	Results and discussion.....	33
4.1	Characterization results	33
4.1.1	BET surface area measurement.....	33
4.1.2	UV-visible spectrophotometry.....	33
4.1.3	TPO analysis	37
4.1.4	TPR analysis	39
4.1.5	XRD analysis	40
4.1.6	SEM and EDS.....	45
4.1.7	Chemisorption results.....	50
4.1.8	Comparison of XRD dispersion and chemisorptions dispersion	51
4.2	Activity measurements	52
4.2.1	Comparison of the photocatalysts	57
5	Conclusion.....	59
6	References.....	61
	List of appendices.....	67

List of symbols and abbreviations

α – angle in a unit cell	k – XRD calculation constant
β – angle in a unit cell	L – particle size
β_{FWHM} – FWHM for peaks in diffractograms	LV-FESEM – Low Voltage Field Emission Scanning Electron Microscope
β_1 – instrumental line broadening in XRD	n – degree of reflection
γ – angle in a unit cell	x_{Ru} – rutile content
λ – X-ray wavelength	FWHM – Full Width at Half Maximum
θ – angle between the incoming X-rays and the normal to the reflecting lattice plane	IWI – Incipient wetness impregnation
η – factor for optical transition	MS – Mass spectrometry
A – absorption coefficient	P – pressure
a – width of a unit cell	P_0 – saturation pressure
BET – Braun, Emmet & Teller	P25 – commercial TiO_2 powder
b – length of a unit cell	PIH – Photo-Induced Hydrophilic effect
C – constant for net heat of adsorption	PSA – Pressure Swing Adsorption
c – height of a unit cell	q_1 – heat of adsorption first layer
D – metal dispersion	q_L – heat of condensation
d – distance between 2 lattice planes in a crystal	R – gas constant
d_p – particle diameter	Redox – Reduction and oxidation reactions
DP – Deposition Precipitation	R – reflectance
E_0 – optical absorption edge energy	S – scattering coefficient
EDS – Energy-Dispersive X-ray Spectrometry	SEM - Scanning Electron Microscope
$h\nu$ – photon energy	T – temperature
I – intensity of XRD peak	TGA – Thermal Gravimetric Analysis
K – Kelvin	TPO – Temperature Programmed Oxidation

TPR – Temperature Programmed
Reduction

UV – Ultra Violet radiation

UV/vis – Ultra Violet-visible light

V – volume

V_m – volume of monolayer adsorbed gas

WGS – Water Gas Shift reaction

WI – Wetness Impregnation

Wt% – weight percentage

XRD – X-Ray Diffraction

1. Background

If we are going to avoid further global warming, we need to develop sustainable renewable energy without toxic or green house gas emissions [1-3]. The most realistic green future will include a great variety of renewable energy sources and energy carriers, including hydrogen. Hydrogen is the most abundant element in nature and is defined as an energy carrier, like electricity. The reason why it is called an energy carrier and not an energy source is because it has to be produced from hydrogen containing sources with the use of energy, since it does not exist available in the nature. This extraction of hydrogen is difficult and demands a lot of energy. Hydrogen can be used as an energy carrier in e. g. fuel cells. The fuel cells can replace gasoline or diesel motors, in which the reaction between hydrogen and oxygen produce electricity and this is then the energy source for the car. The only emission from fuel cells is water, which will not have any impact on the global environment [1-2].

Hydrogen is considered one of the best media for storage and distribution of renewable energy for the future, but new technologies and infrastructure is needed for sustainable hydrogen production, storage and distribution. The biggest challenge with using hydrogen as an energy carrier is how to produce hydrogen in large scale without any pollution [1-3].

Hydrogen can be produced from many different sources and with many different processes. Today hydrogen is produced mainly from natural gas, which is a complicated, energy demanding process with green house gas emissions [4]. Some hydrogen is also produced from biomass pyrolysis. CO and CO₂ are main byproducts achieved from these two processes. To utilize hydrogen in fuel cells there are high purity requirements that has to be met, because CO will poison the fuel cell catalysts. This requires complicated purifying processes like WGS, PSA and so on in addition to the energy demanding and complicated production technology [1].

Another source of hydrogen is water. Splitting the water into hydrogen and oxygen can be done with several methods using renewable energy, like electrolysis with electricity from renewable energy, photoelectrolysis (photocatalysis), thermochemical techniques and biophotolysis [1]. Production of hydrogen from water will give a very pure H₂ gas which is only mixed with O₂, an expensive gas used in many chemical processes. The splitting of water into H₂ and O₂ is a reaction with positive Gibbs energy, i.e. the reaction need energy input. The energy input is given by irradiation with photons, and a photocatalyst is also necessary to induce the reaction. This is the reason why this field is called photocatalysis [5].

Ideally the energy input in photocatalysis should come for the sun, which is the biggest renewable energy source. The definition of renewable energy sources is sources which never get empty and easily can replenish themselves [1]. Wind, biomass utilization, solar energy, tides, waves and ocean currents are examples of renewable energy. The sun emits energy towards the earth equal to 10 000 times the global energy consumption every year. Under 0.05% of the worlds energy production comes from solar energy [3]. Figure 1.1 gives an overview of the capacity in the energy sources used today compared with the annual global energy consumption and the potential in solar energy [1].

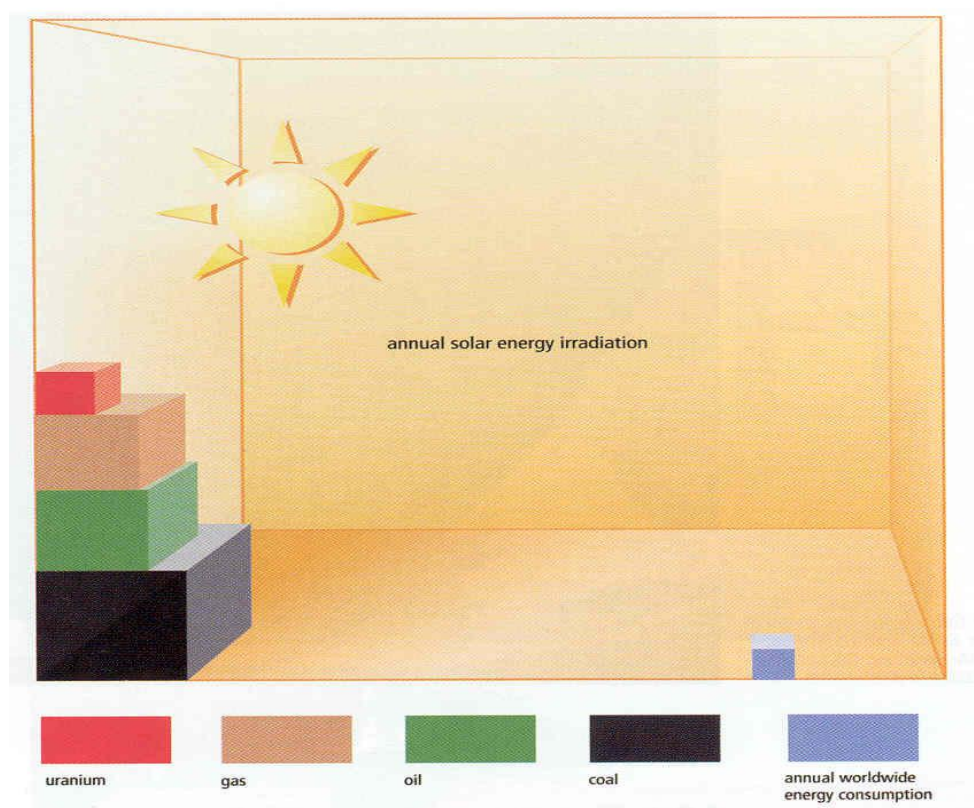


Figure 1.1. Describing the total solar energy capacity compared to energy sources most utilized today and the actual annual global energy consumption[6].

This study is focused on hydrogen production with photocatalysis. Photocatalysis can be used to produce hydrogen from water splitting and from photoreforming of organic compounds like alcohols [2, 4, 7-11]. Earlier studies have showed that pure water splitting has low efficiency [8-10, 12]. The main focus in this study will therefore be on two ways to increase the efficiency; loading the photocatalyst with metal and adding a sacrificial reagent. The addition of a sacrificial reagent in the process is called photoreforming, and the sacrificial reagent is an organic compound.

CO₂ is a major green house contributor and are formed during photoreforming. If the organic compounds used in photoreforming are derived from biomass; a renewable and sustainable resource, the CO₂ formed in the photoreforming process will be “CO₂” neutral. Biomass is formed by the plants uptake of CO₂ from the atmosphere and converting it to sugar, which is the main component in biomass. This sugar can then be converted to alcohols or other organic compounds which can be used in photoreforming, where it will be converted back to CO₂. Photoreforming of organic compounds from biomass will therefore be an environmentally friendly and sustainable hydrogen production process [4].

This study will focus on photoreforming of methanol with CuO loaded TiO₂ photocatalysts. The photoactivity of the photocatalysts will be compared based on preparation method, CuO loading, TiO₂ phase content and surface area.

2. Theory

If solar energy is going to be used for efficient and sustainable photocatalytic production of hydrogen, the photocatalytic process needs to be improved. If the process is made more efficient, photocatalytic hydrogen production would be a great alternative for the development of sustainable energy. The theoretical principles of photoreforming of aqueous methanol solutions for H₂ production will be presented in this chapter, in addition to give an account for the catalyst systems, characterization methods and photocatalytic activity used in this study.

2.1 The principle of photocatalysis

The principle of photocatalysis has evolved over several years. One of the earliest reports on photocatalytic activity was by a swizz named Renz in 1921. He discovered that if TiO₂ or other semi conductive materials were mixed with an organic compound the materials reacted with sunlight. The white color of the TiO₂ turned grey, blue or even black when irradiated, and he reported this reaction as a reduction of the oxides [11, 13]. Other scientists reported a redox mechanism for the formation of H₂O₂ on ZnO in 1927 [14], and in the 1930s researchers started looking at Ti-based paint and explained the chalk formation on these paints with photocatalysis. ZnO was considered the best photocatalyst for a long time, until TiO₂ got more interest in the 1960s. Photocatalysis developed to become a technology for selective and unselective oxidation of organic compounds for water purification and air purification, self-cleaning surfaces and sterilization among others [11]. Photocatalytic water splitting was first done by Fujishima and Honda in 1972 [15], when they photoelectrochemically split water with a titanium electrode [5, 15]. This method of water-splitting was named “Honda-Fujishima effect”, and studies of the field of photocatalysis accelerated after this publication. The method has been developed and improved by many scientists in later years [5, 11].

Photocatalysis can be defined as “a chemical reaction induced by photoabsorption of a solid material, or “photocatalyst”, which remains unchanged during the reaction” [5]. The biggest difference between photocatalysis and catalysis is the thermodynamics. Catalysis is limited to thermodynamically possible reactions with negative Gibbs free energy, since the catalyst only lower the activation energy for the reaction and therefore make the reactions happen faster. Photocatalysis on the other hand can drive reactions with positive Gibbs energy, like for instance water splitting [5].

The photocatalysts usually consist of a semiconductive metal, regardless of which photocatalytic process it will be used in. The semiconductive metal is activated during irradiation. A crucial property of the photocatalyst is the band gap between the conductive band and the valence band. This band gap property is the reason why semiconductors can be activated in photocatalysis. The band gap should be equal to or smaller than the photon energy of the radiation, because if the photon energy is equal to or greater than the band gap energy in the metal, the photon energy will be absorbed by the metal. This absorption leads to excitations of electrons from the valence band to the conductive band, leaving electron holes in the valence band. These electron-hole pairs cause redox reactions similar to the reactions taking place in ordinary electrolysis. In ordinary photocatalytic water splitting the electrons in the conductive band reduce the water molecules to form H₂, and the electron holes in the valence band oxidize the water molecules to form O₂ [2, 5, 7, 9, 11, 16-18]. See figure 2.1 for

a schematic representation of the photocatalytic principle. In photoreforming the reactions are a bit more complex (see chapter 2.1.1), but the electron holes are consumed by the organic compound in the oxidizing step, and the electrons form H_2 gas. In ideal photoreforming the only products will be CO_2 and H_2 [19].

It is important to avoid recombination between the electron and the electron hole, i.e. charge separation is essential [5, 11]. Charge recombination will convert the photoelectronic energy to heat, and there will be no surface reaction to form H_2 . Electrons and electron holes must migrate to different places on the surface. The semiconductive metal should have high crystal quality, meaning minimum of defects, since this will decrease the recombination frequency. The defects in the crystals will trap both the electrons and the electron holes, and recombination will occur. If the crystal particle is small the migration length will be shorter for the electron-hole pair, and this will also reduce the occurrence of recombination [2, 7, 18].

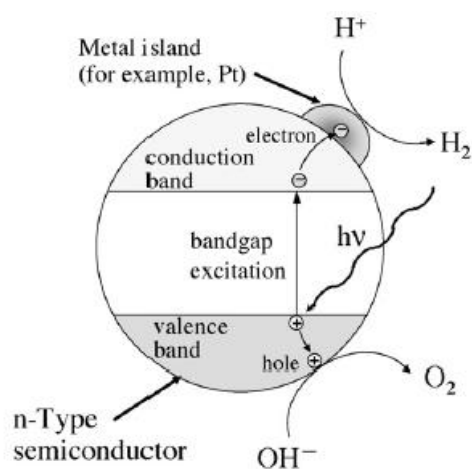


Figure 2.1. Schematic representation of the photocatalytic principle. The semiconductive material absorbs the radiation which creates electron-hole-pairs. In this representation the electron reduces H^+ to H_2 , while the electron hole oxidizes OH^- to O_2 [17].

The next step in the photocatalytic reaction mechanism is the surface reactions. The most important parameters for the surface reaction to take place are the surface area and number of reaction sites. The electrons and electron holes will migrate to the surface and will be trapped there in reaction sites [5]. Addition of a cocatalyst is a way to increase charge separation and decrease the recombination rate [11]. Heller and Gerischer *et al.* were some of the first to add cocatalysts to the photocatalyst, and proposed a model for the mechanism known as the Heller-Gerischer model [20]. This model is the base for most photocatalytic processes investigated today. The electrons will migrate to the cocatalyst if the Fermi level of the cocatalyst is lower than the conductive band in the semiconductor, and make this a reaction site for the hydrogen production. When the electrons have migrated to the cocatalyst they will act as a reducing agent [2, 21]. According to the Heller-Gerischer model photocatalysis require electroneutrality, which means oxidation and reduction must happen by equal rates [20].

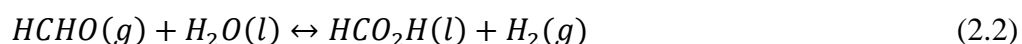
2.1.1 Photoreforming

One of the biggest problems with photocatalytic water splitting is the low process efficiency as mentioned before. In addition to decrease the charge recombination rate it is essential to avoid back reactions between hydrogen and oxygen to form water molecules. To avoid back reactions sacrificial reagents can be added to the system [2, 7, 18]. The sacrificial reagent will both increase charge separation by trapping the electron holes, and produce intermediates that are less reactive towards the hydrogen. Addition of a sacrificial reagent to the water will therefore both increase charge separation and enhance hydrogen production [11, 22]. The sacrificial reagent is an organic compound, and the use of sacrificial reagents is called photoreforming.

The organic compound is an electron donor or a hole scavenger, a reducing reagent, added to the water. It is oxidized by the electron holes faster than water, which result in more electrons in the photocatalyst and this leads to increased H₂ production [2, 7, 11, 21, 23].

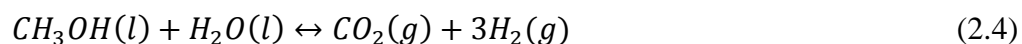
The most common sacrificial reagent used in studies today is methanol [22]. Methanol is one of the most promising sacrificial reagents because it has a high H/C ratio, which will result in more H₂ produced per CO₂. It can also be produced from renewable biomass as well as from fossil feed stocks, making this a very applicable reagent [4]. Patsoura *et al.* presented a study that showed the addition of alcohols enhanced the production rate of H₂, and that methanol showed the best H₂ evolution rate of all the alcohols tested in the study [24].

In a methanol/water solution the reaction mechanism for photoreforming follows the steps shown in reaction (2.1) – (2.3) [16, 22].



The first step is dehydrogenation of the methanol to form formaldehyde. In the next step formaldehyde reacts with water to form formic acid which decomposes to CO₂ and H₂ in the last step. Hydrogen is produced in all the steps in the mechanism [21-22].

These reactions make the overall reaction shown in reaction (2.4).



The photoreforming process also produces some byproducts like trace amount of CO [23], and some studies has also detected methane [4]. If the hydrogen is produced for use in fuel cells, a photocatalyst with low selectivity towards CO has to be developed [4].

Alcohols have shown good efficiency as sacrificial reagents, but to make this a sustainable environmentally friendly process the alcohols have to be made from biomass that does not compete with crop land or food market. If the alcohols is produced from 2nd generation biomass the H₂ produced will be a clean fuel, and the CO₂ produced under the photoreforming process will be “CO₂-neutral”. Ethanol and glycerol is also alcohols that have gained a lot of

interest lately. Ethanol can be formed from fermentation of waste lignocellulosic material and glycerol is the main byproduct in the process for biodiesel production. The use of these alcohols in photoreforming processes will then be a good solution to waste handling problems [23].

The term rate determining step cannot be used in photocatalysis, since the reactions induced by electrons and holes in photocatalysis happens in parallel and not in series. However if the reaction between adsorbed species and electron or electron holes is much faster than the adsorption from a solution or gas, then the rate determining step will be the diffusion of substrates. I. e. the process will be a diffusion-controlled process. The process could also be light intensity-controlled if the surface reactions between electrons and electron holes is slower than the adsorption of substrates [5].

2.2 Photocatalyst

When deciding on photocatalyst material, the band gap between the valence band and the conductive band need to be considered. The bottom level of the conductive band has to be more negative than the reduction potential of H₂ formation (0 V), while the upper level of the valence band has to be more positive than the potential of O₂ formation (1.23 V) in water splitting. The theoretical minimum band gap for pure water splitting therefore is 1.23 V, which is equivalent to light with wavelength around 1100 nm [2]. The minimum band gap is even lower for photoreforming processes, because the splitting energy for the organic compounds used in photoreforming is much lower than for water. The splitting energy of e. g. methanol is only 0.7 V [19].

The ideal photocatalyst should be able to absorb sun light, meaning both UV and visible light. This is a big challenge for the photocatalytic research field, since most photocatalysts only absorb UV radiation. UV radiation has higher energy than visible light, and it is therefore more easily absorbed by semiconductors than visible light [5]. If the researchers can make the photocatalysts absorption range include both visible and UV light, the photoefficiency will be significantly improved. The possibility of using sun light for fuel production from water has been called the holy grail for clean hydrogen production [3].

2.2.1 TiO₂ photocatalyst

TiO₂ is the most popular photocatalyst at the moment, but other semiconductors have also been used for several studies [11, 25-26]. TiO₂ anatase has a band gap around 3.2 eV, and TiO₂ rutile has a band gap around 3.0 eV [5]. This shows TiO₂ is ideal as a photocatalyst in systems with UV irradiation, since the irradiation light should have wavelengths shorter than 380 nm [27]. The UV wavelength range is between 180 and 380 nm [28]. TiO₂ is also a good photocatalyst because of its resistance to photocorrosion, its chemically and biologically inertness and its availability [1, 23]. There are three different TiO₂ phases; anatase, rutile and brookite. Rutile and anatase is the most common phases used in photocatalytic studies. Brookite is an amorphous phase and quite rare and difficult to prepare, without any photocatalytic properties [11, 29].

Degussa P25 is a very stable commercial type of TiO₂ catalyst with relatively high surface area and small particles [18]. The use of small particles in photocatalysis will inhibit the

charge recombination, see chapter 2.1. Degussa P25 consists of both anatase and rutile TiO₂ structure in the relation 4:1 to 9:1 [29]. The anatase and rutile particles in P25 exist separately, but under photocatalytic operational conditions the two phases are in contact. It is this contact between the phases that is assumed to give P25 the high photocatalytic activity [30-31], and this effect is often called the synergetic effect [5]. This has not been proven, and there are some newer studies indicating pure anatase has higher photocatalytic activity than P25 [32]. Ohtani *et al.* reported that Degussa P25 contains anatase, rutile and amorphous TiO₂ in varying composition from package to package, and even with variations in the same package [32].

Rutile TiO₂ is more stable than anatase, and if the anatase structure is treated with sufficiently high temperatures it will transform to rutile structure. This should be avoided since anatase has higher photocatalytic activity than rutile, and the composition of rutile and anatase in P25 is claimed to be optimal in photocatalysis. At temperatures over 1073 K the transition rate is fast, and all the anatase content is transformed to rutile in a couple of hours [33].

When TiO₂ is irradiated with UV light the contact angle between the TiO₂ particle and water or organic liquid is reduced to near 0° [11]. This effect is called the photo-induced hydrophilic effect (PIH), and is the reason for why TiO₂ can be used for instance in photocatalytically self-cleaning surfaces and ant-fogging mirrors. The PIH effect also improves the photocatalytic activity of TiO₂ in photoreforming, since the contact area between the photocatalyst and substrate (water or organic compound) increases.

Loading the TiO₂ with other noble metals has been found to enhance the photocatalytic activity considerably. The metal loading is also called adding of cocatalyst. Adding cocatalyst to the photocatalyst will also decrease the charge recombination rate as mentioned in chapter 2.1. The cocatalyst is the reaction site on the catalyst, where the surface reaction between reactants and electrons takes place [34].

The most common photocatalyst in photocatalytic water splitting and photoreforming consist of TiO₂ as the semiconductive metal and Pt as the cocatalyst [2]. The addition of Pt on the TiO₂ has shown great results for enhanced hydrogen production, but Pt is very expensive and quite rare. It is therefore important to find a sufficiently active cocatalyst with lower costs than Pt and better availability [34].

2.2.2 CuO loaded TiO₂ photocatalyst for photoreforming

Copper is a cheap metal with high availability compared to the more commonly used Pt, and it has been used in combination with TiO₂ in a variety of processes already. Some examples of the use of TiO₂ with Cu-particles as catalyst are:

- In methanol synthesis from CO₂ hydrogenation, where the Cu activates the H₂ to react with the CO₂ [35].
- In NO adsorption, where the Cu oxidizes the NO to NO₂ which facilitates the formation and adsorption of nitrites and nitrates [36-37].
- It can be used with Pt or Pd in photocatalytic reduction of nitrates, nitrite ions, benzenes and methyl tert-butyl ether in groundwater [38-40].

- In photocatalytic degradation of methylene blue in wastewater [41].
- It can be used with Au in partial oxidation of methanol to produce hydrogen [42].
- In photocatalytic reduction of CO₂ with water to produce hydrocarbons. Without Cu the main product is CO but with Cu the selectivity towards methane is improved and the overall CO₂ conversion is increased [43].
- It can be used as a thin film making an antibacterial surface or as nanoparticles where the TiO₂ produces radicals that disrupt the outer lipid membrane after UV radiation, and the Cu⁺ ions damage the cytoplasmic membrane making this a strong biocidal compound [44-45].

CuO loaded TiO₂ can of course also be used in photoreforming [16, 18-19, 22, 27, 46]. CuO also inhibit some photocatalytic properties, like TiO₂ [47]. Wu *et al.* [22], Choi *et al.* [19] and Xu *et al.* [18] has found that impregnating TiO₂ with CuO increases the hydrogen production rate from aqueous methanol solutions considerably compared to pure TiO₂. Xu *et al.* presented a comparison between other reported photocatalysts and their own photocatalysts activity, and reported that their 9.1wt% CuO loaded P25 TiO₂ showed better photoactivity than some results with either Pt, Pd or Au loaded TiO₂ [18]. Some reports in that study also showed Pt loaded P25 showed better photoactivity than the CuO loaded ones [24, 48]. All the studies in the comparison used different operational parameters, and even different sacrificial reagents, so the difference in photoactivity may be caused by the photoreforming parameters rather than the photocatalyst. Sreethawong *et al.* studied the difference between CuO, PdO and Au loaded TiO₂ and reported Au showed best photocatalytic activity and CuO the poorest, but the CuO loaded photocatalyst still showed a significant hydrogen evolution rate [49].

Wu *et al.* and Choi *et al.* used the incipient wetness impregnation method on pure anatase TiO₂, while Xu *et al.* used a different wetness impregnation method on the commercial P25 TiO₂ [18-19, 22]. Zhang *et al.* studied the difference of CuO loaded photocatalyst prepared by different methods; incipient wetness impregnation, sol-gel, chemical reduction and photo-deposition. They found the sol-gel preparation method gave the best stability and photoactivity of the photocatalyst [50]. Different values have been reported for the optimal CuO loading of TiO₂, see table 2.1 for some of the reported values.

Table 2.1. Some different reported optimal CuO loading for photoactivity.

Study	Optimal CuO loading [wt%]	Reference
Wu <i>et al.</i>	1.5	[22]
Dhanalakshmi <i>et al.</i>	1.5	[51]
Choi <i>et al.</i>	10	[19]
Yu <i>et al.</i>	1.3	[52]
Xu <i>et al.</i>	9.1	[18]
Bandara <i>et al.</i>	7.0	[53]

It is important to have the Cu particles deposited on the surface of the TiO₂ rather than doped in the TiO₂ lattice, because Wu *et al.* reported that TiO₂ lattice doped with Cu ions decreased

the activity of the photocatalyst [22]. Choi *et al.* got results that indicated the Cu components exist on the surface of the TiO₂ particles and are unlikely to be incorporated into the TiO₂ lattice with the use of impregnation methods [19].

An energy level diagram showing the electron transfer directions and energy levels of TiO₂ and CuO for photoreforming of methanol is shown in figure 2.2 [53]. The absorption of irradiation with the correct wavelength excites electrons from the valence band to the conduction band. The electron then transfer to the conduction band of the CuO where it reduces water to H₂. The electron hole left in the valence band of TiO₂ oxidize methanol.

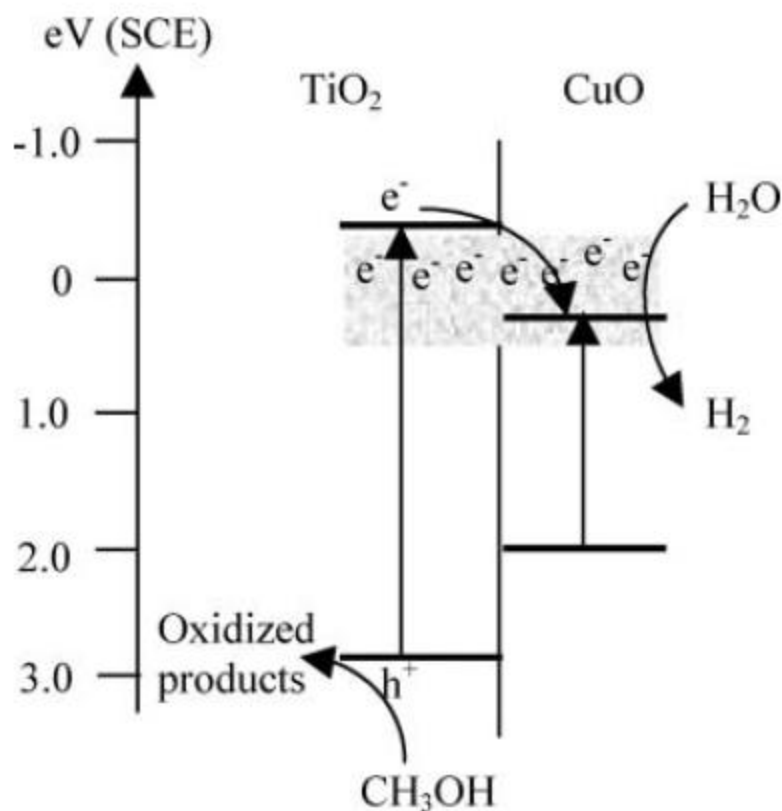


Figure 2.2. An energy level diagram for CuO and TiO₂ showing the electron transfer directions during photoreforming [53].

2.3 Photocatalyst preparation

2.3.1 Incipient wetness impregnation method

To deposit metal particles onto a support, impregnation methods are often used. The incipient wetness impregnation method (IWI) dissolves the desired salt in a solution with a volume equal to the pore volume of the support. The solution is drawn toward the pores by capillary forces, and replaces the air in the pores. The capillary pressure is bigger than the air pressure inside the pores, and the air is either dissolved in the liquid or escapes through bigger pores. If the mechanical strength of the support is not high enough to withstand bubbles, the impregnation should be done under vacuum. The impregnated support is then dried to evaporate the solvent, and the active metal is deposited in the pores of the support [54].

2.3.2 Sol-gel method

The sol-gel preparation method is often used because the synthesis is so easily controlled. The synthesis consists of forming a sol and then developing the sol into a gel, before drying. A sol is a suspension of solid particles in a liquid. The sol is made by hydrolysis and partial condensation of a precursor. The precursor is often a metal alkoxide or an inorganic salt. When the sol particles condensate further a three-dimensional network is produced, and this is called the gel. The gel is basically solids encapsulating the solvent. The gel can also be produced by destabilizing a solution of earlier formed sols. The materials produced are called aquasol if water is used as solvent and alcosol if alcohol is used as solvent [55]. The sol-gel method used in this study was Colón *et al.*'s method described in their article from 2002 where active carbon is used as an additive to increase the surface area of the TiO₂ [56].

2.3.3 Deposition precipitation method

Precipitation is a more demanding catalyst synthesis method than many other methods, but is still one of the most frequently used preparation method. This is because of the possibility for producing very pure materials and because the process is very flexible to the desired quality of the final product [57]. The active metal is mixed in a suspension with the desired support and a salt. pH controlling and monitoring is important, an acid is added to the solution to get the desired starting pH value. The suspension is heated and kept at the reaction temperature for a specific time while stirred, and the reaction taking place is hydrolysis of the salt. The hydrolysis will increase the pH of the suspension and causing the metal ions to precipitate on to the support. The suspension is then filtered and dried, and the obtained powder is the resulting catalyst [58].

2.3.4 Calcination

Calcination is defined as “the heating of a solid to a high temperature, below its melting point, to create a condition of thermal decomposition or phase transition other than melting or fusing” [59] or to cause a loss of moisture and oxidation of the catalyst [60]. Calcination is a thermal treatment of a catalyst in oxidizing atmosphere. The Cu²⁺ particles on TiO₂ are oxidized to CuO during calcination, and nitrates from the solvent used in the IWI will vaporize [61]. Photocatalytic activity for P25 – TiO₂ decreases significantly with calcination temperatures above 973 K, because the rutile content increases and the surface area decrease. Calcination with temperatures below 973 K does not affect the photocatalytic activity compared to uncalcined P25 – TiO₂ when calcined less than 6 hours [33].

2.4 Methods used for characterization of the photocatalysts

2.4.1 Surface area measurements

The surface area of a solid catalyst can be determined by BET measurements. BET is short for Braun Emmet and Teller isotherm, and the measurement use physisorption of an inert species on the surface to calculate how many molecules are needed to form a monolayer. The most commonly used BET species is nitrogen. The physisorption is then done at 77 K which is the boiling point of N₂, and at this temperature the N₂ molecule area is 0.162 nm² [62-63].

The physisorbed species could both condensate in small pores and form multilayers [62]. The BET equation is based on the Langmuir isotherm and some additional assumptions [63]. The Langmuir adsorption assumptions are [64]:

- Homogeneous surface, heat of adsorption is independent of the coverage
- Monolayer adsorption
- Immobile adsorption
- Dynamic equilibrium between gas phase and adsorbed species

Additional assumptions for the BET isotherm [63]:

- The first layer of adsorbed molecules is the site for adsorption in the next layer
- The rate of adsorption in one layer is equal to the rate of desorption from the layer above
- From the second layer of adsorption and up the heat of adsorption is the same as the heat of liquefaction of the adsorbate

The Brauner Emmett and Teller (BET) equation is shown in equation (2.5). V is the total volume of the adsorbed gas at pressure P . V_m is the volume of a monolayer of the adsorbed gas, and P_o is the saturation pressure. C is a constant relating the net heat of adsorption, the equation for C is shown in equation (2.6), where q_1 is the heat of adsorption of the first layer, q_L is the heat of condensation, R is the gas constant and T is the temperature [62, 65].

$$\frac{P}{V(P_o - P)} = \left[\frac{C-1}{V_m C} \right] \frac{P}{P_o} + \frac{1}{V_m C} \quad (2.5)$$

$$C = e^{\frac{q_1 - q_L}{RT}} \quad (2.6)$$

The left side of the BET equation is then plotted against P/P_o and the result will then be a linear plot with slope $\frac{C-1}{V_m C}$ and intercept at $\frac{1}{V_m C}$. For N_2 the equation can be simplified since C is much larger than 1, the slope then equals $\frac{1}{V_m}$. The volume of the monolayer adsorption can then be calculated from the plot [63].

2.4.2 UV-visible spectrophotometry

Absorption of radiation is one of the most important steps in photocatalysis, since absorption of light is essential for a photochemical reaction to take place [5, 66]. A photoabsorption spectrum showing extent of absorption as a function of wavelength is very informative when working with photocatalysis [5].

Absorption of ultraviolet and visible radiation occurs in one or more electronic absorption bands in the molecule. The wavelength at which a molecule absorbs radiation depends on how tightly the electrons are bound. If the electrons are bound tightly to the molecule they absorb radiation with high energy, which means radiation with lower wavelengths. Most transition metals absorb broad bands of visible radiation in at least one oxidation state, and are therefore colored. With these metals, including both copper and titanium, transitions between filled and unfilled d-orbitals are involved in the absorption. The energy of the d-orbitals depend on the

ligands bonded to the metal ions, and the energy difference between them depend on the metals position in the periodic table, oxidation state and what kind of ligand is bonded to the metal [67]. The resulting absorption spectra from the analysis will show an optical absorption edge. The optical absorption edge is the minimum energy a photon needs to excite an electron from the highest occupied orbital, to the lowest unoccupied molecular orbital. The highest occupied molecular orbital is at the top of the valence band, and the lowest unoccupied molecular orbital is at the bottom of the conductive band [68].

It is very difficult to obtain precise measurements of photoabsorption spectrums of solid samples. Such samples can be measured with reflectance spectrophotometry instead, which is an analysis technique that measure the reflection from the sample at different wavelengths [5, 69]. The Kubelka-Munk function transfer reflectance spectra to the equivalent absorption spectra [68-69]. Some assumptions have to be made when using the Kubelka-Munk function; for instance it is assumed that the scattering coefficient is constant throughout the wavelength range of the measurement. The Kubelka-Munk function is shown in equation (2.8), where R_{sample} is the reflectance value of the sample, $R_{\text{reference}}$ is the reflectance value of the reference material, A is the absorption coefficient and S is the scattering coefficient [68-69].

$$R_{\infty} = \frac{R_{\text{sample}}}{R_{\text{reference}}} \quad (2.7)$$

$$F(R_{\infty}) = \frac{(1-R_{\infty})^2}{2R_{\infty}} = \frac{A}{S} \quad (2.8)$$

$$A \propto \frac{(hv-E_0)^{\eta}}{hv} \quad (2.9)$$

The energy dependency of the absorption factor near the absorption edge is shown in equation (2.9), where hv is the photon energy and E_0 is the optical absorption edge energy. η is a factor that depends on the optical transition caused by the photon absorption, for TiO_2 η is 2. If $(Ahv)^{1/\eta}$ is plotted against hv , the resulting plot will be linear near the edge energy. If this linear part of the plot is extrapolated to $(Ahv)^{1/\eta} = 0$, the corresponding hv value is the band gap energy or optical absorption edge energy of the sample [68-69].

2.4.3 Temperature Programmed Reduction and Oxidation

Temperature programmed oxidation and reduction is used to determine the reactivity of the catalyst. The bond strength of the surface species can be found from the temperature at which the species react with, or are desorbed from, the surface. The reagents used in these methods are gaseous. If TPR is desired the reagent gas is reductive, like H_2 , and if TPO is the desired reaction an oxidizing gas is used, like air. The gases are flushed over the catalyst while the temperature increases according to the set temperature program. The change in the catalyst during the program can be monitored by measuring the thermal conductivity of the outlet gas, using MS or GC on the outlet gas, or just by measuring the mass change of the catalyst. TPO and TPR show which changes in the catalyst that can be expected during for instance calcination and activity measurements in reducing environments [65]. TPO is also used to decide the appropriate calcination temperature.

In temperature programmed reduction (TPR) the chemical reduction reaction is monitored while the temperature is linearly increased as a function of time. TPR gives the information about the required temperature for reduction of the catalyst [62]. If the sample changes weight as a result of the temperature change and the reducing environment, this will be recorded. This data give information about thermal stability, solvent or moisture content or other contents, reduction temperature, decomposition temperature and rate. In principle when running CuO in a TPR program it should be possible to see both the reduction step from CuO to Cu₂O and from Cu₂O to Cu(0), but since Cu₂O is very unstable the separation of these two steps is very rarely observed [70].

2.4.4 X-Ray Diffraction

X-Ray Diffraction is one of the oldest and most common catalyst characterization techniques used in the world today. The XRD is used to determine the crystal phases in catalyst powder, by defining the lattice structures inside the catalyst. It is also used to get an indication of the particle size in the samples. When the catalyst is radiated with X-ray photons the atoms in the periodic lattice scatter the X-ray photons. The principle of X-ray photon scattering is shown in figure 2.3. The scattered X-ray photons that are in phase give constructive interference. The path difference between scattered photons from parallel lattices is equivalent to a number of wavelengths for a given X-ray angle; this principle gives the diffraction peaks. The diffraction pattern is then used to describe the crystal structure in the catalyst with the Bragg relation shown in equation (2.10) [62, 71].

$$n\lambda = 2d\sin\theta; \quad n = 1,2, \dots \quad (2.10)$$

λ is the wavelength of the X-ray beams, θ is the angle between the incoming X-rays and the normal to the reflecting lattice plane, d is the distance between two lattice planes, and n is the degree of reflection [62].

The constructively interfering X-ray photons leave the crystal in the angle θ , and if this angle is measured the distance between the lattices which are characteristic for the compound in the sample can be calculated from the Bragg relation in equation (2.10). When characterizing powders with XRD, an image of diffraction lines will occur. This happens because a small fraction of the particles in the powder will have a crystal plane at the angle θ to the incoming X-ray beam. Rotation of the samples during measurements will increase the number of particles that contribute to the diffraction pattern [62].

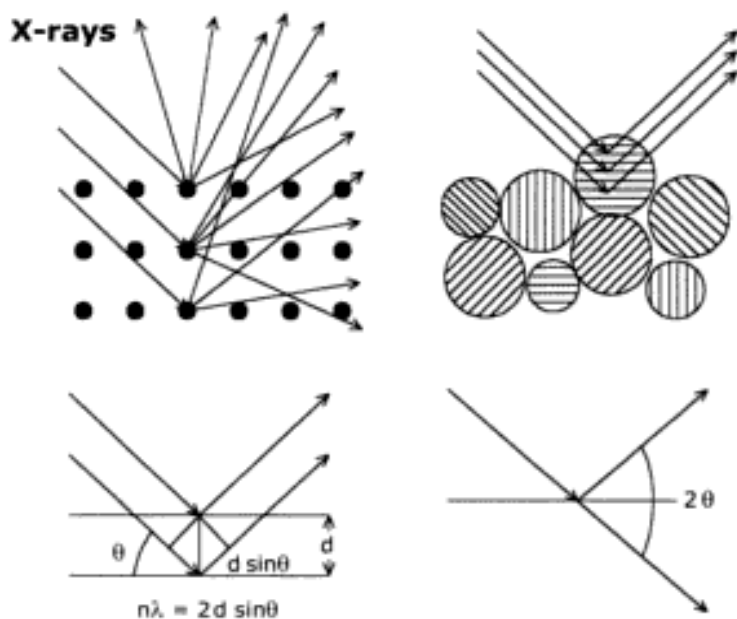


Figure 2.3. Bragg's law determines the directions of which the X-rays are scattered by the lattice in atoms [62].

Information about the dimensions of the reflecting planes can be found from the width of the obtained diffraction peaks. Diffraction peaks from perfect crystals are very narrow, while for crystal sizes below 100 nm the peaks broaden. The diffraction peak gets wider for smaller particles. This broadening occurs because of incomplete destructive interference when the X-rays are out of phase. The crystal size can then be calculated from the peak width with the Scherrer formula shown in equation (2.11) [5, 62].

$$L = \frac{k\lambda}{(\beta_{FWHM}^2 - \beta_l^2)^{0.5} \cos(\theta)} \quad (2.11)$$

L is a measure of the dimension of the particle in the direction perpendicular to the reflecting plane, β_{FWHM} is the peaks full width at half maximum (FWHM) and β_l is the instrumental line broadening. k is a constant, the value is set to 1.00 if the integral width is used in the calculations, or 0.89 if the full width at half maximum is used [5, 62, 72].

XRD will give clear and absolute information about the structure of the catalyst if the particles are large enough. It can also give an estimate on particle size. The analysis cannot show particles that are too small or amorphous, so it can never be certain that there is no other phases present [62].

When the particle size is calculated from the XRD results, the CuO dispersion (D) can be calculated from the simplified equation (2.12) if the CuO particles are assumed to be spherical. d_p is the diameter of the CuO particle in nm [73]. The definition of dispersion for a metal is shown in equation (2.13). The dispersion can also be calculated from chemisorption experiments, see chapter 2.4.7 [64].

$$D = \frac{\text{number of surface atoms of the metal}}{\text{number of metal atoms in the catalyst}} \quad (2.12)$$

$$D = \frac{1.1}{d_p} \quad (2.13)$$

The rutile content can also be calculated from the results in an XRD with equation (2.14) [33], if the assumption of no amorphous TiO₂ phases are present in the sample. X_{Ru} is the rutile content, I_A is the intensity of the anatase peak and I_{Ru} is the intensity of the rutile peak.

$$x_{Ru} = \left(1 + 0.8 \frac{I_A}{I_{Ru}}\right)^{-1} \quad (2.14)$$

2.4.5 Scanning Electron Microscopy

A Scanning Electron Microscope (SEM) is used for examination of the microstructure of solid objects [74-75]. There are different types of SEMs and they are named from what kind of cathode the electrons are accelerated from and which voltage difference is used to accelerate the electrons. The cathode can be either a thermionic, Schottky or field emission (FESEM) cathode. The electrons are accelerated through a voltage difference between the cathode and an anode. The voltage difference can be as low as 0.1 keV or as high as 50 keV. Voltage difference in the range 0.1 – 5 keV is called low-voltage SEM (LV-SEM) [74]. The SEM used in this study was a LV-FESEM.

The smallest beam cross-section is called the crossover, and has a diameter around 10 – 100 nm for field emission SEMs. The crossover is demagnetized by a two- or three-stage electron lens system so that the electron probe is formed at the specimen surface. The electron probe is the focused electron beam at the specimen. The working distance is the distance between the specimen and the bottom of the final lens [74].

Contrast in SEM pictures is caused by the difference in the signal collected from the interaction between the beam and the specimen, which varies from one location to another. Many types of signals are generated when the electrons hit the sample, and all of these signals can be displayed as an image. The detector converts the electron signal to changes in the point-by-point intensity and produces an image. Secondary electrons and backscattered electrons are the signals that are most often used to produce SEM images [75].

2.4.6 Energy-Dispersive X-ray Spectrometry

Energy-Dispersive X-ray Spectrometry (EDS) can be used in combination with a SEM to analyze the elemental composition of a specimen [75]. The EDS uses characteristic X-rays to define the chemical composition of the specimen. A high-energy beam of photons, electrons or X-rays are focused into the specimen, and this beam excites electrons in the molecules. When the electrons relax back to ground state, energy is released in the form of X-rays. These X-rays are specific to the atom that produced them, and are therefore called characteristic X-rays. The X-rays are then measured in an energy-dispersive spectrometer, and the elemental composition of the specimen can be recorded [75-76]. The EDS analysis can be used to get the atom composition on the surface of the sample and to do so-called mapping. EDS mapping shows where the different atoms are located, and can give an indication of the dispersion in the sample. The result from EDS analysis is most accurate if the sample surface is smooth and homogeneous so that no X-rays are “caught” in pores and other obstacles [76].

2.4.7 Chemisorption analysis

Chemisorption analysis can be done on pure metallic phases of copper. The CuO particles must therefore be reduced to Cu(0). Chemisorption on Cu(0) is done with N₂O, which will adsorb dissociatively according to the exothermic reaction shown in reaction (2.15). This reaction gives the stoichiometric relation of two Cu atoms per N₂O molecule [72, 77-78].



If the reaction goes on for too long the oxygen will diffuse into the middle of the particle, and there will be bulk oxidation in addition to surface oxidation [72, 78-79]. Physisorption may also occur. The dispersion can only be calculated when a monolayer of oxygen is chemisorbed on the Cu(0) surface. To ensure only monolayer of oxygen, the sample will be flushed with inert gas after the oxidation step. The TGA program used for obtaining chemisorption measurements was taken from Huber *et al.*'s article [72], but with some adjustments. Since Cu₂O is very unstable the samples need to be handled with care after treatment.

Jensen *et al.* tested the N₂O chemisorptions on Cu(0) with temperatures ranging from 313 K to 493 K, and found the temperature did not affect the Cu(0) dispersion, but the bulk oxidation increase with increasing temperature. They concluded it was best to operate with temperatures under 363 K to avoid too high diffusion rates [78].

The chemisorption analysis results can be used to calculate copper particle dispersion. When N₂O decompose on the surface of Cu(0) particles, the number of surface Cu atoms can be calculated if the amount of adsorbed gas is known [72]. The dispersion is found by equation (2.12) in chapter 2.4.4. The dispersion found by this method is the Cu dispersion, compared with the CuO dispersion found from XRD results. The dispersion from XRD and chemisorption analysis can be compared if the CuO dispersion from XRD analysis is recalculated [80].

The copper atoms in pure Cu(0) metallic state takes up less space than the copper atoms in CuO particles [80]. To take this space reduction into account the differences in the unit cell of CuO and Cu(0) must be investigated. A crystals unit cell is “*the smallest boxlike unit (each box having faces that are parallelograms) from which you can imagine constructing a crystal by stacking units in three dimensions*” [81]. The volume of a unit cell can be calculated from equation (2.16), where a, b, c, α, β and γ is specific constants for each molecule [80-81]. The meaning of the constants and values used in equation (2.16) is shown in figure 2.4, in addition to the different types of unit cells.

$$V_{unit\ cell} = abc\sqrt{(1 - \cos^2\alpha - \cos^2\beta - \cos^2\gamma + 2\cos\alpha\cos\beta\cos\gamma)} \quad (2.16)$$

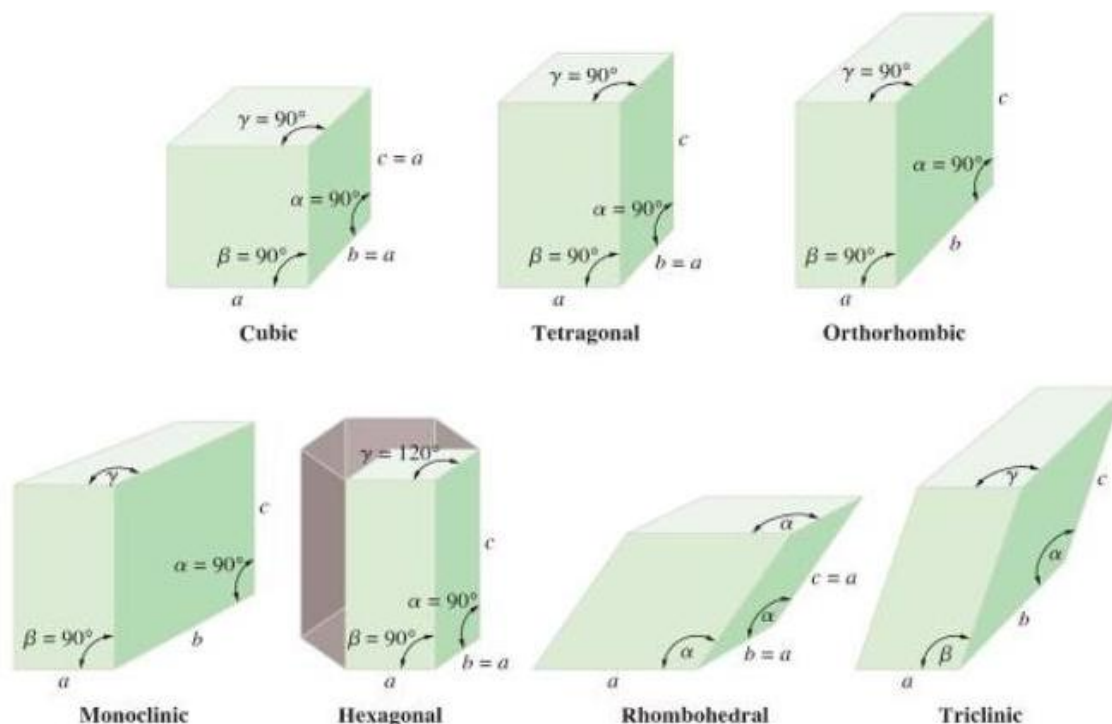


Figure 2.4. Different types of unit cells and the meaning of the angles and constants in the unit cell volume equation[80].

The unit cell for pure Cu(0) is shown in figure 2.5. This unit cell is cubic, which gives $\alpha = \beta = \gamma = 90^\circ$ and $a = b = c = 3.61 \text{ \AA}$. The volume for the Cu crystal unit cell is then calculated to 47.05 \AA^3 , see the calculation in appendix 9.

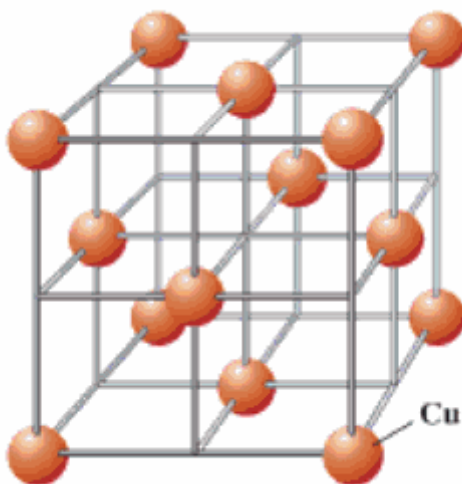


Figure 2.5. The unit cell for metallic copper crystals [81].

The unit cell constants for CuO is: $a = 4.68375 \text{ \AA}$, $b = 3.42265 \text{ \AA}$ and $c = 5.12886 \text{ \AA}$, and the angles is: $\alpha = 90^\circ$, $\beta = 99.54^\circ$, $\gamma = 90^\circ$. This gives a triclinic unit cell with a volume of 81.08 \AA^3 . From these unit cell volumes, the volume uptake by each copper atom in the different unit cells can be calculated. If the assumption of spherical copper particles is introduced, see equation (2.17), the relationship between Cu(0) particle diameter and CuO particle diameter can be calculated to be $d_{\text{CuO}} = 1.198d_{\text{Cu}}$.

$$V_{sphere} = \frac{\pi d_p^3}{6} \quad (2.17)$$

With this information the XRD dispersion can be recalculated to better compare with the dispersion found from chemisorption analysis.

2.5 Photocatalytic activity

Photocatalytic activity is in most cases the same as absolute or relative reaction rate [5]. Catalytic activity in general describes how often an active site produces the reaction products, but photocatalysts does not have active sites in the same meaning. The photocatalytic reaction rate strongly depends on various factors like the intensity of the irradiation. Since the part of the photocatalyst that is not irradiated is inactive, the term active sites is not a proper term for use in photocatalysis, reaction sites is a better term. Photocatalytic activity can therefore not be described based on the turnover frequency of the active sites [5]. See figure 2.6 for an illustration of the difference between classical catalysis and photocatalysis.

The reaction sites in the CuO loaded TiO₂ photocatalysts were found by Xu *et al.* to probably be at the interface between CuO and TiO₂ since they found no hydrogen evolution at pure CuO or TiO₂, and since they found the optimal CuO loading to be close to 10 mol% which is equal to a monolayer coverage of CuO on the TiO₂ surface. This monolayer value also explains why the hydrogen evolution rate decreased at higher CuO loadings than 10 mol%, since the CuO particles would block the TiO₂ from the incoming radiation. They found the adsorption mechanism showed a Freundlich isotherm behavior, which indicates the methanol adsorption on the photocatalyst is a crucial part of the reaction mechanism and that the adsorption is not a uniform monolayer adsorption [18].

Since the photoexcited electrons and holes induce reduction and oxidation reactions, a rate constant for these active species can be estimated. The overall reaction rate depends on the rate constant for the redox reaction and, as mentioned in chapter 2.1, the rate constant for the recombination rate of the excited electrons and holes. There are no methods for measuring the recombination rate constant, since the recombination does not produce any detectable chemical species for estimation of the recombination rate. I. e. there is no way to estimate the intrinsic photocatalytic activity [5].

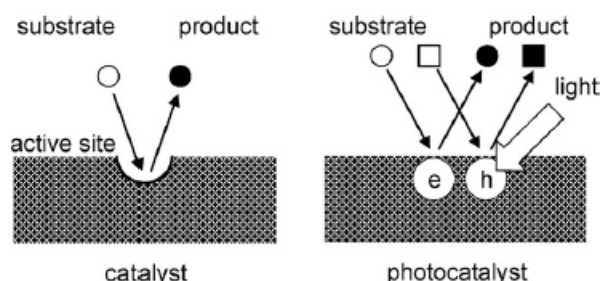


Figure 2.6. The difference in the catalytic concept and the photocatalytic concept, showing no active sites on a photocatalyst [5].

The sacrificial reagent has been shown to influence the photoactivity in many studies. Photocatalysts that have high photoactivity with one sacrificial reagent, does not necessarily have high activity with other organic compounds, as discussed later [31, 82]. For the studies

with methanol as the sacrificial reagent different methanol concentration has been applied [18-19, 22]. Xu *et al.* found that the hydrogen evolution rate increased with increasing methanol concentration up to 80 vol%. From 80 vol% to 100 vol% there was a decrease in the hydrogen evolution rate, but there was still a considerable evolution of hydrogen. This decrease in hydrogen evolution rate in the absence of water was concluded to be because the water molecules also acted as a sacrificial reagent scavenging the electron holes on the surface and producing hydrogen ions [18].

Another important factor that affects the photoactivity is the radiation, as already mentioned. Ryu *et al.* used a variety of TiO₂ photocatalysts, and reported all of them had higher photoactivity for UV radiation than for visible light radiation [31]. This is not surprising considering the band gap of TiO₂ and the wavelength of UV and visible light radiation (chapter 2.2). The most frequently reported radiation power is 400 W or more [8-9, 12, 18, 33, 46, 50, 83-84]. Chen *et al.* studied the effect of light intensity on the photocatalytic rate, and reported the rate increased with increasing intensity [85].

Bandara *et al.* studied the effect of calcination temperature on photocatalytic activity with CuO loaded P25 TiO₂ for photoreforming and found the activity increased with increasing calcination temperature up to about 700 K and then it decreased again [53]. They assumed that since the highest H₂ evolution rate was achieved with a calcination temperature around 700 K, where CuO is fully crystalline, the crystallinity of CuO is important for the photocatalytic activity [53].

Miwa *et al.* also found the photoreforming temperature to be a significant factor for hydrogen generation from methanol/water solutions [86]. They found the quantum yield to be proportional to the temperature, as did Korzhak *et al.* [87], and assumed the reason was because of adsorption and desorption mechanisms.

It is also possible the photoactivity of CuO loaded TiO₂ for photoreforming of methanol is affected by catalyst concentration. The photodegradation of 4-nitrophenol by TiO₂ showed faster reaction rate with increasing TiO₂ concentration up to 2 g/l by Chen *et al.* [85].

Ohtani claims in his review that there is not known how size of photocatalytic structures affect photocatalytic activity [5]. Kim *et al.* on the other hand claims small crystallite size (6 nm) with high crystallinity increase photocatalytic activity [88]. Inagaki *et al.* also report that the crystallite size affect photocatalytic activity, and that different crystallite size is optimal for different reactants [89]. For instance an anatase crystallite size about 32 nm obtained the highest rate constant for photocatalytic decomposition of methylene blue [89]. Many researchers have reported different optimal crystallite sizes in the range of 5 nm to 30 nm [84, 88-93].

Ryu *et al.* also studied the effect of surface area on the photoactivity, and found the correlation to be highly specific for the sacrificial reagent used in the photoreforming [31]. They claim that any single parameter, like the surface area, not could describe the overall properties of the photocatalyst, but they found some tendencies. They reported that high surface area seem to increase photoactivity for organic acids, and lower surface area promotes

photoreforming for alcohols (phenol) [31]. Kim *et al.* studied the photoactivity of pure TiO₂ on degradation on methylene blue, and reported a large surface area (2-300 m²/g) gave the best photoactivity for this reaction [88]. Sreethawong *et al.* also studied the relationship between surface area and photoactivity with CuO loaded TiO₂ for aqueous methanol solutions, and found the optimal surface area to be about 60 m²/g [49]. Ambrus *et al.* on the other hand did not find any relationship between surface area and photoactivity on phenol decomposition [29].

Ambrus *et al.* studied the effect of TiO₂ phases on the photoactivity for phenol decomposition [29]. They found the photoactivity increased with increasing anatase content, pure anatase was 3 times more efficient than pure rutile. The amorphous phase gave lower photoactivity. Their photocatalysts did however not match the photoactivity of P25. The photocatalysts they made with a rutile content like P25 showed a significantly lower photoactivity than P25, and they assume this has something to do with P25's higher surface area or the preparation method not giving the same synergistic effect as P25 [29].

2.5.1 Deactivation of the photocatalyst

The mechanism for photoreforming of aqueous methanol solutions with CuO-TiO₂ systems was found by Choi *et al.* to coincide with the mechanism showed in chapter 2.1.1 [19]. Xu *et al.*, Choi *et al.* and Wu *et al.* concluded that during photoreforming the CuO particles were reduced to Cu₂O or Cu(0) as a consequence of the reducing environment in the solution, and that this decreased the activity of the catalyst [18-19, 22].

Wu *et al.* reported that the H₂ evolution decreased over time because of equilibrium and not because of deactivation [22]. Xu *et al.* does not agree on this point and studied the deactivation mechanisms of the Cu-TiO₂ photocatalyst in photoreforming. They tried to maintain the high hydrogen evolution by adding more methanol after a given time, but that had no effect. Refreshment of the reaction solution increased the activity again, which indicates accumulated byproducts decrease the activity. The byproducts did not poison the catalyst since the activity could be restored (almost) with refreshment of the reaction mixture without any treatment of the catalyst. They also reported a reduction of the CuO to Cu₂O and Cu could be a reason for deactivation, since the activity increased with heat treatment of the catalyst. They concluded that a reduced state of the Cu particles may limit the electron transfer from TiO₂. Also the deactivation could be caused by Cu leaching into the solution because of lower pH values during reaction. 18.3% of the deactivation factors were not discovered, see table 2.2 for an overview of the deactivation mechanisms [18].

Table 2.2. Deactivation mechanisms in photoreforming process with CuO-TiO₂ found by Xu *et al.*[18].

Deactivation mechanisms	Impact %
Accumulation of byproducts	61,7
Reduction of Cu particles	13,3
Cu leaching	6,7
Unknown	18,3

3. Experimental

3.1 Catalyst preparation

3.1.1 Incipient wetness impregnation preparation

Photocatalyst sample 1-7 were prepared by using the incipient wetness impregnation method to deposit the Cu particles on the support with a $\text{Cu}(\text{NO}_3)_2$ solution. In sample 1-4 P25- TiO_2 (Acros Organics Aeroxide, 99.5%) was used as support, sample 5 used pure anatase with low surface area (Alfa Aesar, 99.9%) called anatase1, sample 6 used rutile (Alfa Aesar, 99.9%), and sample 7 anatase with high surface area (Alfa Aesar, 99.9%) called anatase2. For sample 6 the rutile had to be grinded to form powder before the impregnation. See table 3.1 for an overview of all the photocatalyst samples. The incipient wetness point was found by weighing out an exact amount of the TiO_2 in a beaker, and adding water to the powder on a scale. The weight of the water was noted when a change in the TiO_2 state was noticed. The incipient wetness point was then calculated by dividing the mass of the water by the weight of the TiO_2 powder. 2 series were done for each support, and the incipient wetness point was decided as the mean value of these 2 series. This incipient wetness point was used to calculate the amount of $\text{Cu}(\text{NO}_3)_2$ solution needed for each sample. The amount of $\text{Cu}(\text{NO}_3)_2 \cdot 3\text{H}_2\text{O}$ needed to get the desired weight % of Cu^{2+} on the P25 powder was calculated and dissolved in the calculated amount of water, assuming 5 g total catalyst. The CuO amount in each photocatalyst sample is given in table 3.1. For calculations in the preparation, see appendix 1. The samples were then dried over night at 473 K before being calcined for 4 hours at 623 K.

3.1.2 Sol-gel preparation

Photocatalyst sample 8 and 9 were prepared by the sol-gel method. The precursor was $\text{Ti}(\text{OiPr})_4$. The amount of active carbon used were decided based on Colón *et al.*'s article [56] and set to be 20 wt%. The desired amount of carbon was dissolved in ethanol. The volume ethanol used was 3 times the volume of $\text{Ti}(\text{OiPr})_4$. The $\text{Ti}(\text{OiPr})_4$ was added to the ethanol carbon solution, and when the suspension was homogeneous the same amount of water as of $\text{Ti}(\text{OiPr})_4$ was added to the solution. The pH of the sol was then adjusted to 9 with ammonium hydroxide to achieve gel formation. After this the sample was filtrated and washed with ethanol, before drying over night at 373 K. Sample 8 were calcined to burn off the carbon at 773 K for 4 hours before being impregnated with Cu^{2+} by the incipient wetness impregnation method described in the previous chapter. Sample 8 was then calcined again at 623 K for 4 hours. Sample 9 were impregnated with Cu^{2+} before carbon burnoff and calcined only once at 473 K for 4 hours to both oxidize the copper particles and burn off the active carbon.

3.1.3 Deposition precipitation preparation

The desired amount of P25- TiO_2 were dissolved in water, and the desired amount of $\text{Cu}(\text{NO}_3)_2 \cdot 3\text{H}_2\text{O}$ and urea was added to the suspension. The amount of urea used was 5 mol urea/mol $\text{Cu}(\text{NO}_3)_2 \cdot 3\text{H}_2\text{O}$, based on earlier experiments. The pH of the suspension was adjusted to 2 by addition of HNO_3 , and the suspension was thoroughly stirred. The suspension

was slowly heated to 363 K and kept at this temperature for 20 hours. The pH values for the deposition precipitation can be found in appendix 2. The suspension was then filtrated and washed before dried over night at 373 K and calcined at 473 K for 4 hours.

3.1.4 Overview of photocatalysts and preparation parameters

Table 3.1 shows an overview of all the photocatalysts and their preparation parameters.

Table 3.1. An overview of the different photocatalyst samples and their preparation parameters.

Photocatalyst sample no.	Wt% CuO	TiO ₂	Impregnation method	Drying temperature [K]	Calcination temperature [K]
1	1	P25	IWI	373	623
2	5	P25	IWI	373	623
3	10	P25	IWI	373	623
4	15	P25	IWI	373	623
5	10	Anatase1	IWI	373	623
6	10	Rutile	IWI	373	623
7	10	Anatase2	IWI	373	623
8	10	Sol-gel	IWI	373	773&623
9	10	Sol-gel	IWI	373	623
10	10	P25	DP	373	623

3.2 Catalyst characterization

3.2.1 BET surface area measurement

Clean and dried sample holders were weighed without being in contact with anything other than lens paper. An amount of catalyst sample was added to the sample holders, and the new weight of the sample holder with sample was recorded. The samples were degassed over night in a Micromeritics VacPrep 061, before N₂ adsorption in a Micromeritics Tristar 3000 Surface Area and Porosity Analyzer. The mass change was recorded, and the BET surface area was calculated by the BET software.

3.2.2 UV-visible spectrophotometry

The samples were put into sample holders for solid powders, and pressed with a glass cylinder to make the surface of the sample as smooth as possible. Then they were analyzed in a Shimadzu UV-Vis recording spectrophotometer (UV-2401PC) with BaSO₄ as the reference value. The reflectance plot recovered from this analysis was converted with the Kubelka-Munk function and the band gap was found for each photocatalyst and TiO₂ “supports” with the method shown in appendix 3, based on Barton *et al.* [68] and Wang *et al.*'s [69] method.

3.2.3 Temperature programmed analysis

Both TPR and TPO were done in a Netzch STA 449 C thermal gravimetric apparatus. The TGA instrumentation consists of a reactor which is controlled by a processor that heats the reactor. A thermal conductivity detector and/or a mass spectrometer measure the composition of the produced gas. The TPR was done on calcined photocatalysts by increasing the temperature from ambient temperature by 5 K/minute up to 433 K in 50 vol% H₂ in Ar gas. A

correction file was made prior to the analysis with the same temperature program. The mass change was recorded, and the derivative of the mass change with respect to temperature showed at which temperature the reduction was fastest. The TPO plots is shown in appendix 4. The results from the TPR were also used to calculate the amount of CuO present in each sample, according to the calculations in appendix 5 [94].

The TPO analysis was done on uncalcined photocatalysts with increasing temperature in air instead of H₂, to find out which chemisorption temperature was needed for the different photocatalyst samples and at which temperature all the active carbon from the sol-gel preparation was burned off.

3.2.4 X-Ray Diffraction

Small amounts of the photocatalysts were grinded and put onto Si sample holders and suspended in ethanol. The XRD analysis was done in a Bruker axs D8 Focus X-Ray Diffractometer with 2θ from 20° to 80°. The step size used was 0.0199°, step time was 0.5 sec/step and the number of steps was 3001. The calculations for the XRD results are based on Rioux *et al.*'s article [73], and are shown in appendix 6. The calculation of the XRD dispersion for comparison to the chemisorption dispersion was based on Rønning *et al.*'s study [80] and is shown in appendix 8.

3.2.5 SEM and EDS

SEM and EDS mapping was done in a Zeiss Supra 55 VP LV-FESEM. The samples were applied onto a carbon double sided adhesive tape. The SEM was used with different magnifications, electron voltage and work distance, shown in the resulting SEM images.

3.2.6 Chemisorption analysis for dispersion measurements

Chemisorption analysis with N₂O was done in a Netzch STA 449 C thermal gravimetric apparatus with a correction file. The photocatalysts were first heated to 423 K by 5 K/min in Ar atmosphere to evaporate moisture and remaining nitrates, and kept at this temperature for 30 minutes. The photocatalyst was then cooled down to 248 K and kept at this temperature for 80 minutes to stabilize the sample. The next step was a reduction step with 25 vol% H₂ in Ar by heating the samples with 2 K/min up to 533 K and keeping the temperature for 2 hours, and then the sample was cooled down to 248 K again. The temperature was kept at 248 for the rest of the program. After 30 minutes the atmosphere was switched from H₂ in Ar to pure Ar for another 30 minutes. N₂O (5 vol% N₂O in Ar) was then presented to the system to oxidize the Cu(0) particles to Cu₂O. The chemisorption step was held for 15 minutes, before switching to pure Ar again for 30 minutes and ending the experiment. The output gas was analyzed in a Netzch QMS 403 C mass spectrometer. The results from this analysis were calculated [94] as shown in appendix 8.

3.2 Activity measurements

The activity measurements were done in a 1.2 l batch photoreactor with magnetic stirring, continuous inert gas throughput and internal irradiation. The lamp was a 6.5 W UV lamp which were cooled with water in a cooling jacket around it. The lid was made of teflon with glass tubes for gas input and output and temperature control. See figure 3.1 for a schematic figure of the photoreactor.

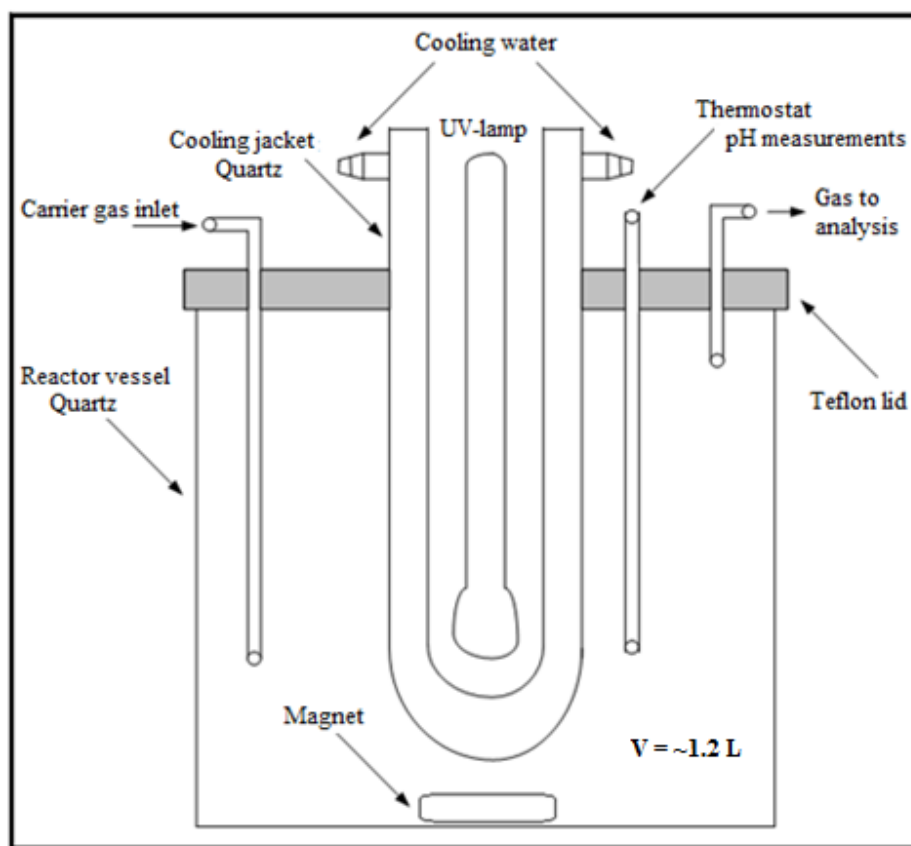


Figure 3.1. The design of the photoreactor.

The activity measurements were conducted with different gas throughput, catalyst concentration, methanol concentration and stirring intensity, and also with a smaller reactor volume, see table 3.2 for the different experiment parameters. The first experiment done was an experiment with pure P25 to have a reference value for the other experiments. All the experiments were done at ambient temperature. The gas output was analyzed in a mass spectrometer (Netzch QMS 403 C mass spectrometer), which were calibrated with an argon-ethylene gas mix, see appendix 7 for the calibration method.

Table 3.2. Overview of experiment parameters for photoreforming experiments.

Experiment	Lamp on [cycle]	Catalyst sample	Catalyst concent. [g/l]	Reactor volume [ml]	MeOH concent. [vol%]	Ar flow [ml/min]	Stirring intensity start [rpm]
030311	9170	3	1	1100	80	20	750
070311	5000	3	0.2	1100	50	20	880
080311	5830	3	0.5	128	50	20	880
090211	2800	3	1	128	50	20	650
100311-1	4340	3	1.5	128	50	8.5	650
100311-2	2000	2	1	128	50	12.8	650
110311-1	1710	7	1	128	50	12.8	650
110311-2	6300	3	1	128	50	12.8	650

In experiment 070311 the stirring intensity was reduced to 500 rpm at cycle 10342. The reactor used in experiment 080311 had quite big gas volume, but this was reduced for the later experiments. The stirring in experiment 080311 was reduced to 500 rpm at cycle 7960, and then increased to 650 at cycle 8000. In experiment 100311-1 the gas flow was increased to 12.8 at cycle 5865. In experiment 110311-2 the gas flow was increased to 24 ml/min at cycle 19400 and then decreased to 8.5 ml/min at cycle 20800. The lamp was turned off at cycle 22800.

4 Results and discussion

4.1 Characterization results

4.1.1 BET surface area measurement

The BET surface area results are shown in table 4.1. The result for photocatalyst 1 is much lower than for the other P25 photocatalysts. This analysis should be done once more to figure out if this was a mistake during the analysis or if this photocatalyst really has this low surface area. The result for photocatalyst 6 is not accurate, since this method is not ideal for such low surface areas, but it is an indication of how low the surface area of photocatalyst 6 is. It is also obvious that photocatalyst 8 and 9 had almost the same surface area before calcination, and that calcination decreased the surface area. Especially photocatalyst 8, which were calcined twice; once at 773 K and then again at 623 K, reduced the surface area considerably. The BET results also show the surface area decrease with increasing CuO loading, and this correspond to the literature [95]. The BET results also shows the incipient wetness impregnation method decreases the surface area of P25 (photocatalyst 1-4) more than the deposition precipitation method (photocatalyst 10). This indicates the IWI method deposit more CuO in the pores of TiO₂ than the DP method. The results also show that it was possible to achieve as high surface area with the sol-gel method used in this study, as the surface area of the commercial anatase TiO₂.

Table 4.1. The BET surface areas for all the photocatalysts, including photocatalyst 8 and 9 before calcination.

Photocatalyst	BET surface area [m ² /g]
1	11 ^a
2	43
3	40
4	38
5	28
6	1 ^b
7	74
8	33
9	74
10	48
8 before calcination	383
9 before calcination	371

a) Possible error during BET analysis

b) BET not an accurate method for such small surface areas

4.1.2 UV-visible spectrophotometry

The band gap energy calculated from the Kubelka-Munk absorption for all the photocatalysts and for the pure P25, anatase and rutile “supports” is shown in table 4.2.

Table 4.2. The calculated band gap from the Kubelka-Munk absorption functions for all the photocatalysts and “supports”.

Photocatalyst	Calculated Band gap [eV]
P25	3,46
Anatase1	3,30
Anatase2	3,40
Rutile	3,01
1	3,30
2	3,23
3	3,20
4	3,12
5	3,28
6	2,95
7	3,29
8	3,28
9	3,23
10	3,37

The DP photocatalyst; photocatalyst 10, has higher band gap energy than the other IWI P25 photocatalysts. The increased band gap could be caused by the difference in the deposition of CuO particles with the two methods. The band gap of the anatase photocatalysts is almost the same, so the difference in surface area does not impact the band gap energy. There was not found any dependency on crystallite size either. The reported values for ideal crystallite size for photocatalytic activity in chapter 2.5 is therefore most likely not dependent on band gap, but other factors like charge recombination.

The Kubelka-Munk absorption plot for all the “supports” is shown in figure 4.1. In figure 4.2 only the Kubelka-Munk absorption for photocatalyst 1-4 and pure P25 is displayed to show the difference with increasing CuO loading, and in figure 4.3 all the rutile and anatase Kubelka-Munk absorptions are shown. Kubelka-Munk absorption plot and reflectance plot for all the photocatalysts can be seen in appendix 3.

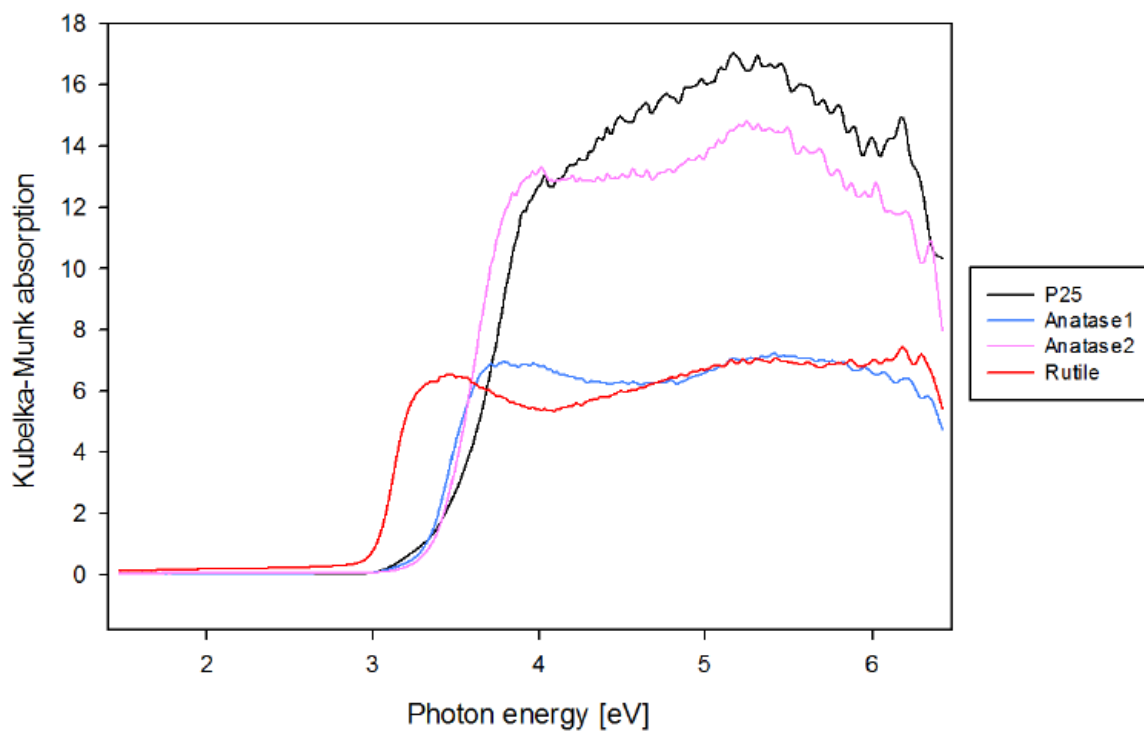


Figure 4.1. The Kubelka-Munk absorption from the pure "supports".

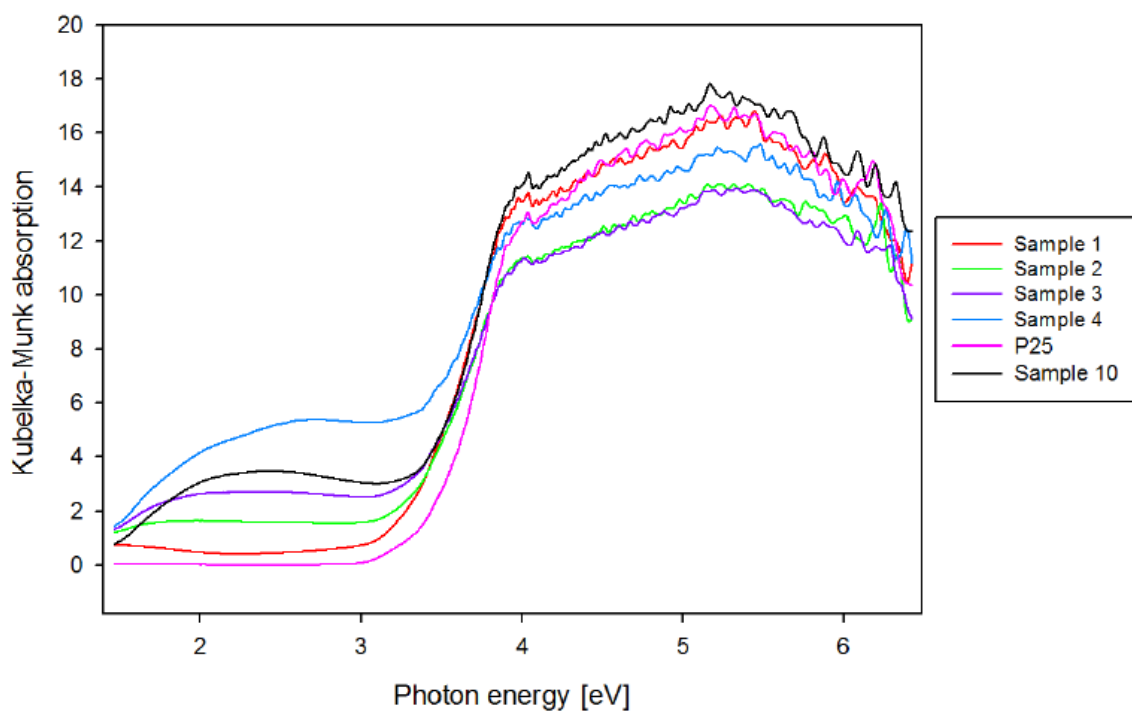


Figure 4.2. The Kubelka-Munk absorption plot from the P25 photocatalysts.

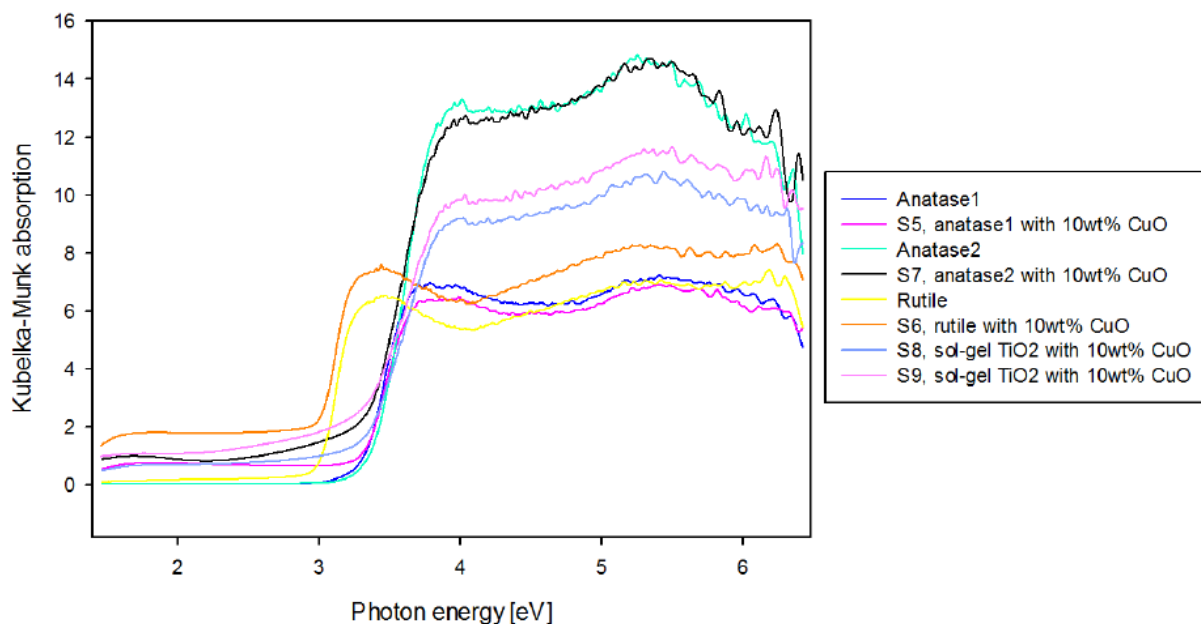


Figure 4.3. The Kubelka-Munk absorption plot from anatase and rutile photocatalysts.

In figure 4.4 the band gap dependency on CuO content is shown, and it is clear the CuO loading decrease the band gap of the photocatalyst. This implies the photocatalyst can absorb more of the sun light, e. g. photons with longer wavelength. The band gap dependency on rutile content is also shown in figure 4.5. The band gap for rutile is lower than for anatase, as expected from the literature. The band gap for P25 however is higher than for anatase, and this could be caused by the synergistic effect discussed in chapter 2.2.1.

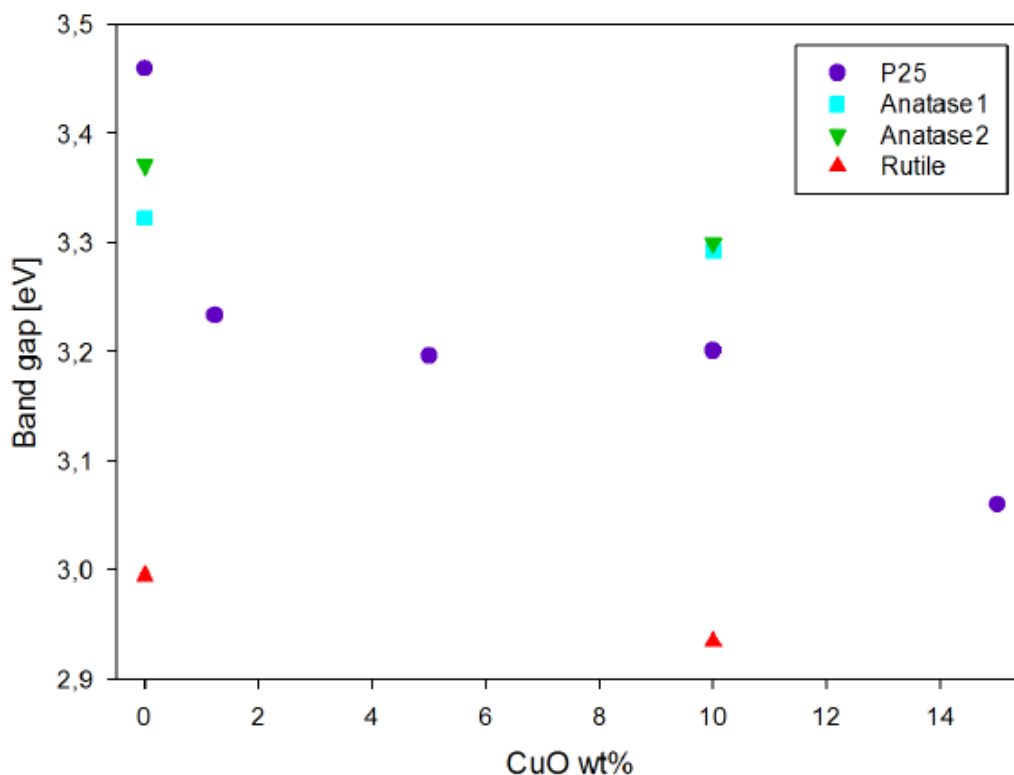


Figure 4.4. A plot showing the band gap dependency on CuO loading.

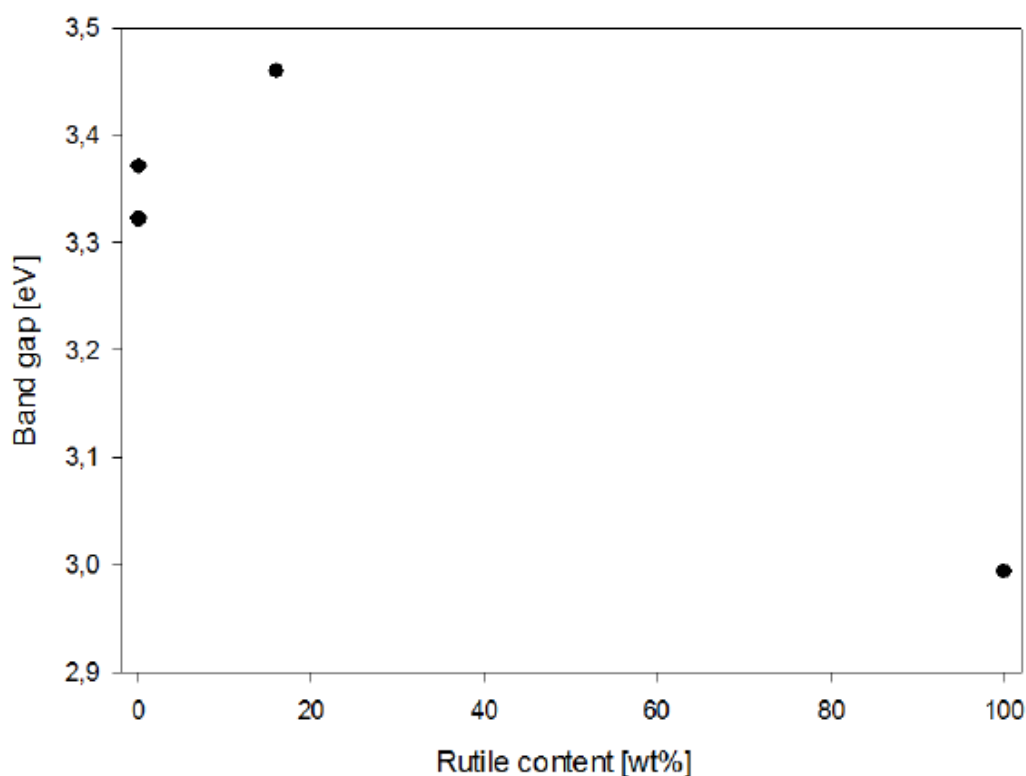


Figure 4.5. A plot showing the band gap dependency on rutile content in the TiO₂.

4.1.3 TPO analysis

Table 4.3 displays the results from the TPO analysis. The TPO of photocatalyst 8 and 9 was done with the active carbon from the sol-gel preparation still in the TiO₂ samples, but photocatalyst 9 was also impregnated with Cu²⁺ ions. As seen from the table, the oxidation temperature was decreased when the photocatalyst was impregnated with Cu²⁺ ions. Photocatalyst 8 was calcined twice, first to burn off the active carbon at 773 K and then at 623 K to oxidize the copper particles. The derivative mass change for photocatalyst 4, 8, 9 and 10 is shown in figure 4.6.

Table 4.3. The oxidation temperature obtained from the TPO analysis.

Photocatalyst	Oxidation temperature [K]
4	492
8	742
9	633
10	521

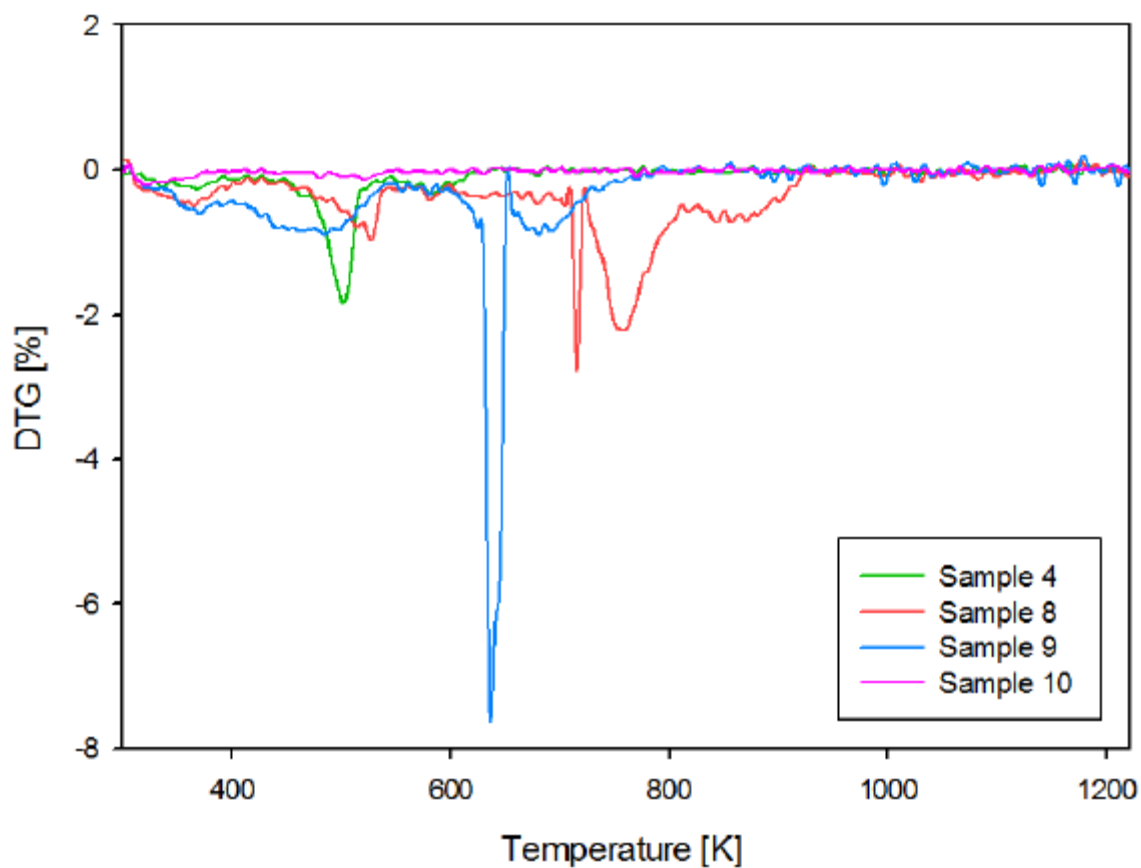


Figure 2.6. The derivative mass change signal for the TPO analysis of photocatalyst 4, 8, 9 and 10.

Figure 4.7 shows an example of the TPO program with the TG signal of photocatalyst 10. There is no significant peak in the mass change rate for photocatalyst 10 in figure 4.6, since the differences was bigger for the other photocatalysts with more content to be oxidized and burned off. The highest mass change rate is more visible in figure 4.7, where the thin green plot shows the derivative TG signal, and gives the highest rate at 521 K.

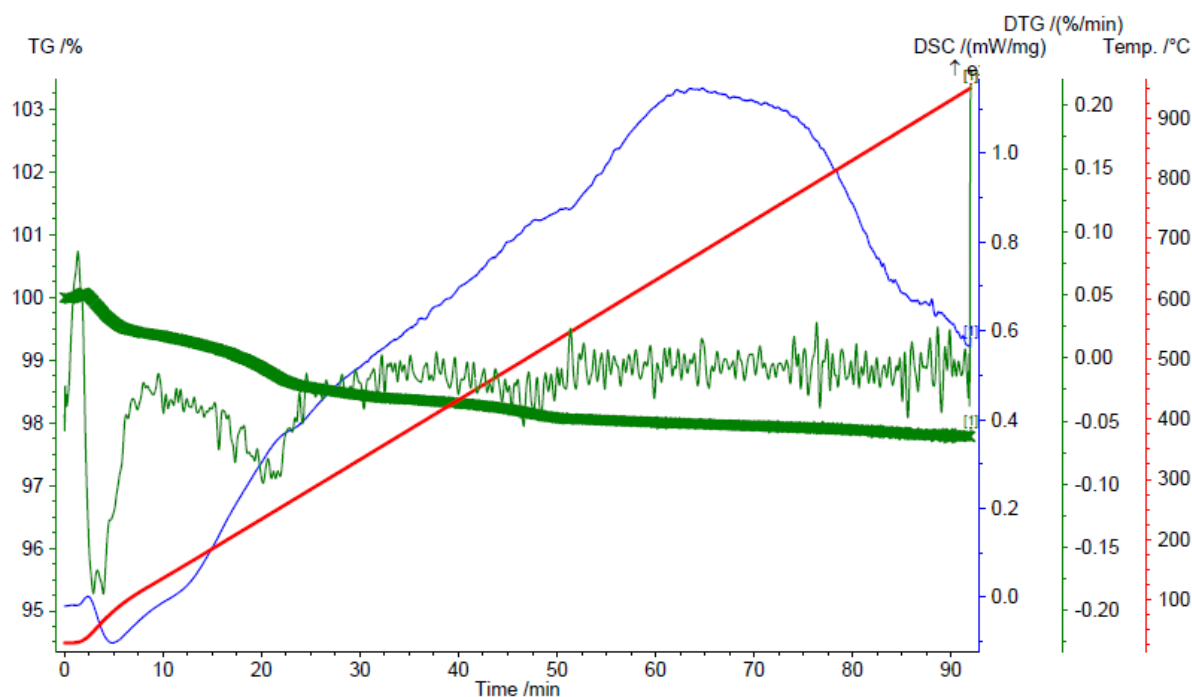


Figure 4.7. The TGA plot of photocatalyst 10, showing the mass change in the thick green plot, the derived mass change in the thin green plot, the DSC signal in the blue plot and the temperature program in the red plot.

4.1.4 TPR analysis

The TPR plot is shown in figure 4.8 showing at which temperature the highest mass change rate is obtained for the different photocatalysts. Photocatalyst 10 has the lowest reduction temperature, while photocatalyst 6 has the highest. The results imply the DP preparation method gives lower reduction temperature than IWI preparation method. The lower reduction temperature support the theory about DP method depositing CuO particles more on the surface and less in the pores of the TiO₂ than IWI method, as discussed later. This could also mean photocatalysts prepared by the DP method is more easily reduced during photoreforming, and therefore earlier deactivated than IWI photocatalysts. The results are also shown in table 4.4.

Table 4.4. The results from the TPR analysis; the reduction temperatures and the calculated CuO content. It was not possible to obtain any reduction results from photocatalyst 1, since the CuO loading is too low for detection.

Photocatalyst	Reduction temperature [K]	Calculated CuO [wt%]
1	-	-
2	408	11
3	408	11
4	393	16
5	408	11
6	417	10
7	382	15
8	379	11
9	408	14
10	371	9

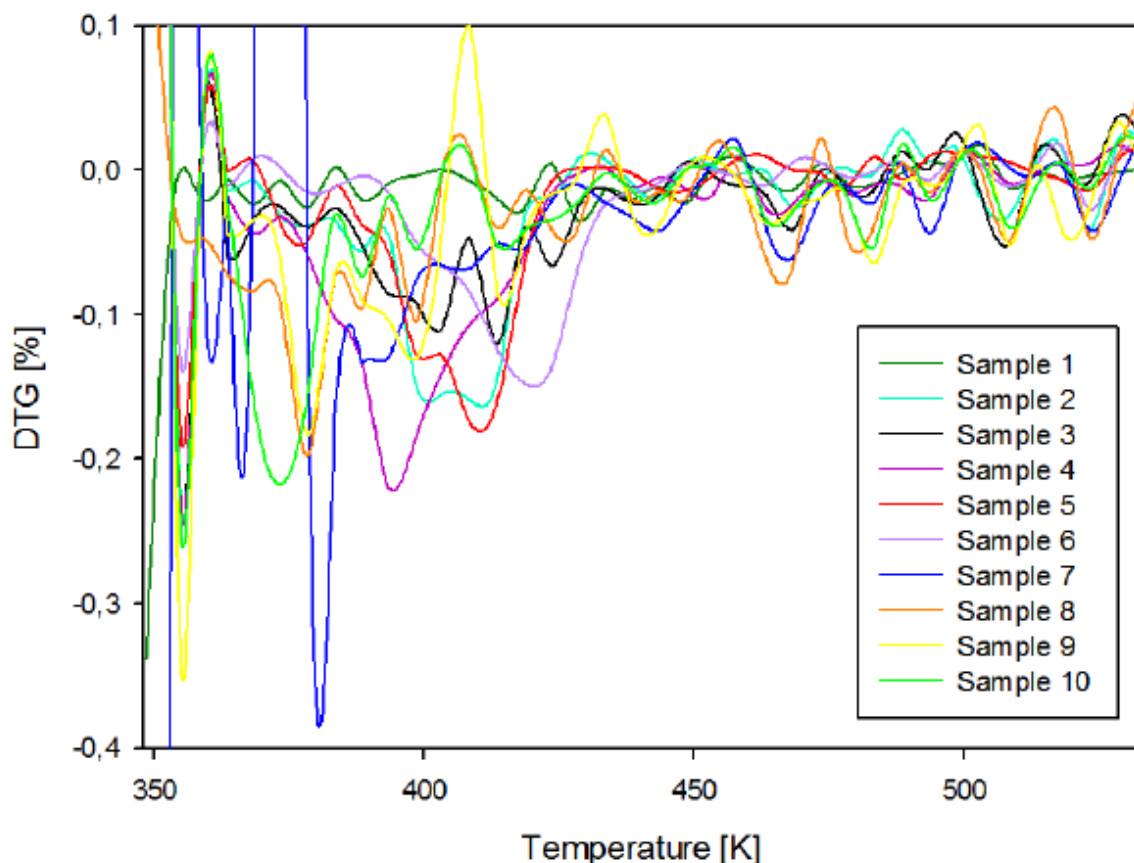


Figure 4.8. The derivative mass change signal for all photocatalysts in the TPR analysis.

The calculated CuO content from the TPR analysis is overestimated compared to the calculated content from the preparation method for all the photocatalysts except for photocatalyst 6 and 10. For samples with high surface area there is often condensed water in the pores of the sample that is hard to evaporate with inert atmosphere. The overestimation of the samples with high surface area could therefore be because of this pore condensate evaporating during the TPR analysis. This would also explain why the CuO content in photocatalyst 6, the rutile photocatalyst, was not overestimated, since this sample has very low surface area (see chapter 4.1.1). It is not certain that all the copper deposited on the P25 during the preparation method for photocatalyst 10, and this might be the reason for the apparent underestimation of the CuO content in this sample. The CuO content calculated for the samples with less than 10 wt% CuO was much higher than the calculated content from the preparation method. This could mean CuO content calculations based on TPR results is uncertain for samples with too low CuO content.

4.1.5 XRD analysis

Figure 4.9 shows the XRD scans for increasing copper content on P25 TiO₂. The CuO peak is not visible for the photocatalyst with 1 wt% CuO, and barely visible in photocatalyst 2 with 5wt% CuO. This correspond to the results presented in Choi *et al.*'s report [19]. All the P25 photocatalysts show more noise in the XRD scans than the photocatalysts with pure anatase or rutile TiO₂, which implies P25 contains more amorphous phase.

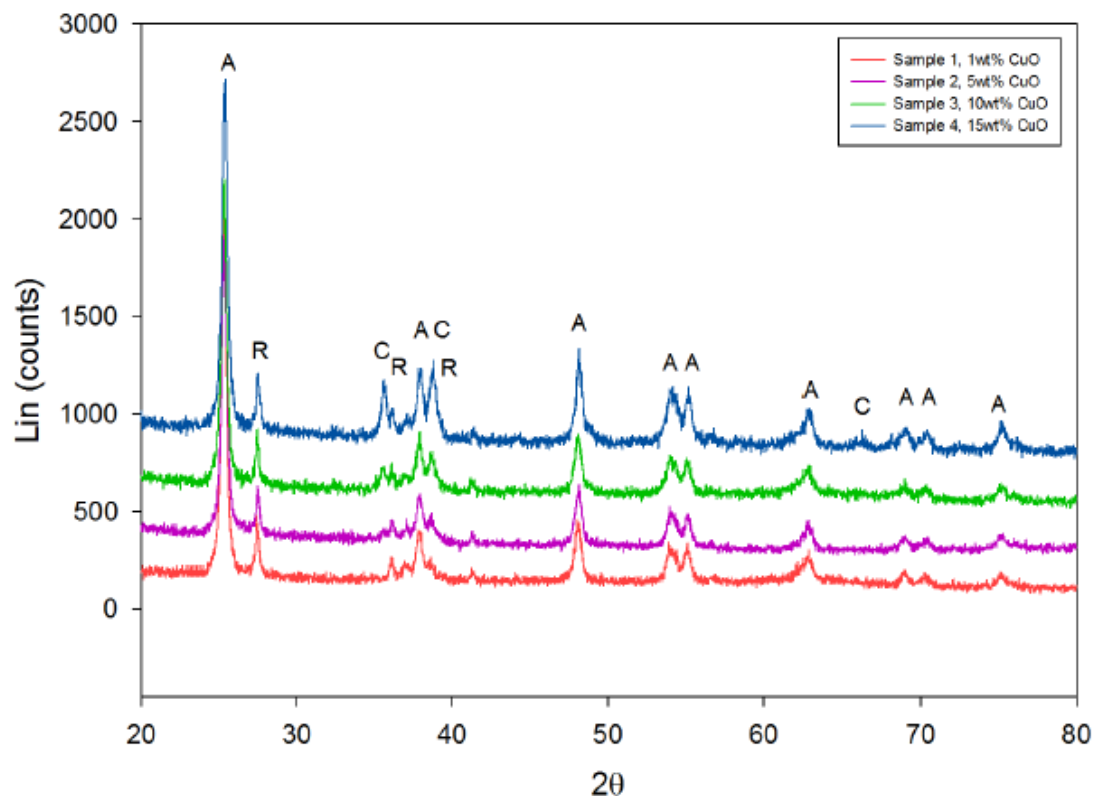


Figure 4.9. The XRD scans of photocatalyst 1-4 showing the difference in XRD signal with increasing CuO loading.

Figure 4.10 shows the difference between the photocatalysts with only anatase TiO_2 . Photocatalyst 5 has higher anatase intensity, than the others. This implies higher anatase crystallinity in this sample, which coincide with literature which says that crystals with lower surface area and bigger crystallite size have higher crystallinity [62]. The CuO peak is also more significant in the samples with lower surface area, where it is harder to get high CuO dispersion and low CuO particle size. Photocatalyst 7, the photocatalyst with high surface commercial anatase, seems to contain less amorphous phase than the other anatase samples.

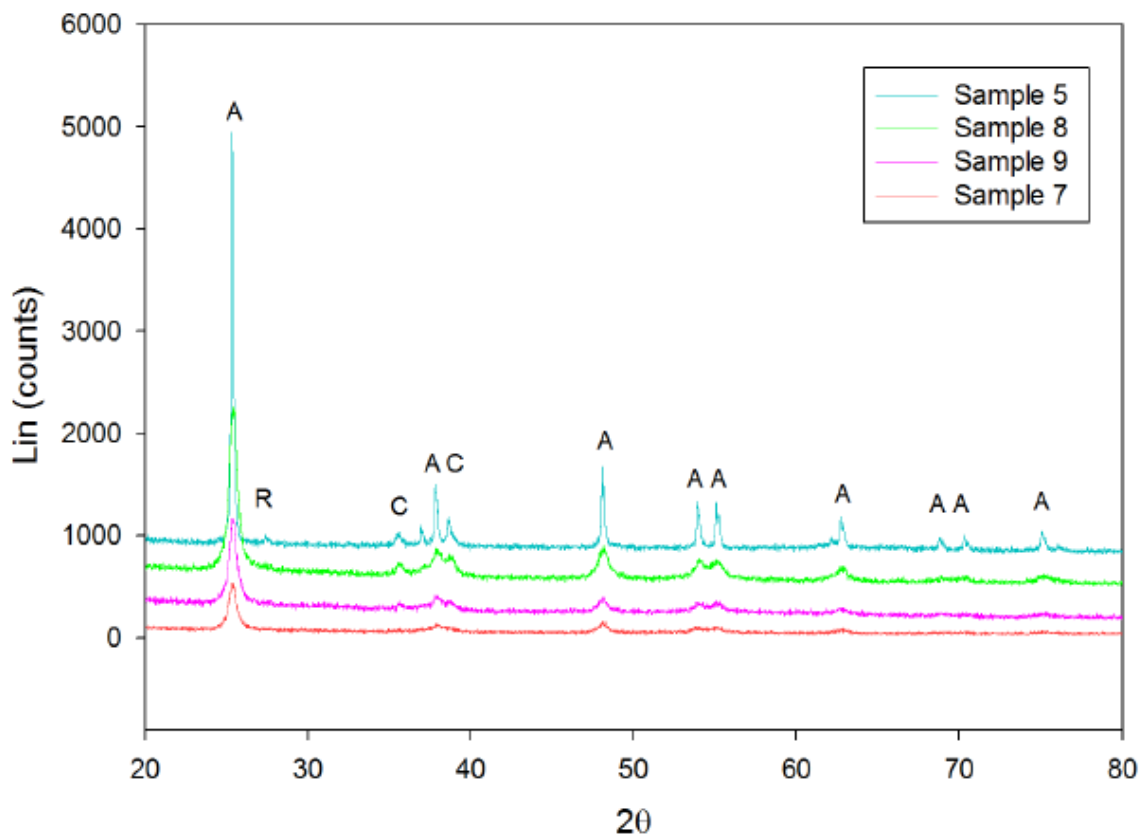


Figure 4.10. The XRD scans from all the anatase photocatalysts; photocatalyst 5, 7, 8 and 9.

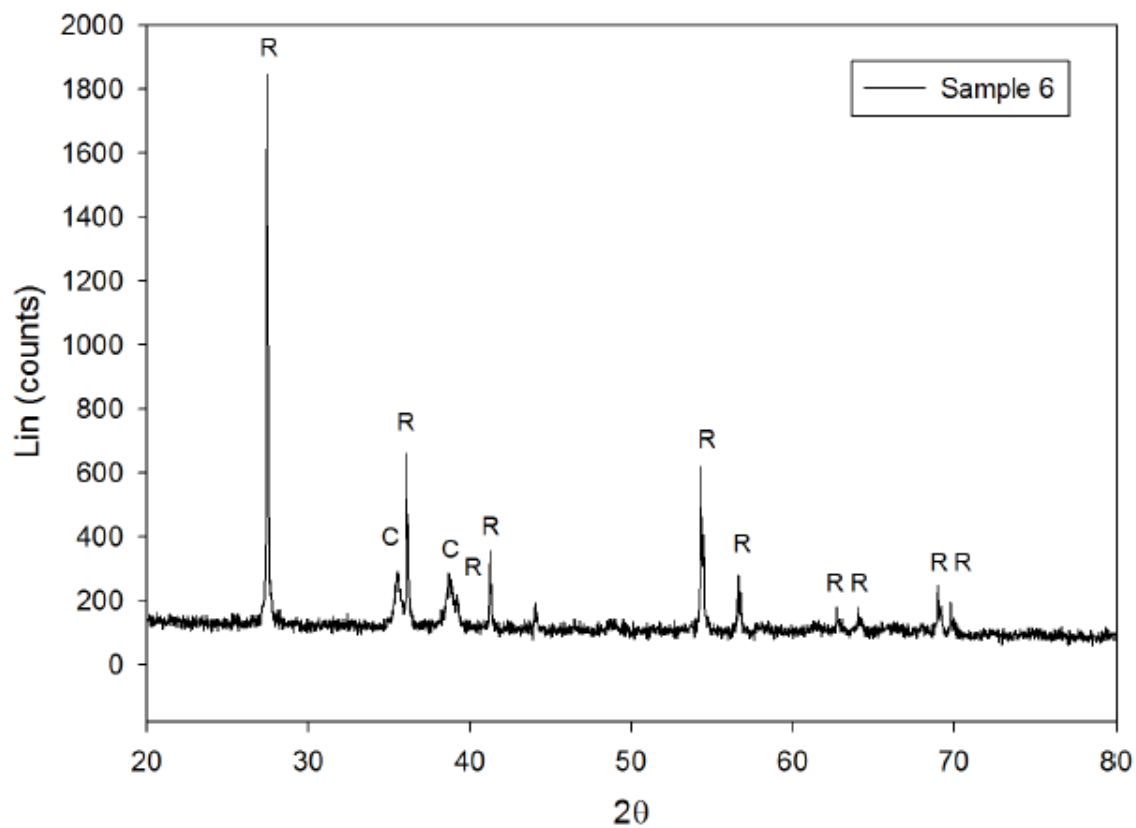


Figure 4.11. The XRD scan of sample 6, 10wt% CuO on rutile TiO₂.

Figure 4.11 shows the XRD scan of photocatalyst 6, the only photocatalyst with only rutile TiO_2 . This XRD plot shows quite high crystallinity of the rutile phase, and significant CuO peaks. The CuO peaks imply big CuO particle size, see table 4.5 for the calculated particle sizes for each phase in all the photocatalysts. Large CuO particles on rutile are logical since the surface area of rutile is very low. The plot also shows high crystallinity and low content of amorphous phases.

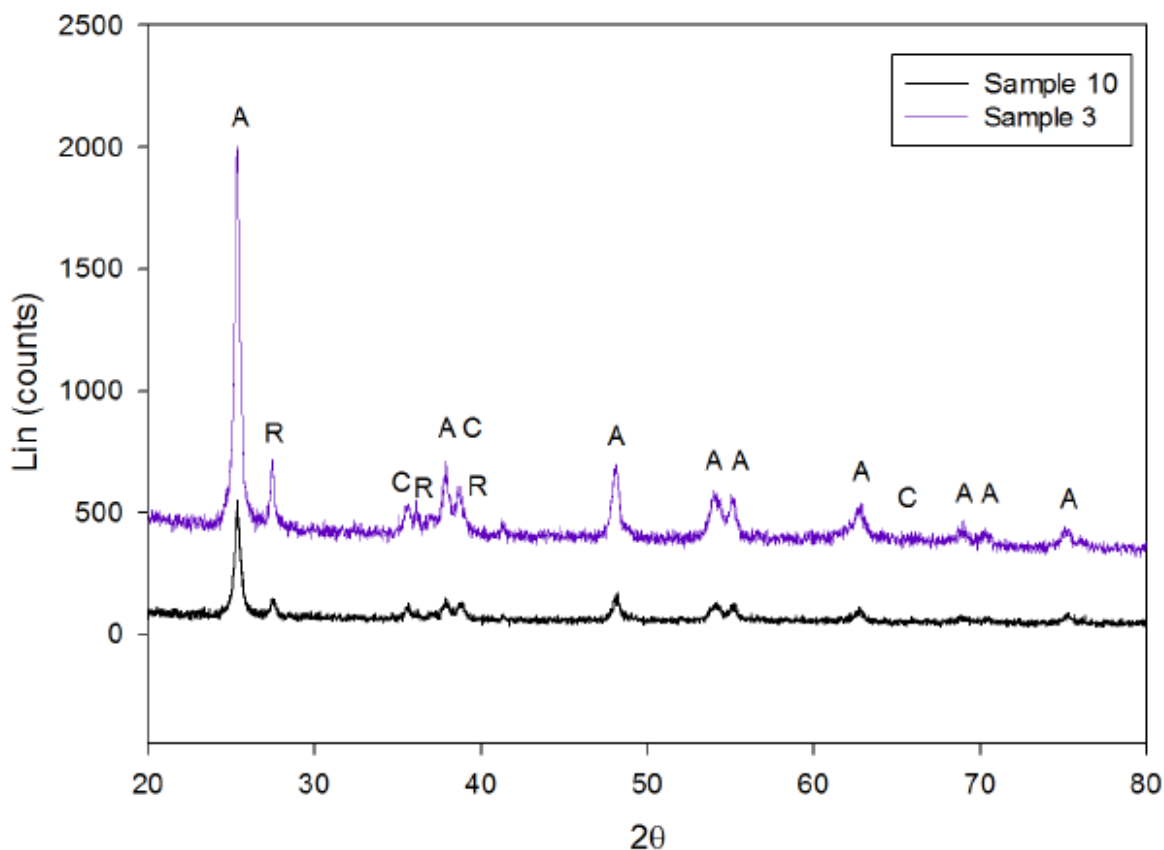


Figure 4.12. Showing the difference in XRD scans between the two photocatalysts with 10wt% CuO on P25; photocatalyst 3 and 10.

Figure 4.12 shows the difference in the two photocatalysts with 10wt% CuO on P25; photocatalyst 3 and photocatalyst 10. The scan implies the deposition precipitation method (photocatalyst 10) might decrease the crystallinity of the P25 TiO_2 , since the anatase and rutile peaks has lower intensity for photocatalyst 10. It also show more noise for photocatalyst 3, which might imply there are more amorphous copper phases with the incipient wetness impregnation method than the deposition precipitation.

In table 4.5 all the calculated results from the XRD scans are shown, FWHM crystallite size, rutile content and CuO dispersion. The crystallite size from XRD scans is often underestimated compared to the real sizes [29], which makes the dispersion calculated based on the crystallite size overestimated compared to the true dispersion. The anatase and CuO particle size is almost the same for all the P25 photocatalysts (photocatalyst 1-4 and 10). The rutile crystallite size varies between 9 – 39 nm. The CuO crystallite size in photocatalyst 1 is not accurate, because XRD has a detection limit around 5 nm and this makes the XRD

analysis an unreliable analysis method for photocatalyst 1, a better characterization method would be TEM or XAS [96].

The smallest obtained CuO crystallite size was obtained in photocatalyst 7, the photocatalyst with the highest surface area. The CuO crystallite size was bigger on the sol-gel photocatalyst which was impregnated with Cu before the active carbon was burned off (photocatalyst 9), than on the sol-gel photocatalyst that was impregnated after the carbon was burned off (photocatalyst 8) even though photocatalyst 9 has higher surface area. This shows the active carbon affect the Cu²⁺ dispersion and CuO particle size. It is possible the active carbon is located in the TiO₂ pores, making the surface area lower when photocatalyst 9 was impregnated with Cu. The difference in calcination process did not affect the crystallite for the sol-gel photocatalysts. See appendix 6 for calculations and errors for the crystallite size.

The rutile content varies by 2% in the P25 photocatalysts used in this study. This coincides with *Ohtani et al.*'s results were they reported 3% variations, but they also found the amount of amorphous TiO₂ phases present in their photocatalysts. The method for rutile content calculations used in this study assumes no amorphous TiO₂ present [33]. The calculated results show the rutile content is not affected by CuO loading. As seen in table 4.5 there were some rutile present in photocatalyst 5. This is most likely caused by some contamination during the calcination process since this was the first of the anatase photocatalysts to be calcined in the calcination reactor used for both P25 and rutile samples before.

Table 4.5. Showing crystallite size of the different phases in the photocatalyst and dispersion calculation based on XRD analysis. The CuO dispersion was calculated based on the method used by Rioux and Vannice [97].

Photocatalyst	CuO crystallite size [nm]	Anatase crystallite size [nm]	Rutile crystallite size [nm]	Rutile content [wt%]	CuO dispersion [%]
1	1 ^a	21	39	16	100 ^b
2	26	21	18	16	4
3	23	21	16	18	5
4	26	19	33	17	4
5	24	102	12	1	5
6	24	155	125	100	5
7	12	11	0	0	9
8	23	12	1	0	5
9	30	13	2	0	4
10	27	18	9	17	4

a) Not an accurate crystallite size value, since the XRD cannot detect that small particles and the error has a higher value than the crystallite size.

b) The calculated dispersion was higher than 100%, too small amount of CuO to use XRD as a reliable analysis method.

From table 4.5 it is also clear that the sol-gel TiO₂ has much lower anatase crystallite size than P25 TiO₂. Some literature claims smaller crystallite size is better, but the ideal crystallite size of anatase has been reported to be everything from 5 nm to 30 nm and all the photocatalysts except 5 and 6 has anatase crystallite size in this range. Even though there are reported a crystallite size for rutile in photocatalyst 8 and 9 and for anatase in photocatalyst 6, the peaks

were so low that the rutile content was calculated to be 100% for photocatalyst 6 and 0% for photocatalyst 8 and 9. However there was trace amounts of rutile in photocatalyst 8 and 9, but the calcination of photocatalyst 9 at 773 K did not increase the rutile content more than for photocatalyst 8.

4.1.6 SEM and EDS

The structure of the P25 samples is shown in figure 4.13 with photocatalyst 2. The difference in structure between the two sol-gel photocatalysts is also shown in figure 4.14. It is obvious from the SEM pictures that photocatalyst 8 has less surface area than photocatalyst 9, which is also proved in chapter 4.1.1.

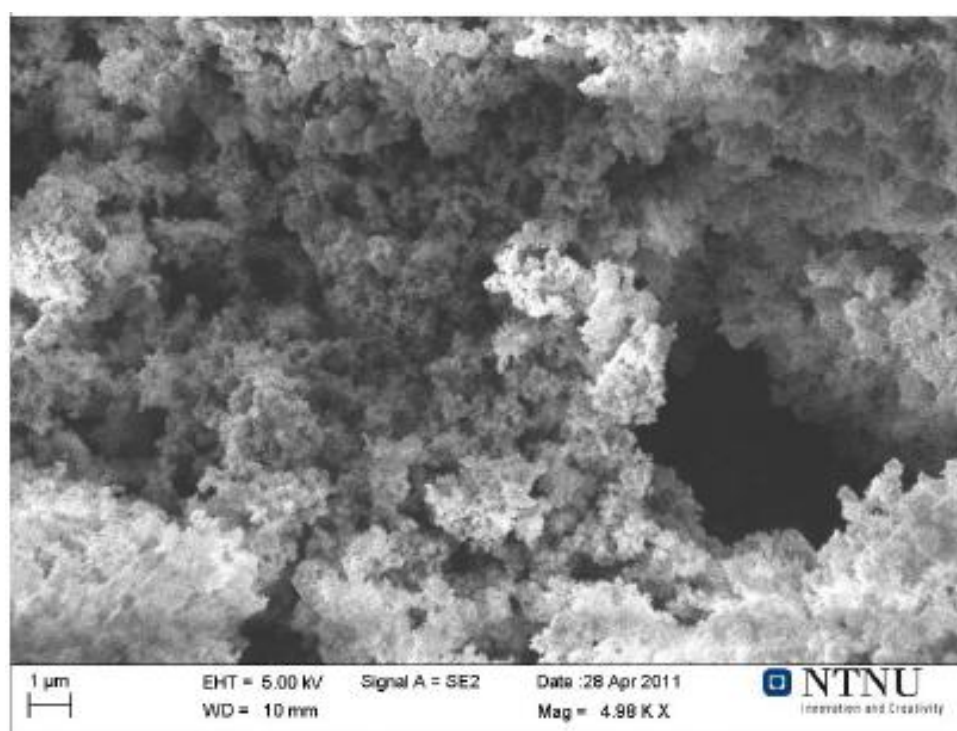


Figure 4.13. SEM picture of photocatalyst 2 showing the structure of P25 TiO₂.

Table 4.6. Atom% of Ti, Cu and O at the surface from EDS measurement.

Photocatalyst	Atom% Ti	Atom% Cu	Atom% O
1	28	1	71
2	23	2	75
3	25	2	74
4	23	5	72
5	30	2	68
6	26	8	66
7	26	3	71
8	28	3	69
9	27	5	68
10	29	6	65

Table 4.6 shows the atom% of Ti, Cu and O at the surface from the EDS analysis. The highest Cu% at the surface was obtained in photocatalyst 6, the photocatalyst with the lowest surface

area. This is logical since more copper will deposit deeper in the sample for samples with more pores. The EDS analysis is also not very accurate for this kind of sample, since the surface of the substance should be homogeneous and smooth to get good EDS results. The EDS result also show the deposition precipitation method most likely deposit the copper particles more on the surface of the TiO₂, while the copper particles might more easily deposit in the pores of the TiO₂ with the incipient wetness impregnation method. This theory is also confirmed by BET, XRD and TPR results. The atom% at the surface of photocatalyst 9 is also quite high, and that corresponds to the results in chapter 4.1.4 indicating the TiO₂ pores probably were filled with active carbon during the Cu²⁺ impregnation making the Cu²⁺ particles deposit more on the surface of TiO₂ than in the pores.

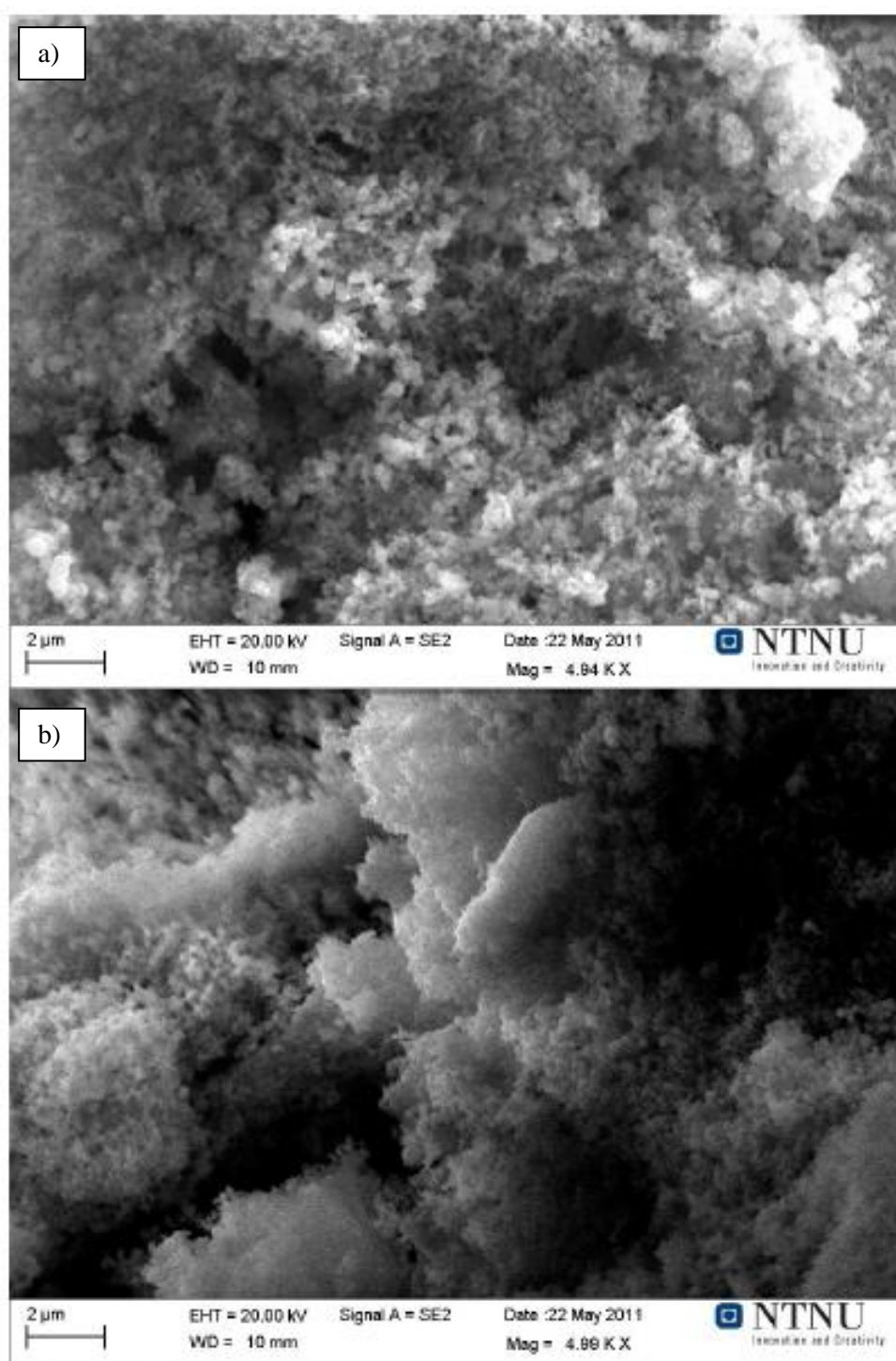


Figure 4.14. Showing the difference in structure between the two sol-gel photocatalysts; a) photocatalyst 8 and b) photocatalyst 9.

Figure 4.15 shows the SEM and EDS picture of photocatalyst 6 (rutile) and 7 (anatase2), the blue in the EDS pictures is copper and the purple is titanium. The figure shows both the difference in structure and in dispersion. Photocatalyst 6 has low surface area and big copper particles and photocatalyst 7 has bigger surface area and the copper particles are small and well dispersed.

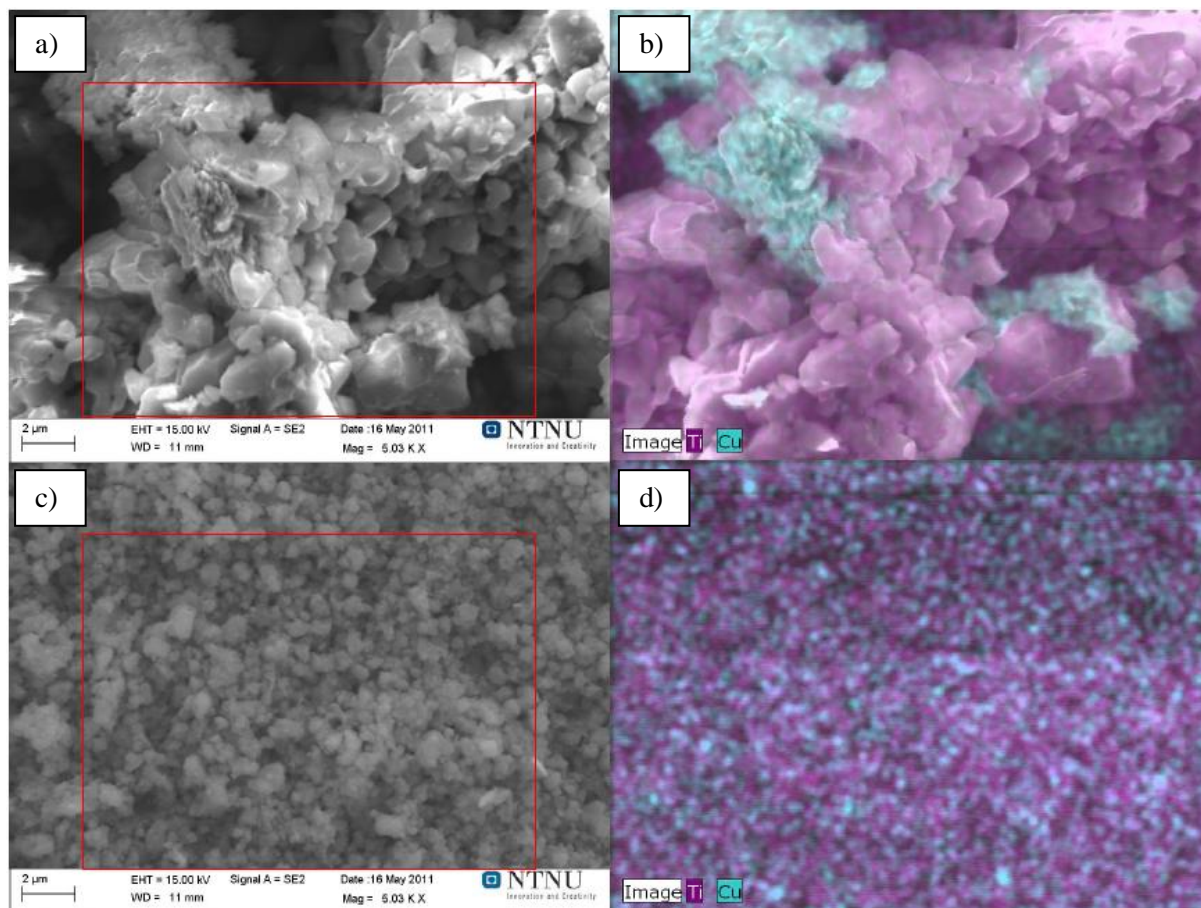


Figure 4.15. Showing the difference in CuO dispersion in photocatalyst 6 and 7. Picture a) is the SEM picture of photocatalyst 6, b) is the EDS picture of photocatalyst 6, c) is the SEM picture of photocatalyst 7 and d) is the EDS picture of photocatalyst 7.

Figure 4.16 shows the difference between photocatalyst 6 and 9 at higher magnification. In this figure the difference between TiO₂ structure and CuO structure is displayed. The rutile structure is smooth “rocks”, the CuO structure is flowerlike and the high surface sol-gel anatase structure looks like cotton.

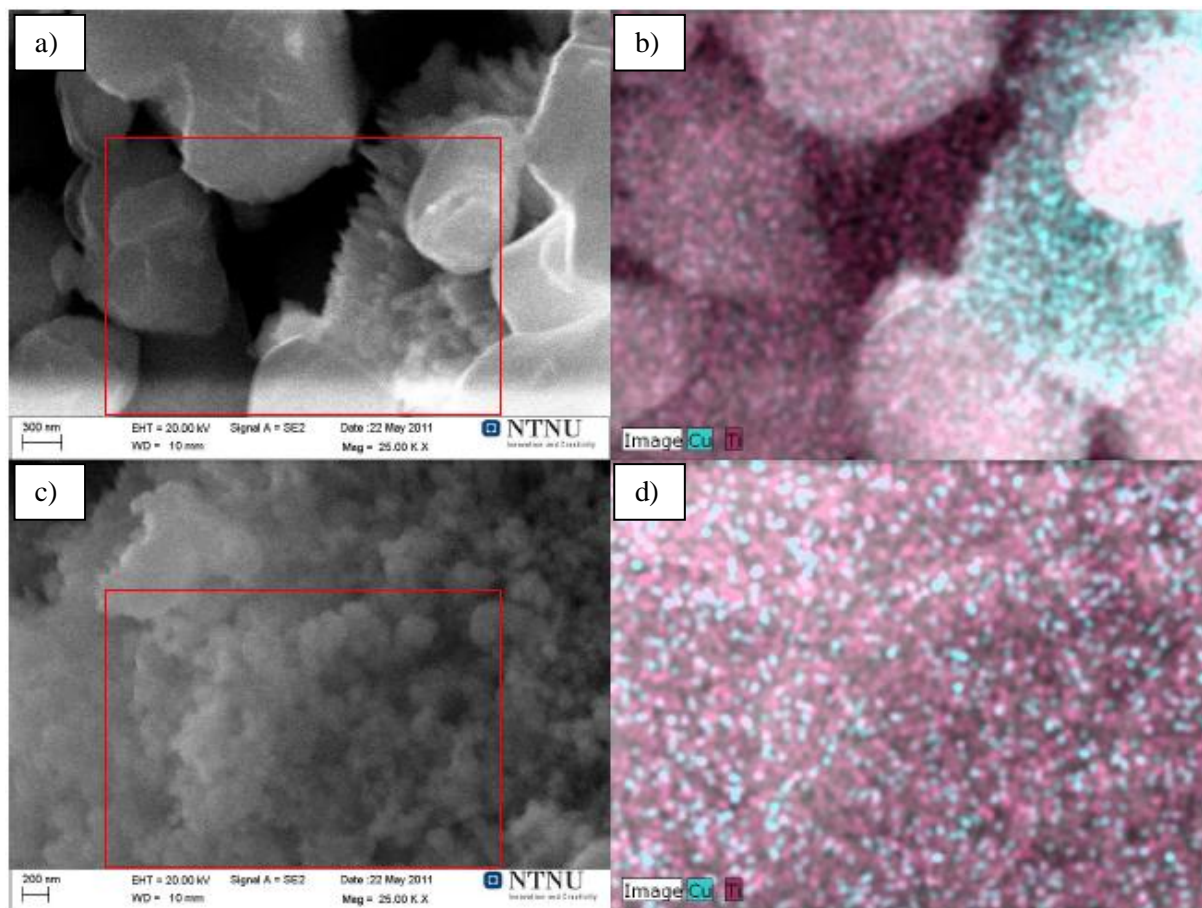


Figure 4.16. SEM picture of a) photocatalyst 6 and c) photocatalyst 9 shows the difference in structure for photocatalyst with low surface area and high surface area. EDS picture of b) photocatalyst 6 and d) photocatalyst 9 shows the difference in dispersion for samples with high surface area and low surface area.

4.1.7 Chemisorption results

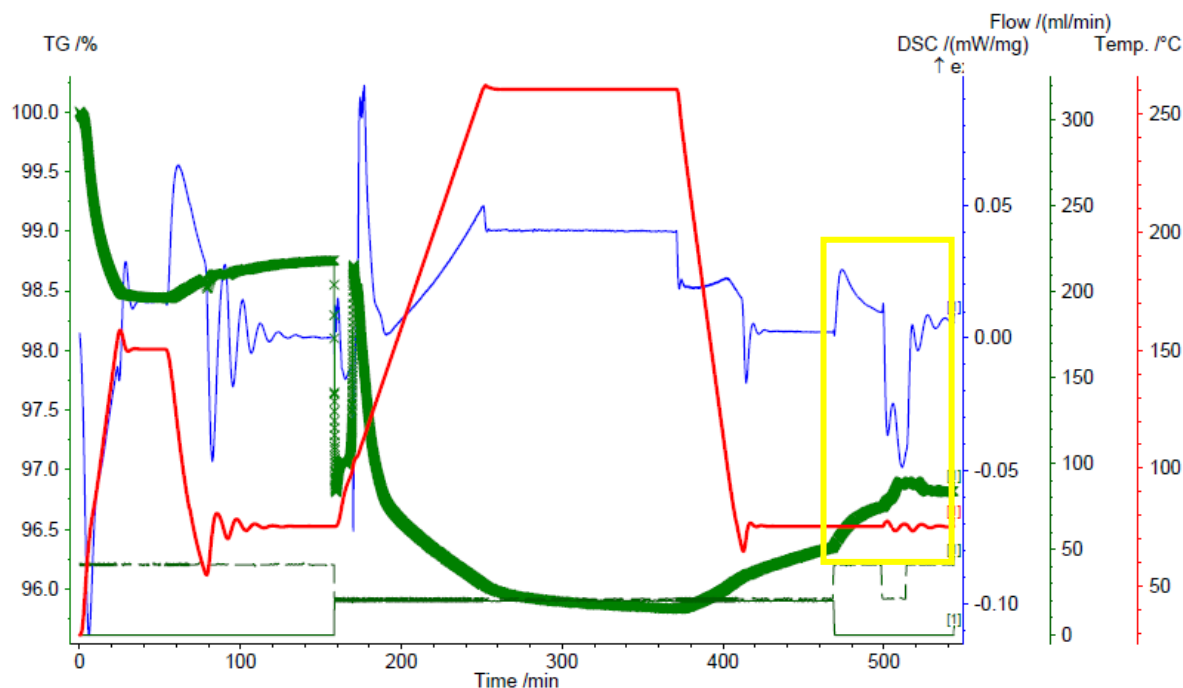
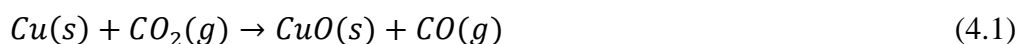


Figure 4.17. Shows the plot of mass loss, DSC signal, gas flow and temperature program for the chemisorption analysis for photocatalyst 7. The mass signal is green, DSC signal is blue and temperature program is red.

Figure 4.17 shows a typical chemisorption plot from the TGA software. The green plot is the mass signal, the red is the temperature program and the blue is the DSC signal. The TG signal stabilized after the nitrate evaporation step, and after the reduction step. The mass increased because of the temperature change when the temperature decreased to 248 K in reducing environment. A further increase in mass was seen when the gas atmosphere was changed to Ar, the yellow frame in figure 4.17 shows the oxidation and chemisorption step. This increase is most likely caused by impurities in the argon gas, like CO_2 oxidizing the sample. This was also confirmed by the MS signal where the CO_2 signal increased when the atmosphere was changed. The gas quality used during these measurements was 5.0, 6.0 is therefore most likely necessary to get precise chemisorptions results. If the element oxidizing the sample is CO_2 , the most likely oxidation is bulk oxidation. This is also seen by the DSC signal showing an endothermic reaction when the gas atmosphere is switched to pure argon. If the mass change is caused by bulk oxidation, the reaction will be as shown in reaction (4.1). Bulk oxidation of $\text{Cu}(0)$ by CO_2 is an endothermic reaction (126 kJ/mol), see appendix 10 for calculations of heat of reactions.



There was a further increase in mass when N_2O was introduced to the system. When N_2O decompose on Cu particles Cu_2O is formed, as discussed in chapter 2.4.3. This reaction is exothermic, as also seen by the DSC signal which decreases while N_2O is present in the TGA chamber. This indicates the N_2O adsorptive decomposition does take place on the surface of the Cu particles. Since there obviously is some oxidation of the particles before N_2O is

present, these chemisorption measurements are not accurate. It is most likely the CO₂ oxidation of the copper particles is bulk oxidation, but some surface oxidation might also have taken place.

Table 4.6. Calculated CuO dispersion and specific surface area of CuO from chemisorption measurements.

Photocatalyst	Specific surface area of Cu particles [m²/g]	Dispersion of Cu particles [%]
1	7	32
2	2	3
3	6	9
4	9	11
5	1 ^a	1 ^a
6	0 ^a	0 ^a
7	7	9
8	3	6
9	6	8
10	4	6

a) Photocatalyst 5 and 6 showed almost no response to the chemisorption step.

Table 4.6 shows the calculated Cu(0) dispersion and specific surface area of the Cu(0) particles from the chemisorption results. The specific surface area of the copper particles shows high surface area for small Cu particles. Photocatalyst 6 gave no results at all during the chemisorption measurement, and there was almost no chemisorption on photocatalyst 5. These were the photocatalysts with the lowest surface area, and this might have affected the chemisorption abilities.

4.1.8 Comparison of XRD dispersion and chemisorptions dispersion

Table 4.7 displays the results from XRD, the calculated Cu(0) dispersion from XRD and the Cu(0) dispersion from the chemisorption analysis. The dispersion for photocatalyst 1 from XRD can, as discussed earlier (chapter 4.1.4), not be used as an accurate value. Photocatalyst 7 show quite high dispersion with both analysis methods. Photocatalyst 4, the sample with the highest CuO loading, showed higher dispersion with the chemisorption method than with XRD scans, this could indicate some bulk chemisorption in addition to the uncertainty of the chemisorption results. From the literature it is logic if the XRD gives an overestimated dispersion, and this is true for all the samples except photocatalyst 3, 4, 9 and 10. The inconsistency of the results could be caused by the uncertainty of the chemisorption analysis.

The chemisorption dispersion shows the opposite relationship between photocatalyst 8 and 9 as the XRD dispersion. XRD needs crystallinity and two calcination processes could increase the crystallinity of the sample. XRD dispersion is also calculated based on an average particle size. The two methods measures by different principles, making a comparison difficult.

Photocatalyst 8 was calcined before impregnation making the surface area much lower during Cu-impregnation. This could decrease the dispersion for photocatalyst 8. Photocatalyst 9 still contained active carbon in the TiO₂ pores during Cu-impregnation, also making the surface area smaller for photocatalyst 9. It is therefore hard to tell which of the two photocatalysts have the highest dispersion, but since there was bulk oxidation during chemisorption

measurements this method is less precise than desired, and the XRD results is more reliable. The EDS results also indicates photocatalyst 9 has lower dispersion than photocatalyst 8, since photocatalyst 9 had more Cu atoms present on the surface and less in the pores and photocatalyst 8 most likely had more Cu atoms in the pores.

Table 4.7. The dispersion results from chemisorption measurements and XRD analysis for comparison.

Photocatalyst sample	CuO dispersion (XRD)	Cu(0) dispersion (XRD)	Cu(0) dispersion (chemisorption)
1	100 ^a	100 ^a	32
2	4	5	3
3	5	6	9
4	4	5	11
5	5	6	1 ^b
6	5	6	0 ^b
7	9	11	9
8	5	6	6
9	4	4	8
10	4	5	6

a) Not an accurate value because of too low CuO content in sample and too small particle size.

b) Photocatalyst 5 and 6 showed almost no response to the chemisorption

4.2 Activity measurements

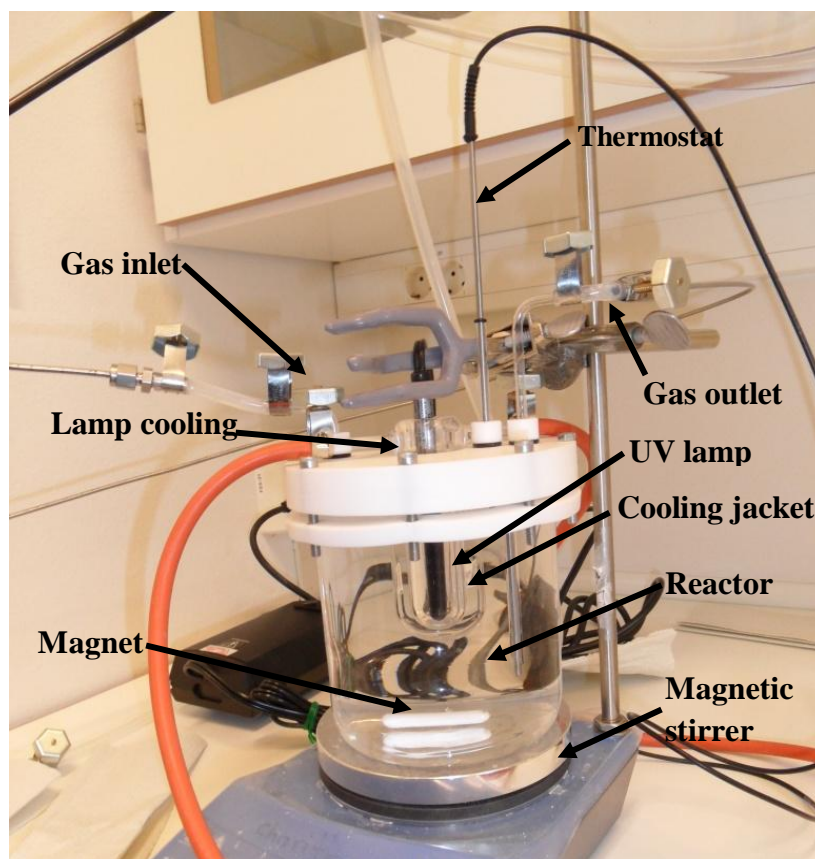


Figure 4.18. The original photoreforming setup.

Figure 4.18 shows the original photoreforming setup, with gas throughput, thermostat, lamp, magnetic stirring and lamp cooling. Figure 4.19 shows the setup after modification of the reactor volume. The outer reactor volume was filled with water to reduce the gas volume in the reactor, while the inner reactor contained the reaction suspension.

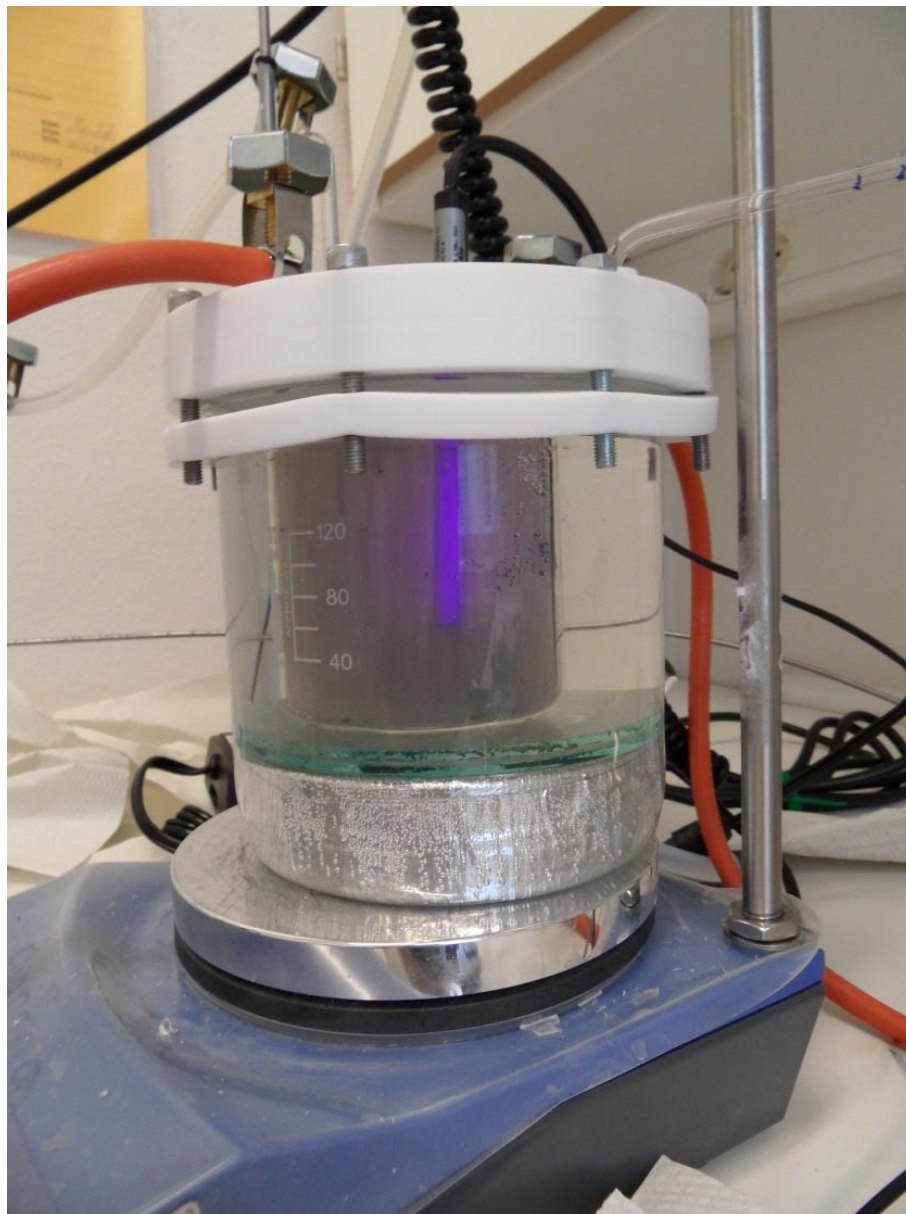


Figure 4.19. The reactor after volume modification.



Figure 4.20. The color of the P25 in 80 vol% methanol suspension after hours of UV radiation.

Figure 4.20 shows the photoreforming suspension after UV-radiation for several hours. The suspension contained 80 vol% methanol and pure P25. The suspension changed color from white to blue-grey. This is most likely caused by a photocatalytic reduction of the P25, as discussed in chapter 2.1. There was not any change in the hydrogen signal from the MS in this experiment.

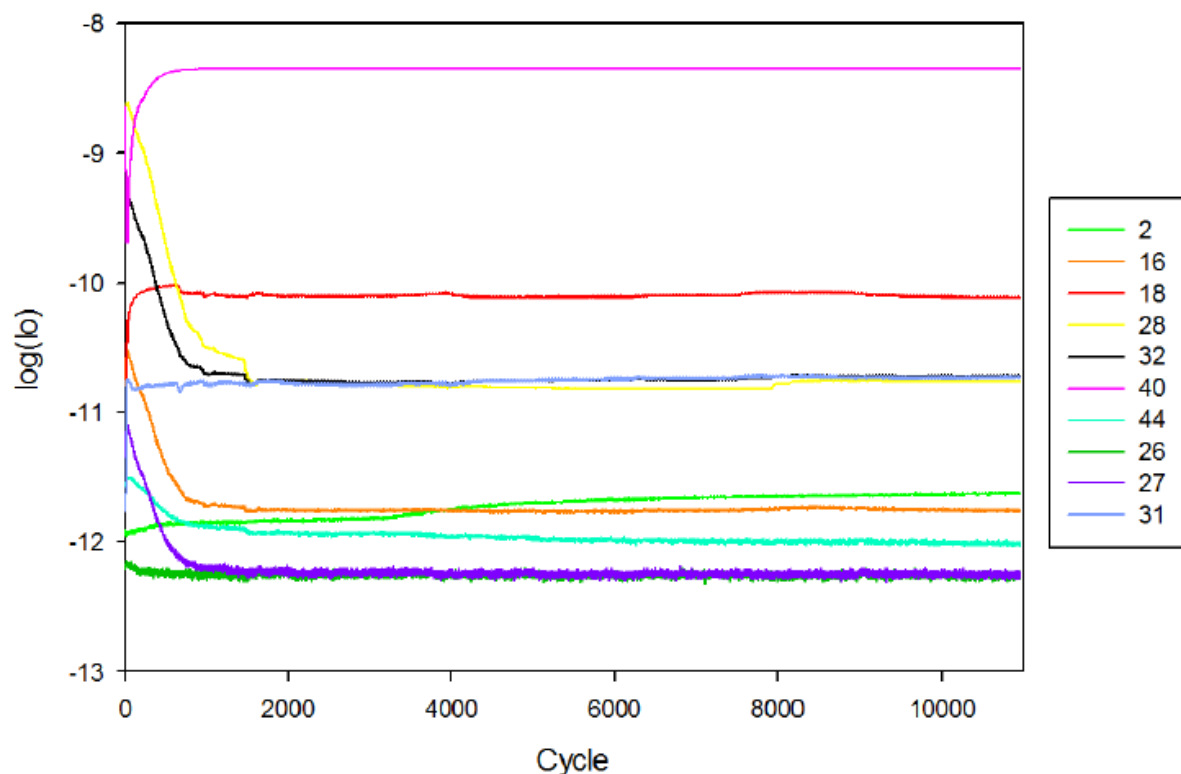


Figure 4.21. A plot of all the MS signals from experiment 10032011-2. Signal 2 is the signal for H_2 , signal 16 is the signal for O, signal 18 is the signal for H_2O , signal 28 is the signal for N_2 , signal 32 is the signal for O_2 , signal 40 is the signal for Ar, signal 44 is the signal for CO_2 , signal 31 is the signal for CH_3OH , and signal 26 and 27 is the signal for C_2H_2 .

Figure 4.21 shows the logarithmic MS signal for experiment 10032011-2. Signal 40 is the signal for Ar, and the signal that was going to be used to calculate the hydrogen evolution. As seen from the plot, there was not a big enough change in the Ar signal to be able to use these results in any calculations.

The reason for the poor hydrogen evolution is most likely the low intensity of the UV radiation, since most of the published articles on photocatalysis use UV lamps with 400 W or more (chapter 2.5) and the lamp used in this study only was 6.5 W. The size and design of the reactor could also affect the poor photoreforming results, since gas leakage was observed and an improvement in the results was obtained when the reactor was modified to a smaller volume. A different analysis method, like a gas chromatograph, could also make the activity calculations easier.

Since the results were so poor and the reactor setup not matched the expectations, not many experiments were conducted. However photoreforming was detected and hydrogen was produced, as seen in figure 4.22, even though the amounts were too small to use in any calculations.

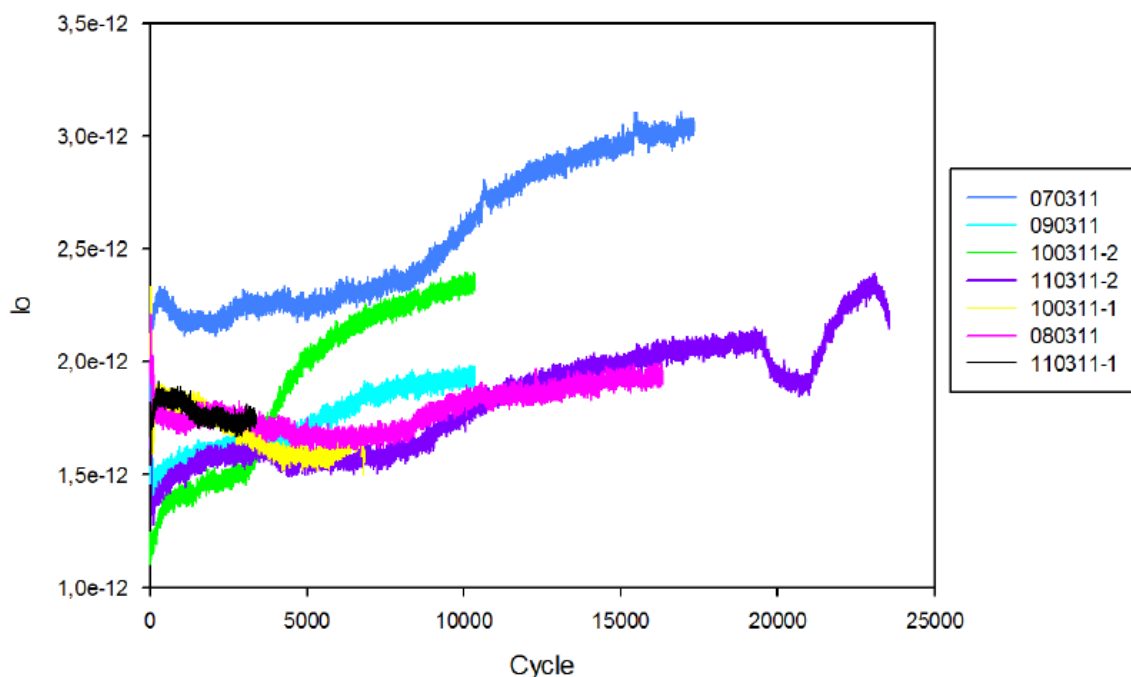


Figure 4.22. The MS signal for hydrogen from some of the photoreforming experiments.

Figure 4.22 displays the MS signal for hydrogen from some of the photoreforming experiments. In experiment 07032011 the lamp was turned on at cycle 5000, and there was no real response from the MS before the stirring was reduced from 880 rpm to 500 rpm giving the photocatalyst more time for irradiation.

Experiment 08032011 had higher catalyst concentration (0.5 g/l) but showed little hydrogen evolution. There was a small increase in the MS signal for hydrogen after the magnetic stirring was decreased from 880 rpm to 650 rpm (cycle 8000). Magnetic stirring below this value was not enough to stir the photocatalysts in the suspension. In this experiment the gas volume above the fluid in the reactor was quite big. This was reduced by experiment 09032011 and later experiments.

In experiment 09032011 the magnetic stirring was 650 rpm, the catalyst concentration was 1.0 g/l and the lamp was turned on at cycle 2800. In figure 4.22 the MS signal from this experiment shows some hydrogen evolution. In all the experiments discussed so far the Ar gas throughput was 20 ml/min.

Experiment 10032011-1 shows no response in the hydrogen signal, this is possibly because of a leakage in the reactor. The gas throughput was also very low in this experiment (8.5 ml/min); it could be the throughput was too low to carry the hydrogen out from the reactor. The catalyst concentration was also higher; 1.5 g/l, it could be the catalyst concentration was too high to let the UV photons irradiate the suspension. This also confirms the theory about too low UV radiation intensity.

The hydrogen evolution was much better in experiment 10032011-2. The lamp was turned on at cycle 2000. The catalyst used in this experiment was not the same as used in the previous experiments (photocatalyst 3, 10wt% CuO on P25), it was photocatalyst 2 with 5wt% CuO on

P25 with a concentration at 1.0 g/l. The gas throughput was also lower; 12.8 ml/min. There was leakage in this experiment also, even though the hydrogen signal from the MS showed the best hydrogen evolution rate in this experiment.

In experiment 11032011-1 the conditions was the same as in experiment 10032011-2, except the catalyst was changed to photocatalyst 7 with 10wt% CuO on anatase with high surface area. There was no response from the MS, and it was not possible to see any UV light through the suspension. It is possible the high surface anatase acts different in the suspension than P25, making it harder for the UV light to irradiate more of the suspension.

Experiment 11032011-2 shows how the hydrogen signal responds to changes in the gas throughput. The experimental parameters were the same as in experiment 09032011 except the gas throughput was only 12.8 ml/min. The Ar gas throughput was increased to 24 ml/min at cycle 19 400, and the MS signal for hydrogen decreased. This is logical since the MS signal depends on concentrations and not masses. The throughput was then decreased to 8.5 ml/min and the signal increased. This shows the gas throughput was not too low to carry the gases out of the reactor in experiment 10032011-1. At cycle 22 800 the lamp was turned off, and there was a clear drop in the MS signal. This shows there really was photocatalytic hydrogen production in the reactor.

4.2.1 Comparison of the photocatalysts

From the activity measurements it is hard to decide which photocatalyst had the best activity since so few experiments were done and the setup did not work as assumed. Photocatalyst 2 showed the faster photocatalytic rate than photocatalyst 3 from the experiments. However it is not certain this was because of the CuO loading or because the suspension with photocatalyst 2 was slightly less dark than with photocatalyst 3 making it easier for the UV light to irradiate the suspension. Gas leakage and other error parameters could also have inflicted the results.

From Sreethawong *et al.*'s report [49], the ideal surface area for CuO loaded TiO₂ was 60 m²/g for photoreforming of methanol. Photocatalyst 7 and 9 is closest to this value in BET surface area with 74 m²/g. It could therefore be assumed these samples would show higher photoactivity. From the theory (chapter 2.1) a higher dispersion of CuO would also be assumed to increase photoactivity, and photocatalyst 7 could then be assumed to show the best photoactivity of these two samples.

From the theory chapter the anatase crystallite size for all the samples except photocatalyst 5 and 6 is in the optimal crystallite range reported in chapter 2.5 (5 – 30 nm), and it can therefore be assumed photocatalyst 5 and 6 could provide lower photocatalytic activity than the others.

Ambrus *et al.* [29] claims higher anatase content gives better photoactivity, although they did not obtain as good activity as P25. This could suggest P25 really has a synergistic effect giving it a higher photoactivity. They also reported higher amorphous content gave lower photoactivity. The P25 photocatalysts in this study showed higher amorphous content than the anatase and rutile photocatalysts (chapter 4.1.4), and this could decrease the photoactivity of these photocatalysts. The P25 used in this study is not from the same supplier as in Ambrus *et*

al.'s study, so the phase content and photoactivity for the samples in this study might vary from their results. For the two photocatalysts with 10 wt% CuO on P25 (photocatalyst 3 and 10), photocatalyst 10 showed lower content of amorphous phase but also lower crystallinity. This is also the same result as for photocatalyst 7 which shows lower content of amorphous phase and lower crystallinity than the other anatase TiO₂ photocatalysts with 10 wt% CuO. Low amorphous content decrease the photoactivity, while high crystallinity increase the photoactivity.

It is very difficult to make assumptions on which photocatalysts would exhibit the highest photoactivity. Without any activity measurements it is hard to tell if pure anatase or P25 shows higher photoactivity. Photocatalyst 7 has both high dispersion and high surface area making this a good candidate, but has only anatase TiO₂ which makes it difficult to know for sure if makes this a better or poorer photocatalyst than P25 photocatalysts. There is also reported ideal CuO content of 10wt% and 1.5 wt%, so it is difficult to predict if photocatalyst 1 or 3 would show higher photoactivity.

The DP preparation method gives higher surface area and less amorphous phase than IWI, but it is also more easily reduced, has lower dispersion and crystallinity and higher band gap. The latter is assumed to influence the activity more than the small difference in surface area and band gap, and IWI photocatalysts is therefore assumed to obtain higher activity than DP photocatalysts.

5 Conclusion

The BET results showed calcination reduced the BET surface area, and the photocatalyst that was calcined twice had significantly lower surface area than the corresponding photocatalyst that was calcined once. It also showed the incipient wetness impregnation reduced the surface area more than the deposition precipitation method.

From the UV-visible spectrophotometry results it was clear that CuO loading decreased the band gap of TiO₂. This implies the CuO loaded TiO₂ catalysts can absorb a broader specter of the sunlight than pure TiO₂. The results also showed the band gap of P25 was higher than for pure anatase, which correspond to the synergetic effect theory. The DP preparation also increased the band gap compared to the IWI preparation. The band gap of the photocatalysts does not depend on surface area or crystallite size.

The TPO analysis showed that loading the sol-gel TiO₂ with Cu²⁺ decreased the burn off temperature of active carbon, so that the sol-gel could be calcined at the same temperature as the other photocatalysts and still burn off all the active carbon. The TPO analysis also showed the DP prepared photocatalysts are more easily reduced than IWI prepared photocatalysts.

The TPR, BET, EDS and XRD results indicate the CuO particles is deposited more on the surface with DP preparation and more in the pores with IWI preparation.

High surface area gives an overestimation of the CuO content in TPR analysis, and TPR is an inaccurate analysis method for determination of CuO content less than 10 wt%.

XRD scans show the photocatalysts with lowest content of amorphous phase also is the photocatalysts with lowest crystallinity. It also shows the DP preparation decrease the crystallinity of the photocatalyst and gave less amorphous copper phases than the IWI preparation method. The photocatalysts with larger surface area obtained smaller CuO crystallite size. P25 photocatalysts contain more amorphous phases than the anatase and rutile photocatalysts.

SEM images showed the difference in structure and surface area of the photocatalyst samples. The EDS images showed the dispersion of CuO particles was much better for samples with large surface area than for samples with low surface area. It also showed higher Cu content on the surface for samples with low surface area. The Cu atom% on the surface was higher with DP method than with IWI method, showing the CuO particles were more likely to be deposited in pores with IWI than with DP.

A gas with higher purity is needed for accurate chemisorption measurements, since bulk oxidation of the samples made the method less precise. The dispersion calculations from XRD analysis and chemisorption analysis can hardly be compared because of the uncertain chemisorption results.

Copper impregnation of sol-gel TiO₂ after carbon burn off gave higher dispersion, while carbon burn off after copper impregnation gave higher surface area. The active carbon affect CuO dispersion and increase CuO particle size.

To perform accurate and reliable activity measurements a significant improvement in the photoreforming setup is required. Higher intensity of the UV radiation, better designed photoreactor and a better analysis method is needed. The results presented in this study gives proof that photocatalytic H₂ production did take place, but not in big enough quanta to use the results in any activity calculations. A proper comparison of the photoactivity between the photocatalysts could therefore not be provided.

6 References

1. Grimes, C.A., O.K. Varghese, and S. Ranjan, *Light, Water, Hydrogen - The Solar Generation of Hydrogen by Water Photoelectrolysis*. 2008, Pennsylvania: Springer Science + Business Media.
2. Kudo, A. and Y. Miseki, *Heterogeneous photocatalyst materials for water splitting*. Chemical Society Reviews, 2009. **38**(1): p. 253-278.
3. Miller, E.L., *Solar Hydrogen Production by Photoelectrochemical Water Splitting: The Promise and Challenge*, in *On Solar Hydrogen & Nanotechnology*, L. Vayssieres, Editor. 2009, John Wiley & Sons (Asia) Pte Ltd: Clementi Loop.
4. Wu, G., *H₂ production with ultra-low CO selectivity via photocatalytic reforming of methanol on Au/TiO₂ catalyst*. International Journal of Hydrogen Energy, 2008. **33**(4): p. 1243-1251.
5. Ohtani, B., *Photocatalysis A to Z—What we know and what we do not know in a scientific sense*. Journal of Photochemistry and Photobiology C: Photochemistry Reviews, 2011.
6. Blanco, J., S. Malato, P. Fernández-Ibañez, D. Alarcón, W. Gernjak, and M.I. Maldonado, *Review of feasible solar energy applications to water processes*. Renewable and Sustainable Energy Reviews, 2009. **13**(6-7): p. 1437-1445.
7. Chiarello, G.L., E. Selli, and L. Forni, *Photocatalytic hydrogen production over flame spray pyrolysis-synthesised TiO₂ and Au/TiO₂*. Applied Catalysis B: Environmental, 2008. **84**(1-2): p. 332-339.
8. Bowker, M., P.R. Davies, and L.S. Al-Mazroai, *Photocatalytic Reforming of Glycerol over Gold and Palladium as an Alternative Fuel Source*. Catalysis Letters, 2008. **128**(3-4): p. 253-255.
9. Al-Mazroai, L., M. Bowker, P. Davies, A. Dickinson, J. Greaves, D. James, and L. Millard, *The photocatalytic reforming of methanol*. Catalysis Today, 2007. **122**(1-2): p. 46-50.
10. Ni, M., M. Leung, D. Leung, and K. Sumathy, *A review and recent developments in photocatalytic water-splitting using TiO₂/TiO₂ for hydrogen production*. Renewable and Sustainable Energy Reviews, 2007. **11**(3): p. 401-425.
11. Fujishima, A., X. Zhang, and D. Tryk, *TiO₂ photocatalysis and related surface phenomena*. Surface Science Reports, 2008. **63**(12): p. 515-582.
12. Bahruji, H., M. Bowker, P.R. Davies, L.S. Al-Mazroai, A. Dickinson, J. Greaves, D. James, L. Millard, and F. Pedrono, *Sustainable H₂ gas production by photocatalysis*. Journal of Photochemistry and Photobiology A: Chemistry, 2010.
13. Renz, C., *Lichtreaktionen der Oxyde des Titans, Cers und der Erdsäuren*. Helvetica Chimica Acta, 1921. **4**(1): p. 961-968.
14. Baur, E. and C. Neuweiler, *Über photolytische Bildung von Hydrperoxyd*. Helvetica Chimica Acta, 1927. **10**(1): p. 901-907.
15. Fujishima, A. and K. Honda, *Electrochemical Photolysis of Water at a Semiconductor Electrode*. Letters to nature, 1972. **238**: p. 37-38.
16. Jeon, M.-K., J.-W. Park, and M. Kang, *hydrogen production from methanol/water decomposition in a liquid photosystem using the anatase and rutile forms of Cu-TiO₂*. Journal of Industrial and Engineering Chemistry, 2006. **13**(1): p. 84-91.
17. Matsuoka, M., M. Kitano, M. Takeuchi, K. Tsujimaru, M. Anpo, and J. Thomas, *Photocatalysis for new energy production; Recent advances in photocatalytic water splitting reactions for hydrogen production*. Catalysis Today, 2007. **122**(1-2): p. 51-61.

18. Xu, S. and D.D. Sun, *Significant improvement of photocatalytic hydrogen generation rate over TiO₂ with deposited CuO*. International Journal of Hydrogen Energy, 2009. **34**(15): p. 6096-6104.
19. Choi, H. and M. Kang, *Hydrogen production from methanol/water decomposition in a liquid photosystem using the anatase structure of Cu loaded TiO₂*. International Journal of Hydrogen Energy, 2007. **32**(16): p. 3841-3848.
20. Wang, C.M., A. Heller, and H. Gerischer, *Palladium catalysis of O₂ reduction by electrons accumulated on TiO₂ particles during photoassisted oxidation of organic compounds*. Journal of the American Chemical Society, 1992. **114**(13): p. 5230-5234.
21. Chiarello, G.L., L. Forni, and E. Selli, *Photocatalytic hydrogen production by liquid- and gas-phase reforming of CH₃OH over flame-made TiO₂ and Au/TiO₂*. Catalysis Today, 2009. **144**(1-2): p. 69-74.
22. Wu, N., *Enhanced TiO₂ photocatalysis by Cu in hydrogen production from aqueous methanol solution*. International Journal of Hydrogen Energy, 2004. **29**(15): p. 1601-1605.
23. Gombac, V., L. Sordelli, T. Montini, J.J. Delgado, A. Adamski, G. Adami, M. Cargnello, S. Bernal, and P. Fornasiero, *CuOx-TiO₂ Photocatalysts for H₂ Production from Ethanol and Glycerol Solutions*. Journal of Physical Chemistry, 2010. **114**: p. 3916-3925.
24. Patsoura, A., D.I. Kondarides, and X.E. Verykios, *Photocatalytic degradation of organic pollutants with simultaneous production of hydrogen*. Catalysis Today, 2007. **124**: p. 94-102.
25. Yan, J.-h., M.-h. Yao, L. Zhang, Y.-g. Tang, and H.-h. Yang, *Photocatalytic H₂ evolution activity of CuO/ZrO₂ composite catalyst under simulated sunlight irradiation*. Journal of Central South University of Technology, 2011. **18**(1): p. 56-62.
26. Karunakaran, C. and R. Dhanalakshmi, *Selectivity in photocatalysis by particulate semiconductors*. Central European Journal of Chemistry, 2008. **7**(1): p. 134-137.
27. Xin, B., *Effect of surface species on Cu-TiO₂ photocatalytic activity*. Applied Surface Science, 2008. **254**(9): p. 2569-2574.
28. Skoog, D.A., D.M. West, F.J. Holler, and S.R. Crouch, *Fundamentals of Analytical Chemistry*. 8th ed. 2004: Brooks/Cole - Thomson Learning.
29. Ambrus, Z., K. Mogyorósi, Á. Szalai, T. Alapi, K. Demeter, A. Dombi, and P. Sipos, *Low temperature synthesis, characterization and substrate-dependent photocatalytic activity of nanocrystalline TiO₂ with tailor-made rutile to anatase ratio*. Applied Catalysis A: General, 2008. **340**(2): p. 153-161.
30. Ohno, T., K. Sarukawa, K. Tokieda, and M. Matsumura, *Morphology of a TiO₂ Photocatalyst (Degussa, P-25) Consisting of Anatase and Rutile Crystalline Phases*. Journal of Catalysis, 2001. **203**(1): p. 82-86.
31. Ryu, J. and W. Choi, *Substrate-Specific Photocatalytic Activities of TiO₂ and Multiactivity Test for Water Treatment Application*. Environmental Science & Technology, 2008. **42**(1): p. 294-300.
32. Ohtani, B., O.O. Prieto-Mahaney, D. Li, and R. Abe, *What is Degussa (Evonik) P25? Crystalline composition analysis, reconstruction from isolated pure particles and photocatalytic activity test*. Journal of Photochemistry and Photobiology A: Chemistry, 2010. **216**(2-3): p. 179-182.
33. Porter, J.F., Y.-G. Li, and C.K. Chan, *The effect of calcination on the microstructural characteristics and photoreactivity of Degussa P-25 TiO₂*. Journal of Materials Science, 1999. **34**(7): p. 1523-1531.
34. Ikeda, M., Y. Kusumoto, S. Somekawa, P. Ngweniform, and B. Ahmmad, *Effect of graphite silica on TiO₂ photocatalysis in hydrogen production from water-methanol*

- solution*. Journal of Photochemistry and Photobiology A: Chemistry, 2006. **184**(3): p. 306-312.
35. Bando, K.K., K. Sayama, H. Kusama, K. Okabe, and H. Arakawa, *In-situ FT-IR study on CO₂ hydrogenation over Cu catalysts supported on SiO₂, Al₂O₃, and TiO₂*. Applied Catalysis A: General, 1997. **165**: p. 391-409.
 36. Guerrero, S., I. Guzmán, G. Aguila, and P. Araya, *Sodium-promoted NO adsorption under lean conditions over Cu/TiO₂ catalysts*. Catalysis Communications, 2009. **11**(1): p. 38-42.
 37. Kustov, A.L., S.B. Rasmussen, R. Fehrmann, and P. Simonsen, *Activity and deactivation of sulphated TiO₂- and ZrO₂-based V, Cu, and Fe oxide catalysts for NO abatement in alkali containing flue gases*. Applied Catalysis B: Environmental, 2007. **76**(1-2): p. 9-14.
 38. Li, L., Z. Xu, F. Liu, Y. Shao, J. Wang, H. Wan, and S. Zheng, *Photocatalytic nitrate reduction over Pt-Cu/TiO₂ catalysts with benzene as hole scavenger*. Journal of Photochemistry and Photobiology A: Chemistry, 2010. **212**(2-3): p. 113-121.
 39. Gao, W., J. Chen, X. Guan, R. Jin, F. Zhang, and N. Guan, *Catalytic reduction of nitrite ions in drinking water over Pd-Cu/TiO₂ bimetallic catalyst*. Catalysis Today, 2004. **93-95**: p. 333-339.
 40. Arana, J., A. Penaalonso, J. Donarodriguez, J. Herreramelian, O. Gonzalezdiaz, and J. Perezpena, *Comparative study of MTBE photocatalytic degradation with TiO₂ and Cu-TiO₂*. Applied Catalysis B: Environmental, 2008. **78**(3-4): p. 355-363.
 41. Carvalho, H.W.P., A.P.L. Batista, P. Hammer, and T.C. Ramalho, *Photocatalytic degradation of methylene blue by TiO₂-Cu thin films: Theoretical and experimental study*. Journal of Hazardous Materials, 2010. **184**(1-3): p. 273-280.
 42. Ou, T.-C., F.-W. Chang, and L.S. Roselin, *Production of hydrogen via partial oxidation of methanol over bimetallic Au-Cu/TiO₂ catalysts*. Journal of Molecular Catalysis A: Chemical, 2008. **293**(1-2): p. 8-16.
 43. Li, Y., W.-N. Wang, Z. Zhan, M.-H. Woo, C.-Y. Wu, and P. Biswas, *Photocatalytic reduction of CO₂ with H₂O on mesoporous silica supported Cu/TiO₂ catalysts*. Applied Catalysis B: Environmental, 2010. **100**(1-2): p. 386-392.
 44. Ondok, V., J. Musil, M. Meissner, R. Čerstvý, and K. Fajfrlík, *Two-functional DC sputtered Cu-containing TiO₂ thin films*. Journal of Photochemistry and Photobiology A: Chemistry, 2010. **209**(2-3): p. 158-162.
 45. Karunakaran, C., G. Abiramasundari, P. Gomathisankar, G. Manikandan, and V. Anandi, *Cu-doped TiO₂ nanoparticles for photocatalytic disinfection of bacteria under visible light*. Journal of Colloid and Interface Science, 2010. **352**(1): p. 68-74.
 46. Colon, G., M. Maicu, M. Hidalgo, and J. Navio, *Cu-doped TiO₂ systems with improved photocatalytic activity*. Applied Catalysis B: Environmental, 2006. **67**(1-2): p. 41-51.
 47. Vaseem, M., A. Umar, Y.B. Hahn, D.H. Kim, K.S. Lee, J.S. Jang, and J.S. Lee, *Flower-shaped CuO nanostructures: Structural, photocatalytic and XANES studies*. Catalysis Communications, 2008. **10**(1): p. 11-16.
 48. Galinska, A. and J. Walendziewski, *Photocatalytic Water Splitting over Pt-TiO₂ in the Presence of Sacrificial Reagents*. Energy & Fuels, 2005. **19**(3): p. 1143-1147.
 49. Sreethawong, T. and S. Yoshikawa, *Comparative investigation on photocatalytic hydrogen evolution over Cu-, Pd-, and Au-loaded mesoporous TiO₂ photocatalysts*. Catalysis Communications, 2005. **6**(10): p. 661-668.
 50. Xu, S., J. Ng, X. Zhang, H. Bai, and D.D. Sun, *Fabrication and comparison of highly efficient Cu incorporated TiO₂ photocatalyst for hydrogen generation from water*. International Journal of Hydrogen Energy, 2010. **35**(11): p. 5254-5261.

51. Dhanalakshmi, K.B., S. Latha, S. Anandan, and P. Maruthamuthu, *Dye sensitized hydrogen evolution from water*. International Journal of Hydrogen Energy, 2001. **26**(7): p. 669-674.
52. Yu, J., Y. Hai, and M. Jaroniec, *Photocatalytic hydrogen production over CuO-modified titania*. Journal of colloid and interface science, 2011. **357**(1): p. 223-8.
53. Bandara, J., C.P.K. Udawatta, and C.S.K. Rajapakse, *Highly stable CuO incorporated TiO₂ catalyst for photocatalytic hydrogen production from H₂O*. Photochemical & Photobiological Sciences 2005. **4**(11): p. 857-861.
54. Marceau, E., X. Carrier, and M. Che, *Impregnation and Drying*, in *Synthesis of Solid Catalysts*, K.P.d. Jong, Editor. 2009, Wiley-VCH.
55. Ko, E.I., *Sol-Gel Process*, in *Preparation of solid catalysts*, G. Ertl, H. Knözinger, and J. Weitkamp, Editors. 1999, Wiley-VCH Verlag GmbH: Weinheim.
56. Colón, G., M.C. Hidalgo, and J.A. Navío, *A novel preparation of high surface area TiO₂ nanoparticles from alkoxide precursor and using active carbon as additive*. Catalysis Today, 2002. **76**: p. 91-101.
57. Schüth, F. and K. Unger, *Precipitation and Coprecipitation*, in *Preparation of solid catalysts*, G. Ertl, H. Knözinger, and J. Weitkamp, Editors. 1999, Wiley-VCH Verlag GmbH: Weinheim.
58. Grift, C.J.G.V.d., P.A. Elberse, A. Mulder, and J.W. Geus, *Preparation of silica-supported copper catalysts by means of deposition-precipitation*. Applied Catalysis, 1990. **59**(1): p. 275-289.
59. Schubert, U. and N. Hüsing, *Synthesis of Inorganic Materials*. 2nd ed. 2005: Wiley-VCH.
60. Merriam-Webster, in *Merriam-Webster's collegiate dictionary*. 2004, Merriam-Webster, Incorporated.
61. Lind, A., *Lecture notes in HES intro-course in catalysis 2010: Calcination and Spray Drying*. 2010, Norwegian University of Science and Technology: Trondheim.
62. Chorkendorff, I. and J.W. Niemantsverdriet, *Concepts of Modern Catalysis and Kinetics*. 2nd ed. 2007: Wiley-VCH Verlag GmbH & Co. KGaA.
63. Vannice, M.A., *Kinetics of Catalytic Reactions*. Vol. 9. 2005: Springer Science+Business Media Inc.
64. Holmen, A., *Heterogen Katalyse*: Institutt for kjemisk prosessteknologi, NTNU.
65. Rothenberg, G., *Catalysis: Concepts and Green Applications*. 2008: Wiley-VCH Verlag GmbH & Co. KGaA.
66. Calvert, J.G. and J.N. Pitts, *Photochemistry*. 1966: Wiley. 899.
67. Skoog, D.A., D.M. West, F.J. Holler, and S.R. Crouch, *Fundamentals of Analytical Chemistry*. 8th ed, ed. S. Kiselica. 2004, Belmont: Thomson Learning, Inc, Brooks/Cole. 1019.
68. Barton, D.G., M. Shtein, R.D. Wilson, S.L. Soled, and E. Iglesia, *Structure and Electronic Properties of Solid Acids Based on Tungsten Oxide Nanostructures*. Journal of physical Chemistry B, 1999. **103**: p. 630-640.
69. Wang, L., G. Liang, and G. Dang, *A study on the protection to relics and the related problems with diffuse reflectance spectroscopy*. Spectrochimica Acta Part A: Molecular and Biomolecular Spectroscopy, 2005. **61**(5): p. 1021-1024.
70. Dragsten, K., *Lecture notes in HES intro-course in catalysis 2010: Thermal analysis TGA, DSC, DTA*. 2010, Norwegian University of Science and Technology: Trondheim.
71. Blake, A.J., W. Clegg, J.M. Cole, J.S.O. Evans, P. Main, S. Parsons, and D.J. Watkin, *Crystal Structure Analysis, Principle and Practice*. 2nd ed. IUCr Texts on Crystallography, ed. W. Clegg. 2009, New York: Oxford University Press.

72. Huber, F., Z. Yu, S. Lögdberg, M. Rønning, D. Chen, H. Venvik, and A. Holmen, *Remarks on the passivation of reduced Cu-, Ni-, Fe-, Co-based catalysts*. Catalysis Letters, 2006. **110**(3-4): p. 211-220.
73. Rioux, R.M. and M.A. Vannice, *Hydrogenation/dehydrogenation reactions: isopropanol dehydrogenation over copper catalysts*. Journal of Catalysis, 2003. **216**(1-2): p. 362-376.
74. Reimer, L., *Scanning Electron Microscopy Physics of Image Formation and Microanalysis*. 2nd ed, ed. H.K.V. Lotsch. 1998, Heidelberg: Springer-Verlag Berlin.
75. Goldstein, J., D. Newbury, D. Joy, C. Lyman, P. Echlin, E. Lifshin, L. Sawyer, and J. Michael, *Scanning Electron Microscopy and X-Ray Microanalysis*. 3rd ed. Vol. 1. 2003: Springer.
76. Garratt-Reed, A.J. and D.C. Bell, *Energy-dispersive X-ray Analysis in the Electron Microscope*. 2003, Oxford: BIOS Scientific Publishers Limited.
77. Ma, J., C. Park, N.M. Rodriguez, and R.T.K. Baker, *Characteristics of Copper Particles Supported on Various Types of Graphite Nanofibers*. The Journal of Physical Chemistry B, 2001. **105**(48): p. 11994–12002.
78. Jensen and J., *An improved N2O-method for measuring Cu-dispersion*. Applied Catalysis A: General, 2004. **266**(1): p. 117-122.
79. Sato and S., *Distinction between Surface and Bulk Oxidation of Cu through N2O Decomposition*. Journal of Catalysis, 2000. **196**(1): p. 195-199.
80. Rønning, M., N.E. Tsakoumis, A. Voronov, R.E. Johnsen, P. Norby, W.v. Beek, Ø. Borg, E. Rytter, and A. Holmen, *Combined XRD and XANES studies of a re-promoted Co/ γ -Al₂O₃ catalyst at Fischer-Tropsch synthesis conditions*. Catalysis Today, 2009.
81. Ebbing, D.D. and S.D. Gammon, *States of Matter; Liquids and Solids*, in *General Chemistry*. 2011, Brooks/Cole, Cengage Learning. p. 418-478.
82. Egerton, T.A., R.W. Harrison, S.E. Hill, J.A. Mattinson, and H. Purnama, *Effects of particle dispersion on the measurement of semi-conductor photocatalytic activity*. Journal of Photochemistry and Photobiology A: Chemistry, 2010. **216**(2-3): p. 268-274.
83. Daskalaki, V.M. and D.I. Kondarides, *Efficient production of hydrogen by photo-induced reforming of glycerol at ambient conditions*. Catalysis Today, 2009. **144**(1-2): p. 75-80.
84. Rivera, A.P., K. Tanaka, and T. Hisanaga, *Photocatalytic degradation of pollutant over TiO₂ in different crystal structures*. Applied Catalysis B: Environmental, 1993. **3**(1): p. 37-44.
85. Chen, D. and A.K. Ray, *Photodegradation kinetics of 4-nitrophenol in TiO₂ suspension*. Water research, 1998. **32**(11): p. 3223-3234.
86. Miwa, T., S. Kaneco, H. Katsumata, T. Suzuki, K. Ohta, S. Chand Verma, and K. Sugihara, *Photocatalytic hydrogen production from aqueous methanol solution with CuO/Al₂O₃/TiO₂ nanocomposite*. International Journal of Hydrogen Energy, 2010. **35**(13): p. 6554-6560.
87. Korzhak, A.V., N.I. Ermokhina, A.L. Stroyuk, V.K. Bukhtiyarov, A.E. Raevskaya, V.I. Litvin, S.Y. Kuchmiy, V.G. Ilyin, and P.A. Manorik, *Photocatalytic hydrogen evolution over mesoporous TiO₂/metal nanocomposites* Journal of Photochemistry and Photobiology A: Chemistry, 2008. **198**(2-3): p. 126-134.
88. Kim, D.S. and S.-Y. Kwak, *The hydrothermal synthesis of mesoporous TiO₂ with high crystallinity, thermal stability, large surface area, and enhanced photocatalytic activity*. Applied Catalysis A: General, 2007. **323**: p. 110-118.

89. Inagaki, M., R. Nonaka, B. Tryba, and A.W. Morawski, *Dependence of photocatalytic activity of anatase powders on their crystallinity*. *Chemosphere*, 2006. **64**(3): p. 437-45.
90. Shapovalov, V.I., *Nanopowders and films of titanium oxide for photocatalysis: A review*. *Glass Physics and Chemistry*, 2010. **36**(2): p. 121-157.
91. Maira, A.J., K.L. Yeung, C.Y. Lee, P.L. Yue, and C.K. Chan, *Size effects in Gas-Phase Photo-oxidation of Trichloroethylene Using Nanometer-Sized TiO₂ Catalysts*. *Journal of Catalysis*, 2000. **192**: p. 185-196.
92. Wang, C.-C., Z. Zhang, and J.Y. Ying, *Photocatalytic decomposition of halogenated organics over nanocrystalline titania*. *Nanostructured Materials*, 1997. **9**(1-8): p. 583-586.
93. Xu, N., Z. Shi, Y. Fan, J. Dong, J. Shi, and M.Z.-C. Hu, *Effects of Particle Size of TiO₂ on Photocatalytic Degradation of Methylene Blue in Aqueous Suspensions*. *Industrial & Engineering Chemistry Research*, 1999. **38**(2): p. 373-379.
94. Aylward, G. and T. Findlay, *SI Chemical Data*. 5th ed. 2002: John Wiley & Sons Australia.
95. Sakthivel, S., M.V. Shankar, M. Palanichamy, B. Arabindoo, D.W. Bahnemann, and V. Murugesan, *Enhancement of photocatalytic activity by metal deposition: characterisation and photonic efficiency of Pt, Au and Pd deposited on TiO₂ catalyst*. *Water research*, 2004. **38**: p. 3001 - 3008
96. Hammer, N., *PhD, Chemisorption - mail*, I.L. Bjørnstad, Editor. 2011: Trondheim.
97. Rioux, R., *Hydrogenation/dehydrogenation reactions: isopropanol dehydrogenation over copper catalysts*. *Journal of Catalysis*, 2003. **216**(1-2): p. 362-376.

List of appendices

Appendix 1	Preparation calculations
Appendix 2	pH values during DP preparation method
Appendix 3	UV/vis calculations and plots
Appendix 4	TPO plots
Appendix 5	TPR calculations and plots
Appendix 6	XRD calculations and plots
Appendix 7	MS calibration for activity measurements
Appendix 8	Chemisorption calculations and plots
Appendix 9	Dispersion comparison calculations
Appendix 10	Heat of reaction calculations
Appendix 11	Hazardous activity identification
Appendix 12	Risk assessment
Appendix 13	HSE action plan
Appendix 14	Material Safety Data Sheets

APPENDIX

Appendix 1 – Preparation calculations

Total amount of photocatalyst: 5 g

Desired CuO content: 10 wt%

Mass $\text{Cu}(\text{NO}_3)_2 \cdot 3\text{H}_2\text{O}$:

$$m_{\text{Cu}(\text{NO}_3)_2} = \frac{5\text{g} \times 10\% \times M_{\text{Cu}(\text{NO}_3)_2}}{100\% \times M_{\text{CuO}}} = \frac{5\text{g} \times 10\% \times 241.6\text{g/mol}}{100\% \times 79.5\text{g/mol}} = 1.52\text{g}$$

Mass TiO_2 :

$$m_{\text{TiO}_2} = \frac{5\text{g} \times 90\%}{100\%} = 4.5\text{g}$$

IWI:

Mass water: incipient wetness point * m_{TiO_2}

DP:

Mass urea:

$$m_{\text{urea}} = \frac{m_{\text{Cu}(\text{NO}_3)_2} \times M_{\text{urea}}}{M_{\text{Cu}(\text{NO}_3)_2}} = \frac{1.52\text{g} \times 5 \times 60.1\text{g/mol}}{241.6\text{g/mol}} = 1.9\text{g}$$

Sol-gel:

Concentration TiP:

$$C = \frac{\text{vol}\% \text{Ti} \times \rho}{M_{\text{TiP}}} = \frac{97\text{l} \times 960\text{g/l}}{100\text{l} \times 284.22\text{g/mol}} = 3.28\text{M}$$

Volume TiP:

$$V_{\text{TiP}} = \frac{m_{\text{TiO}_2}}{C \times M_{\text{TiO}_2}} = \frac{4.5\text{g}}{3.28\text{M} \times 79.87\text{g/mol}} = 0.017\text{l}$$

Volume ethanol:

$$V_{\text{TiO}_2} = 3 \times V_{\text{TiP}} = 51\text{ml}$$

Mass carbon:

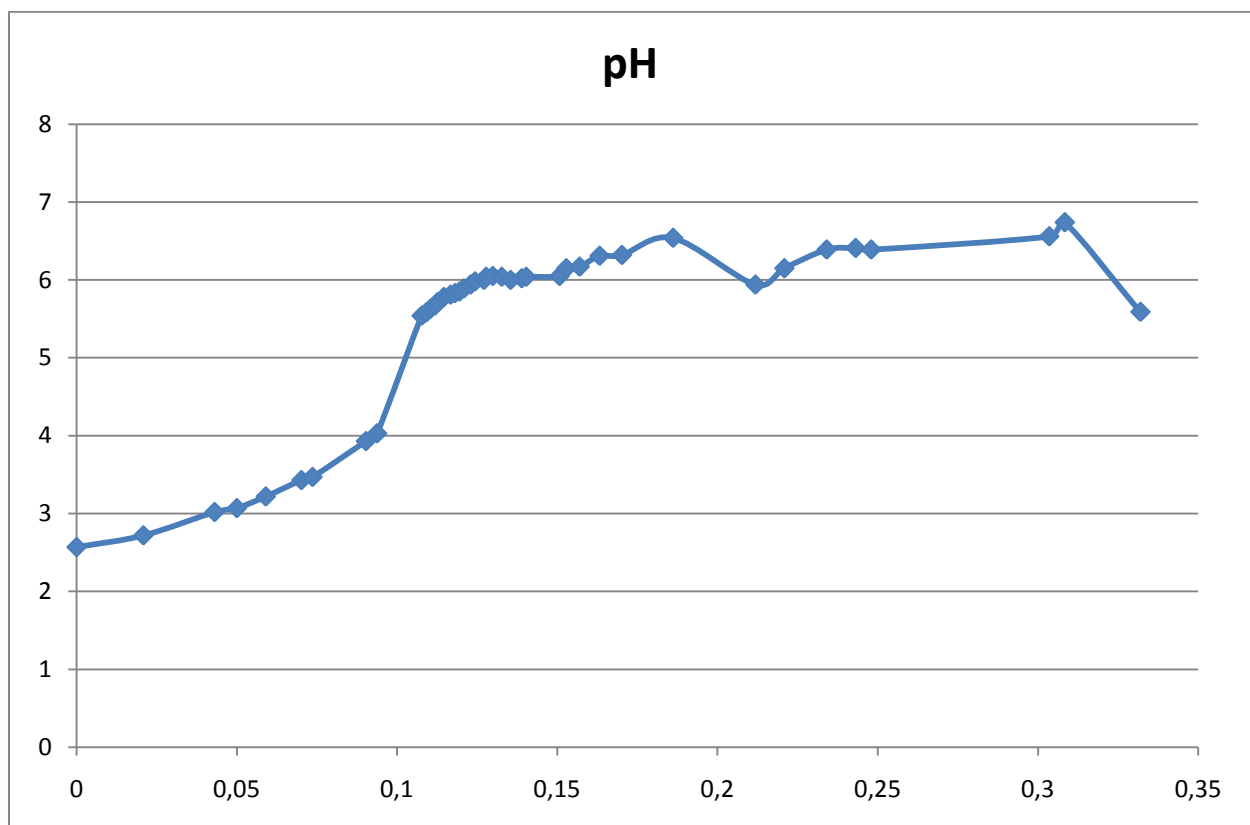
$$m_{\text{total}} = \frac{m_{\text{TiO}_2}}{0.8} = \frac{4.5\text{g}}{0.8} = 5.625\text{g}$$

$$m_{\text{carbon}} = 5.625\text{g} - 4.5\text{g} = 1.125\text{g}$$

Appendix 2 – Deposition Precipitation preparation pH

Tid	pH	Temperatur
0	2,57	20
00:30	2,72	43,7
01:02	3,02	70,7
01:12	3,07	75,6
01:25	3,22	80,2
01:41	3,43	83,9
01:46	3,47	84,5
02:10	3,93	86,2
02:15	4,03	86,3
02:35	5,54	86,6
02:37	5,58	86,7
02:39	5,63	86,7
02:41	5,67	86,7
02:42	5,71	86,8
02:45	5,78	86,8
02:48	5,81	86,7
02:50	5,83	86,7
02:52	5,85	86,7
02:54	5,89	86,7
02:57	5,94	86,8
02:59	5,98	86,8
03:03	6	86,9

Tid	pH	Temperatur
03:04	6,04	86,9
03:07	6,05	87,1
03:11	6,04	87,2
03:15	6	87,5
03:20	6,02	87,8
03:22	6,04	87,8
03:37	6,05	88,4
03:40	6,15	88,5
03:46	6,17	88,5
03:55	6,31	88,6
04:05	6,32	88,6
04:28	6,54	89
05:05	5,94	87,3
05:18	6,15	87,6
05:37	6,39	87,7
05:50	6,41	87,5
05:57	6,39	87,5
07:17	6,56	86,7
07:24	6,74	86,6
07:58	5,59	86,7
22:05	7,32	86,3
00:00	7,37	84,8



Appendix 3 – UV/Vis calculations and plots

The reflectance spectras were converted with the Kubelka-Munk function:

$$R_{\infty} = \frac{R_{sample}}{R_{reference}}$$
$$F(R_{\infty}) = \frac{(1 - R_{\infty})^2}{2R_{\infty}} = \frac{\alpha}{S}$$
$$\alpha \propto \frac{(h\nu - E_0)^n}{h\nu}$$

The reflectance reference used was BaSO₄. Figure 1 shows the reflectance spectra for sample 4, while figure 2 shows the converted Kubelka-Munk absorption spectra.

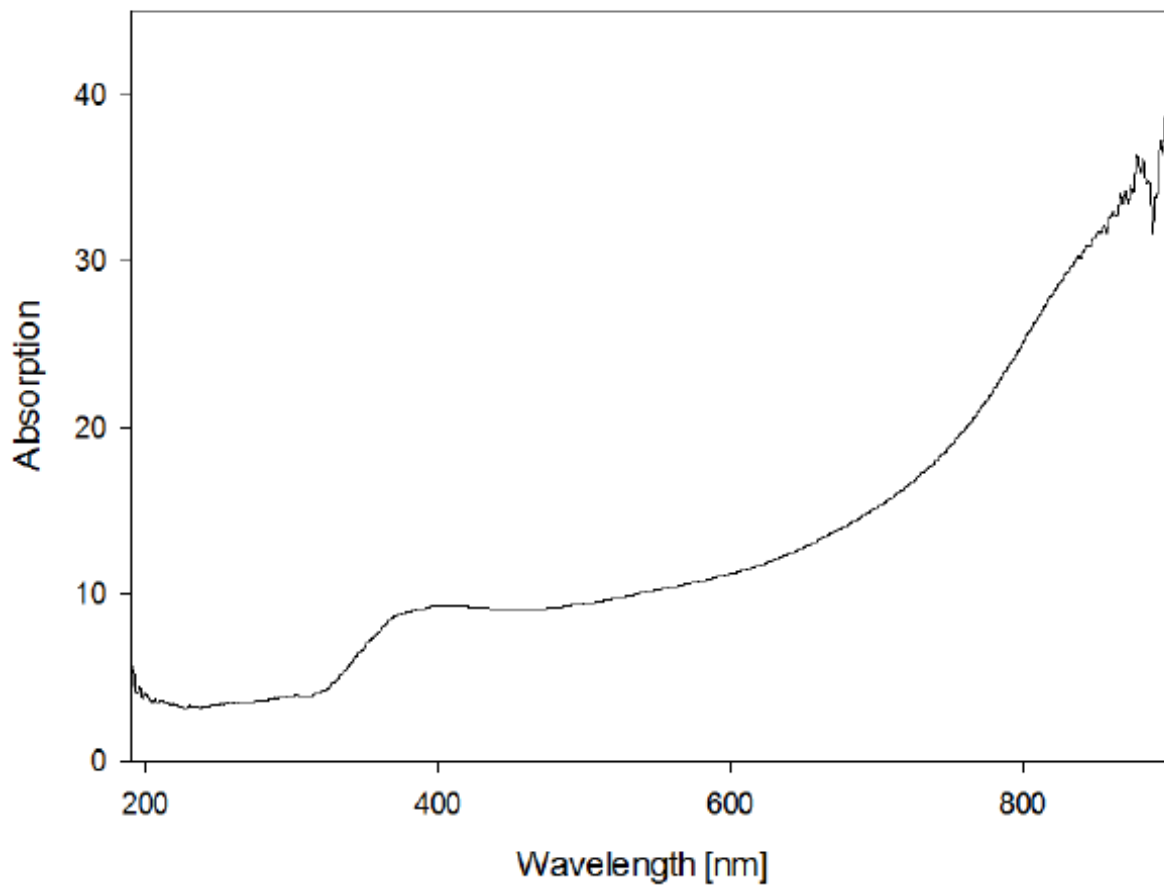


Figure 1. Reflectance spectra of sample 4.

Appendix 3 - UV/Vis calculations and plots

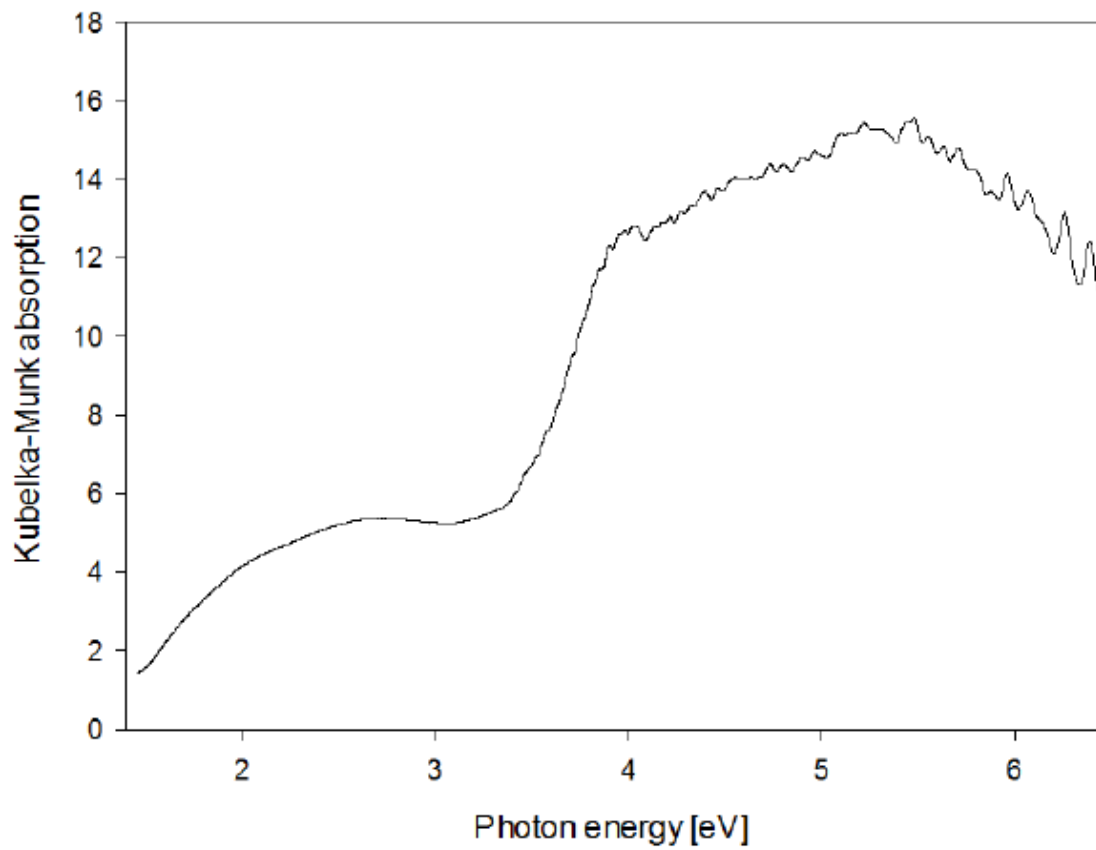


Figure 2. Kubelka-Munk absorption spectra for sample 4.

Figure 3 shows the extrapolated linear part of the Kubelka-Munk absorption curve, and the corresponding absorption edge value.

Appendix 3 - UV/Vis calculations and plots

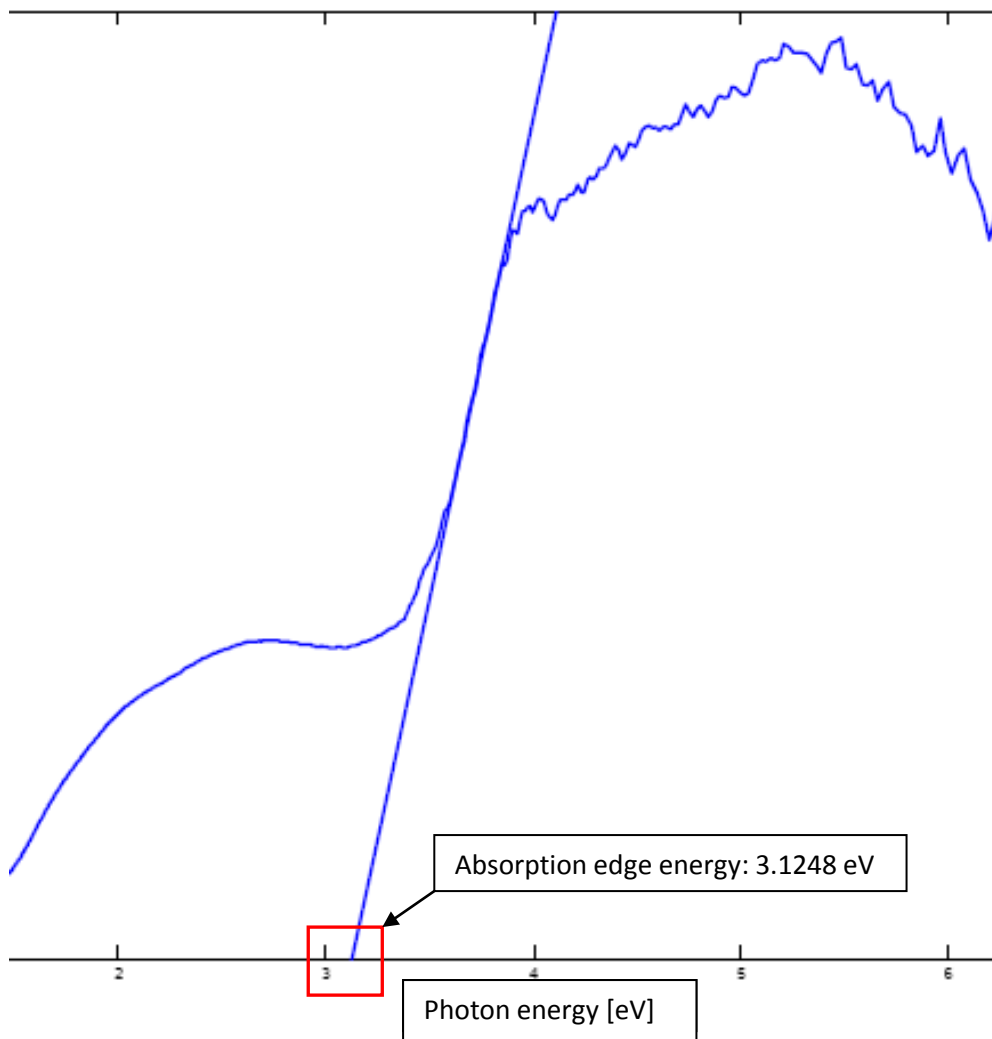
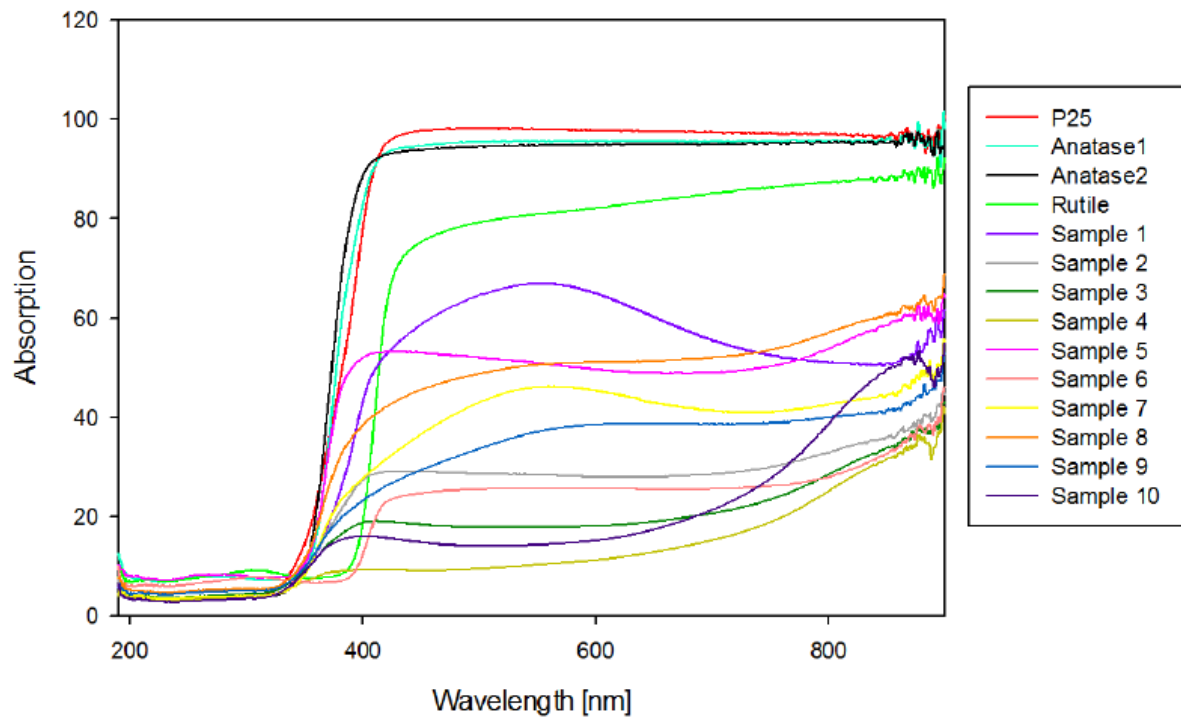


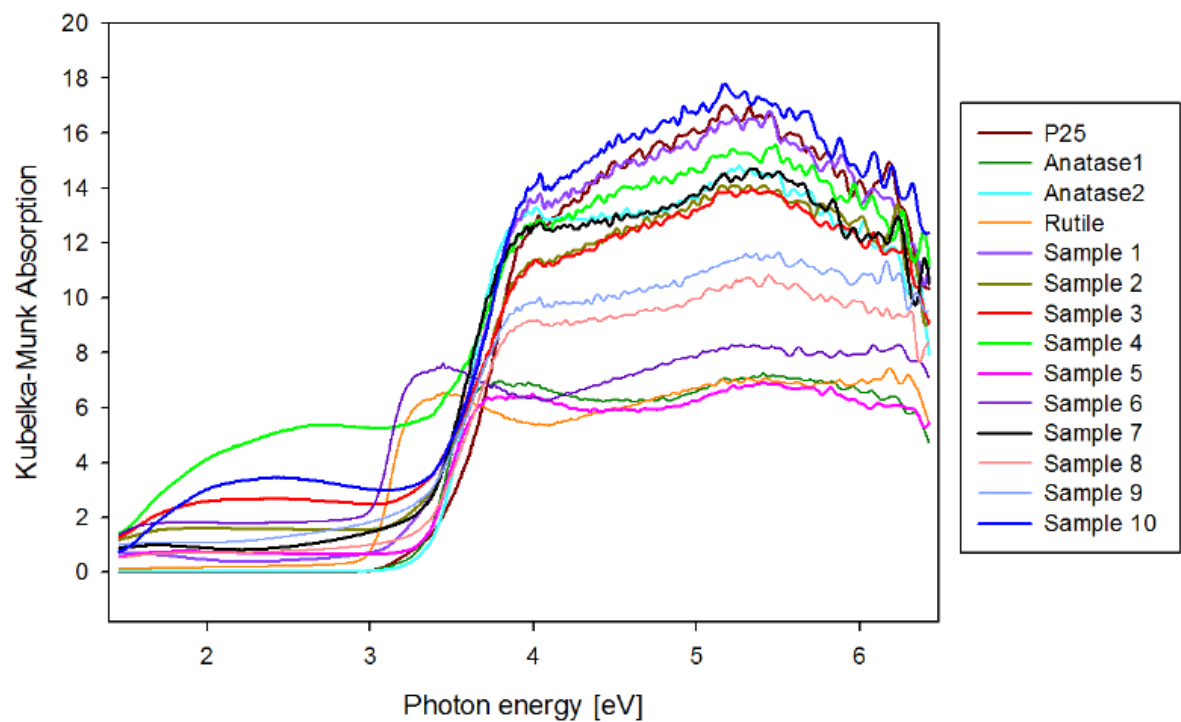
Figure 3. Kubelka-Munk absorption with an extrapolated line through the linear part of the plot, showing the absorption edge value.

Appendix 3 - UV/Vis calculations and plots

All the reflectance spectras:

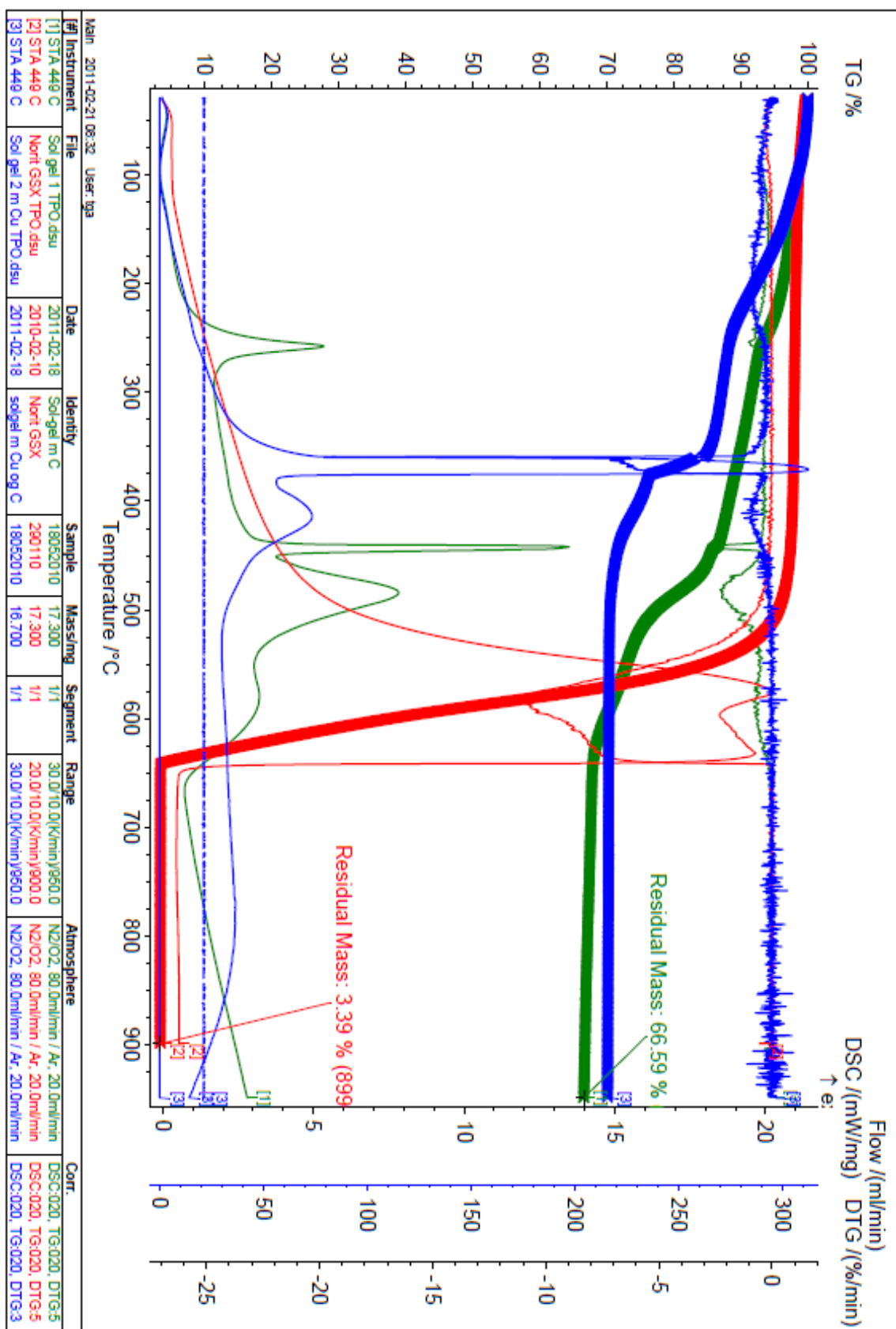


All the kubelka-munk functions:



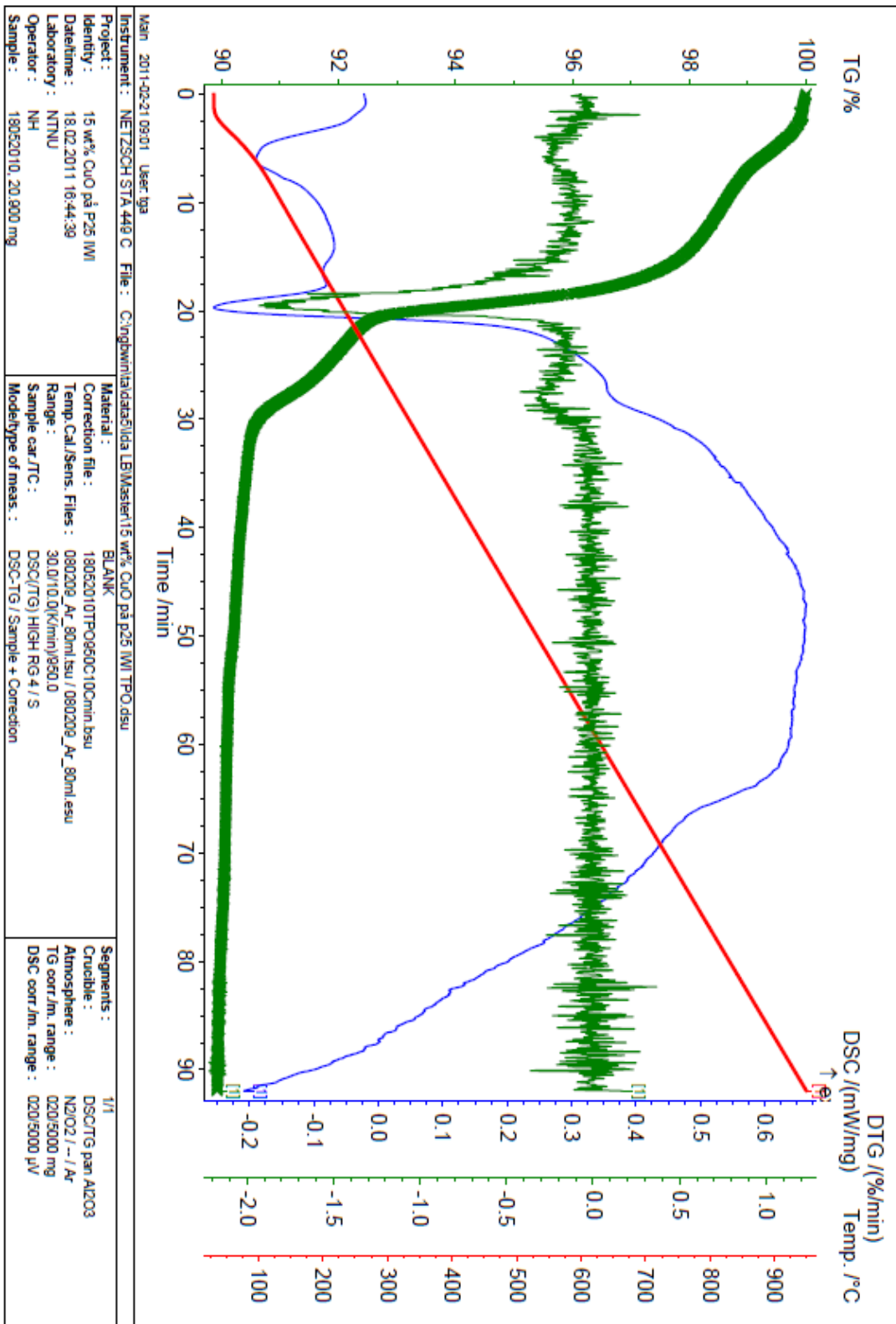
Appendix 4 - TPO plots

Green: sample 8, blue: sample 9, red: pure active carbon



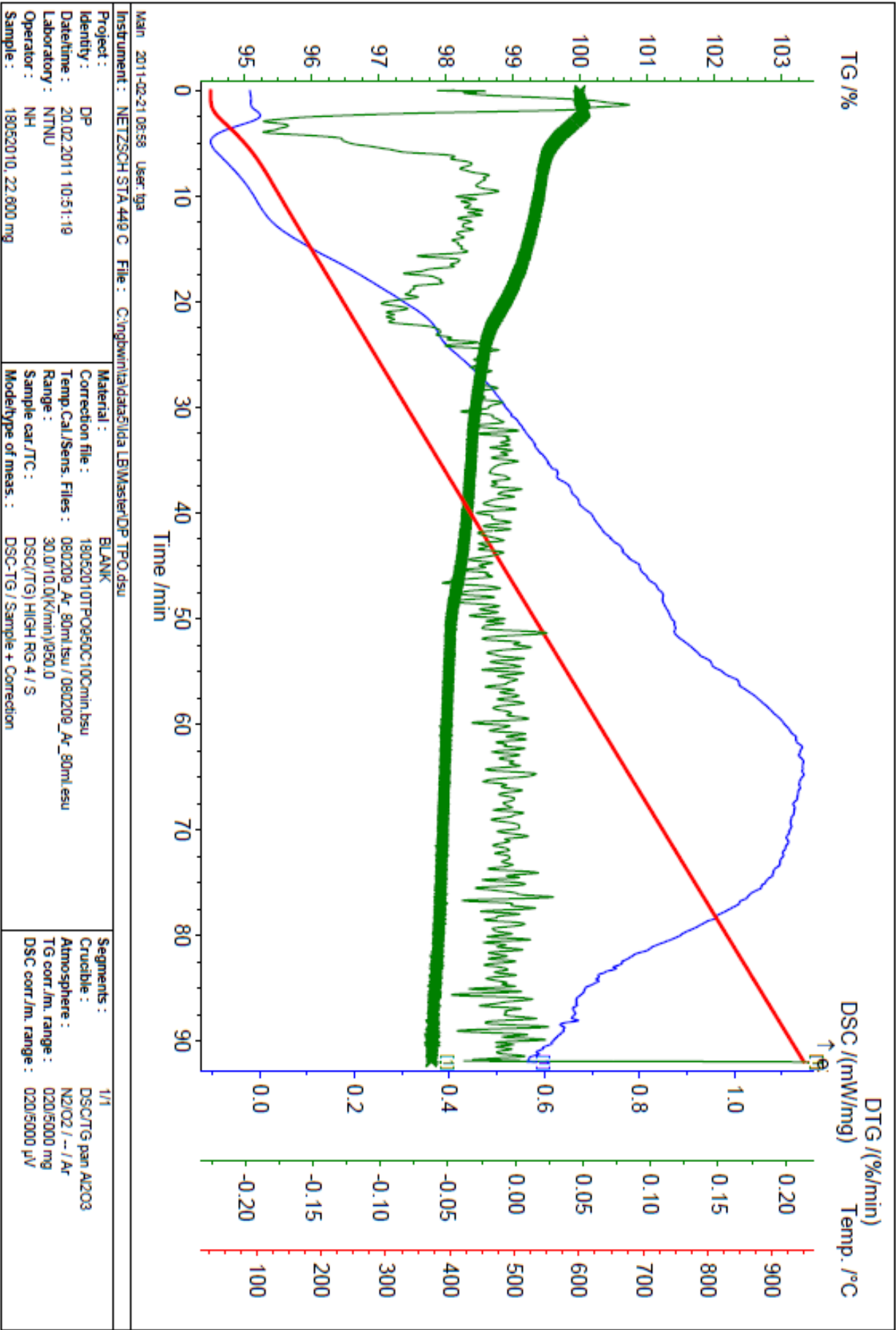
Appendix 4 - TPO plots

Sample 4:



Appendix 4 - TPO plots

Sample 10:



Appendix 5 – TPR calculations

The wt% of CuO in the samples were calculated from the following equations:

$$m_{Cu} = \frac{(m_{sample} - m_{red}) \times M_{Cu}}{1000mg / g \times M_O}$$

$$wt\% Cu = \frac{m_{Cu} \times 1000mg / g \times 100\%}{m_{red}}$$

$$n_{Cu} = \frac{m_{Cu}}{M_{Cu}}$$

$$n_{Cu} = n_{CuO}$$

$$wt\% CuO = \frac{n_{CuO} \times M_{CuO} \times 100\% \times 1000mg / g}{m_{sample}}$$

m_{Cu} = mass Cu [g],

m_{sample} = mass sample after first step [mg],

m_{red} = mass sample after reduction [mg],

M_{Cu} = 63.55 g/mol,

M_O = 16 g/mol,

n_{Cu} = mol Cu,

n_{CuO} = mol CuO,

M_{CuO} = 79,55 g/mol

Calculation example:

Sample 4:

$$m_{Cu} = \frac{(57mg - 55.78mg) \times 63.55g / mol}{1000mg / g \times 16g / mol} = 0.004846g$$

$$wt\% Cu = \frac{0.004846 \times 1000mg / g \times 100\%}{55.78mg} = 8.69wt\%$$

$$n_{Cu} = \frac{0.004846g}{63.55g / mol} = 7.6 \times 10^{-5} mol$$

$$n_{CuO} = 7.6 \times 10^{-5} mol$$

$$wt\% CuO = \frac{7.6 \times 10^{-5} mol \times 79.55g / mol \times 100\% \times 1000mg / g}{57mg} = 16wt\%$$

Appendix 6 – XRD calculations and plots

XRD calculations

The FWHM crystallite size was gotten from TOPAS software, which separate XRD peaks that are too close for manual calculations. The crystallite size and respective errors are listed in table 1.

Table 1 Crystallite size, errors and k-values from TOPAS

Sample	CuO			Anatase			Rutile		
	Str	Error	k	Str	Error	k	Str	Error	k
1	1.0	4.2	0.9	21.2	0.7	0.9	38.5	2.4	0.9
2	26.2	5.5	0.9	21.1	0.7	0.9	18.3	3.6	0.9
3	23.1	2.6	0.9	20.9	0.7	0.9	15.7	3.3	0.9
4	26.3	1.9	0.9	19.4	0.7	0.9	32.5	1.8	0.9
5	24.1	3.3	0.9	101.9	3.2	0.9	12.0	6.6	0.9
6	24.0	2.2	0.9	154.8	24.1	0.9	125.3	42.3	0.9
7	12.2	6.6	0.9	10.9	4.7	0.9			0.9
8	23.4	4.8	0.9	11.9	1.3	0.9	1.3	0.7	0.9
9	29.9	9.6	0.9	13.5	3.2	0.9	1.5	0.5	0.9
10	26.7	4.5	0.9	18.2	3.2	0.9	8.5	1.8	0.9

The dispersion calculated from the XRD analysis is shown in the following equation:

$$D = \frac{1.1}{d_{CuO}} \times 100\%, \quad D = \text{dispersion}, \quad d_{CuO} = \text{crystallite size of CuO [nm]}$$

Example: Sample 4: $D = \frac{1.1}{26.3} \times 100\% = 4.18\%$

The rutile content was calculated from the following equation:

$$wt\% Ru = 100 \times \left(\frac{1 + 0.8 \times I_A}{I_{Ru}} \right)^{-1}, \quad I_A = \text{intensity of anatase peak}, \quad I_{Ru} = \text{intensity of rutile peak}$$

Example: Sample 4: $wt\% Ru = 100 \times \left(\frac{1 + 0.8 \times 2176}{355} \right)^{-1} = 16.9wt\%$

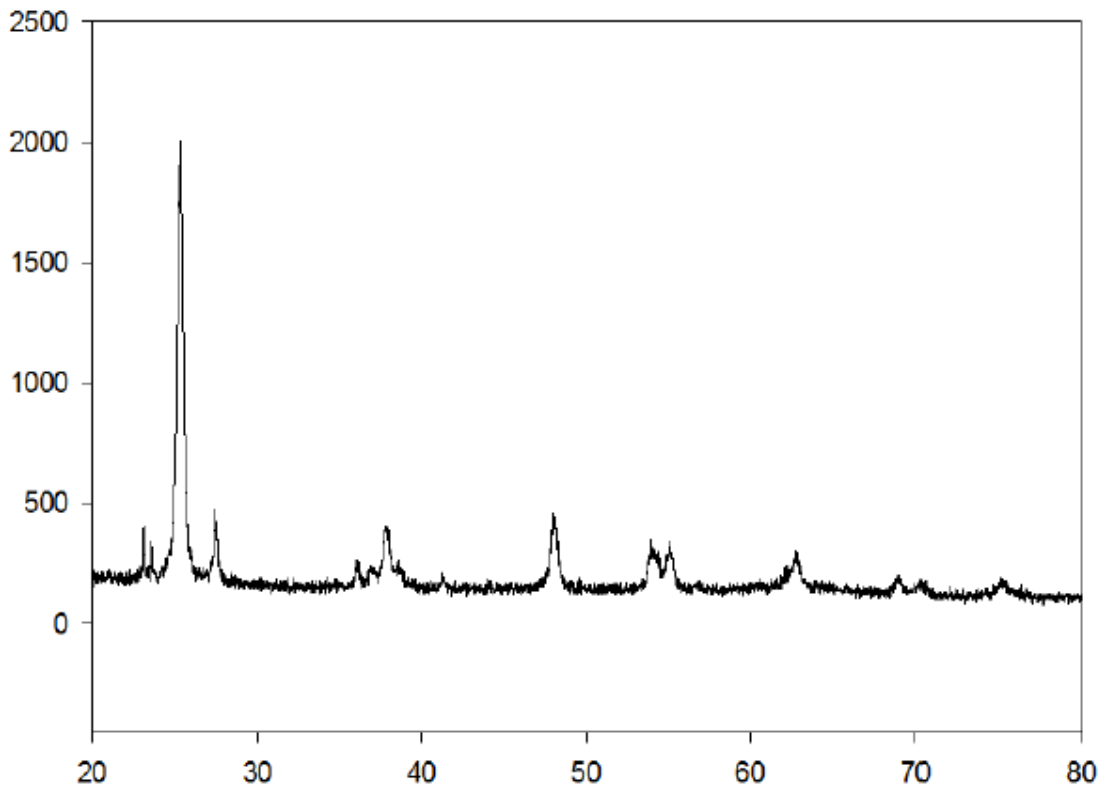
Table 2 shows the intensity of the anatase and rutile peaks for all the samples.

Table 2 Intensity of anatase and rutile peaks, and he resulting calculated rutile content

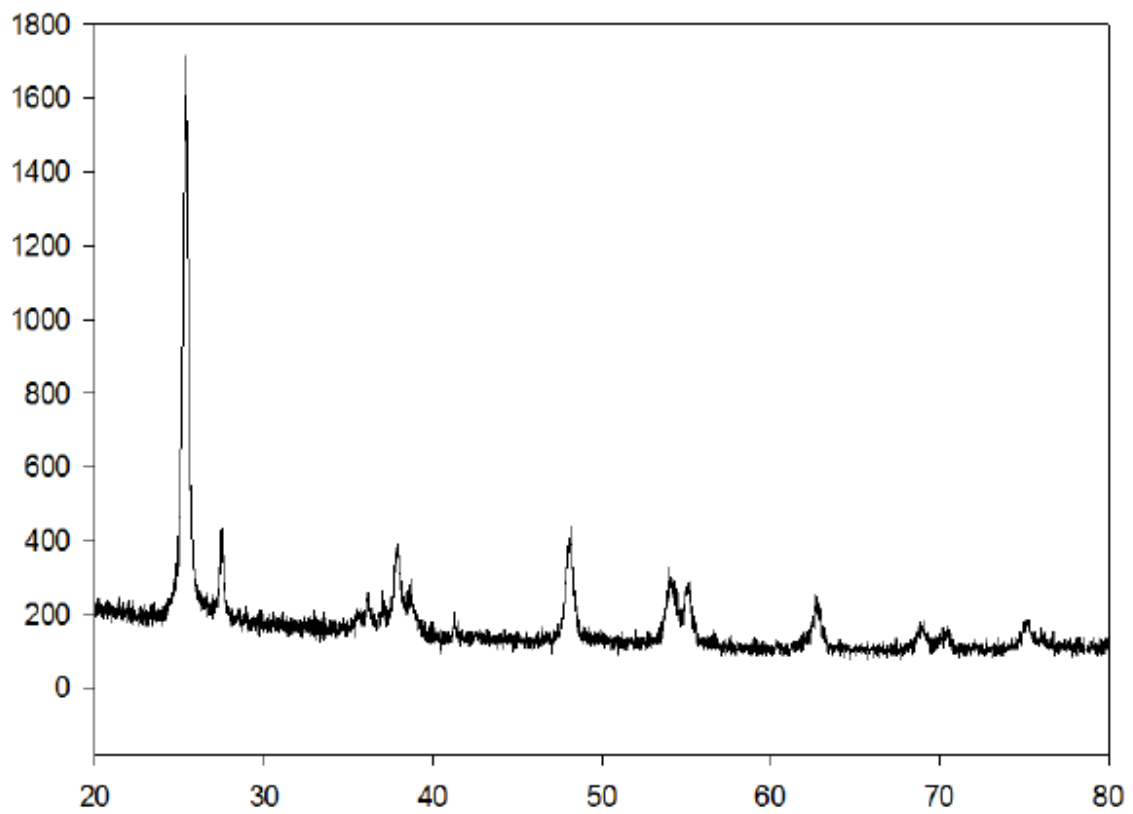
Sample	I _A	I _{Ru}	%Ru
1	2765	416	16
2	1665	258	16
3	1918	336	18
4	2176	355	17
5	3867	31	1
6	0	1703	100
7	437	0	0
8	1493	0	0
9	795	0	0
10	1639	267	17

Appendix 6 - XRD calculations and plots

Sample 1

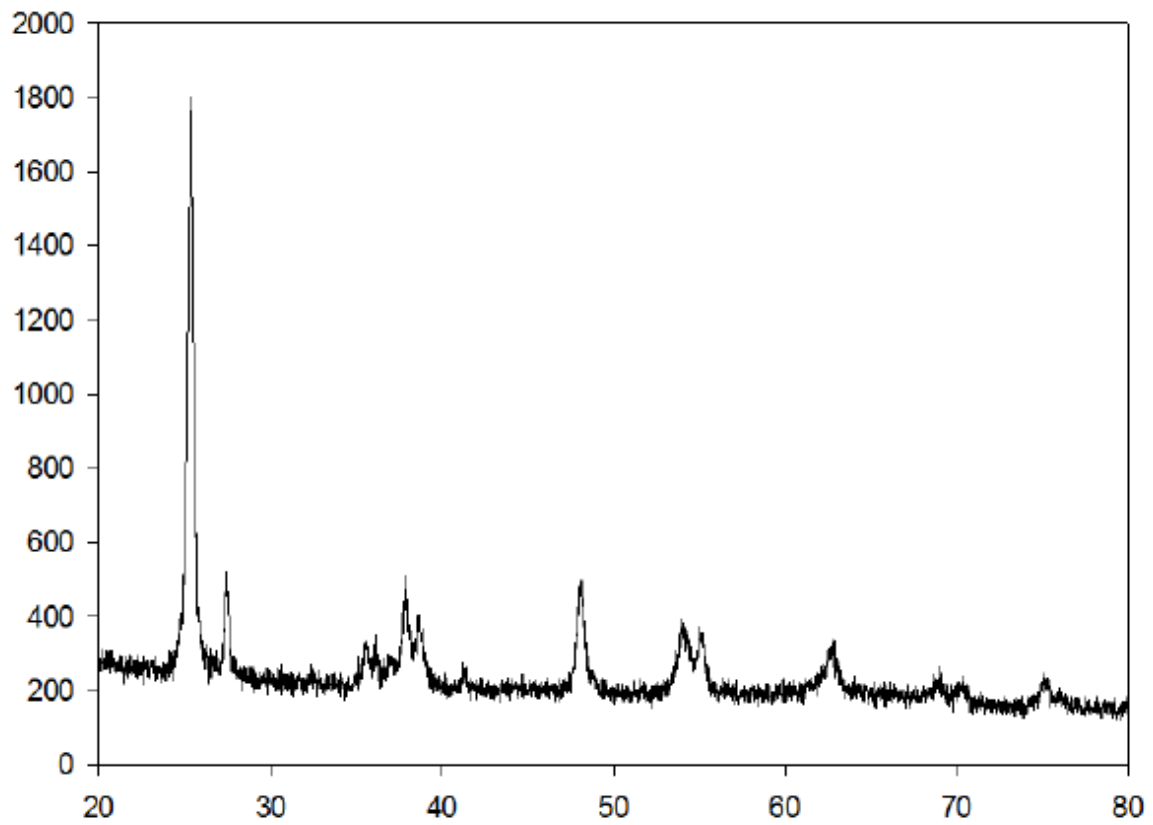


Sample 2

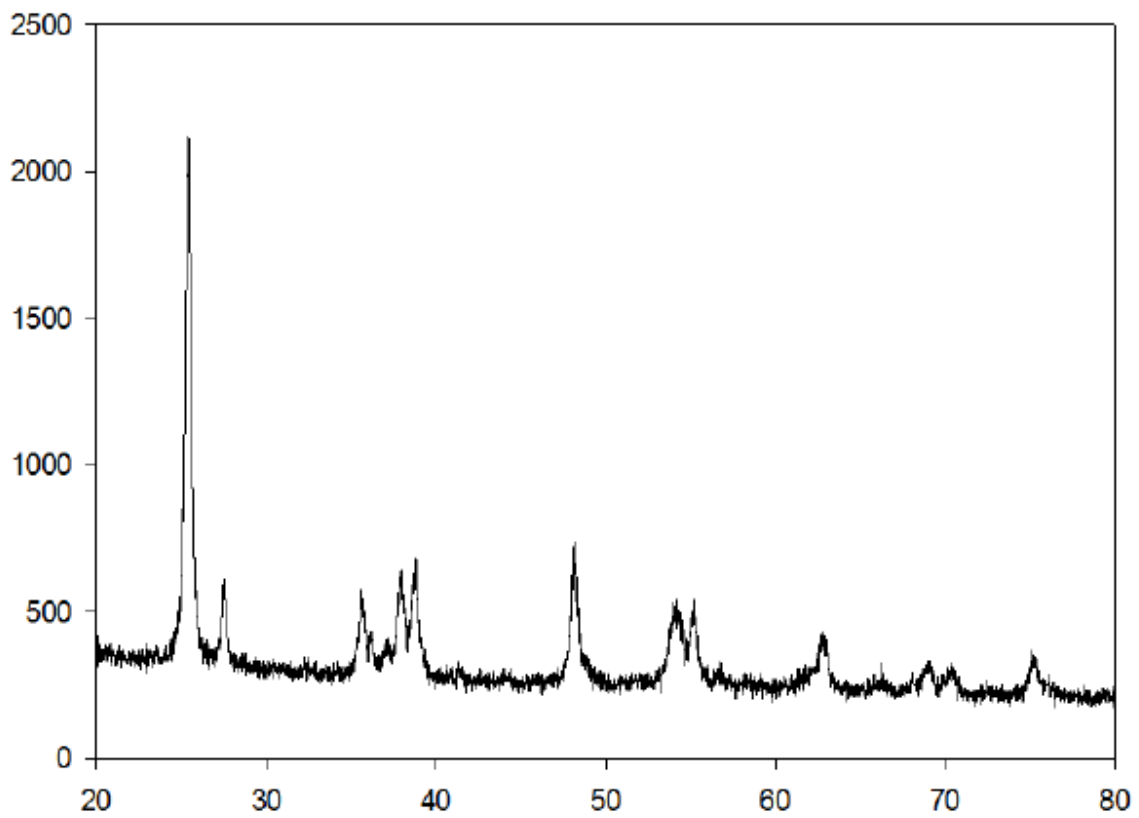


Appendix 6 - XRD calculations and plots

Sample 3

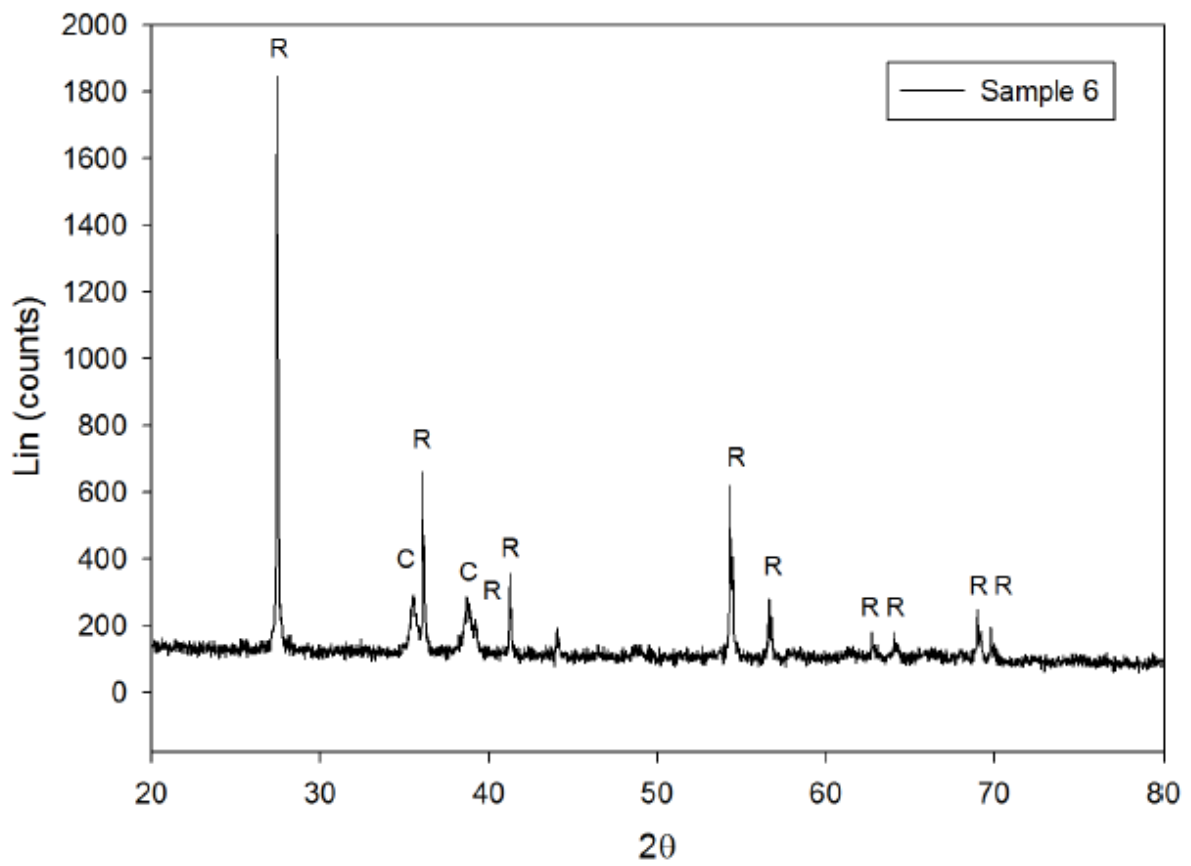
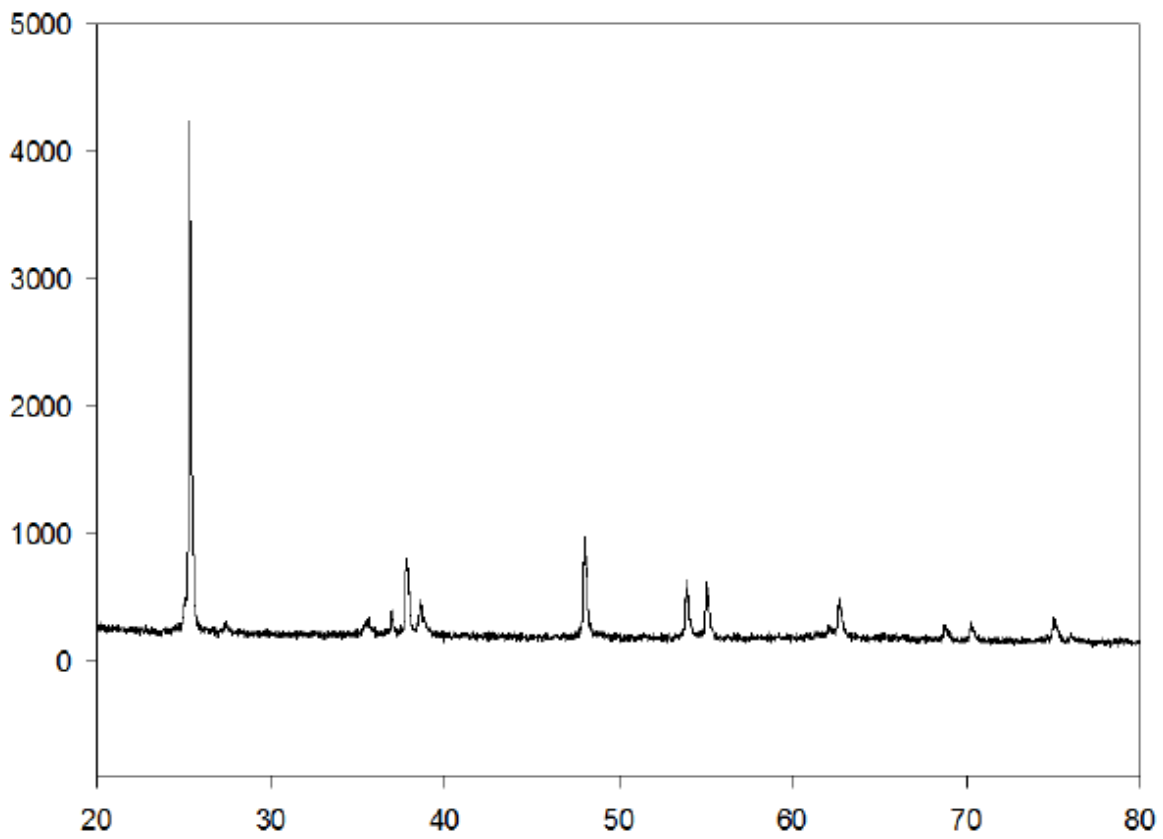


Sample 4

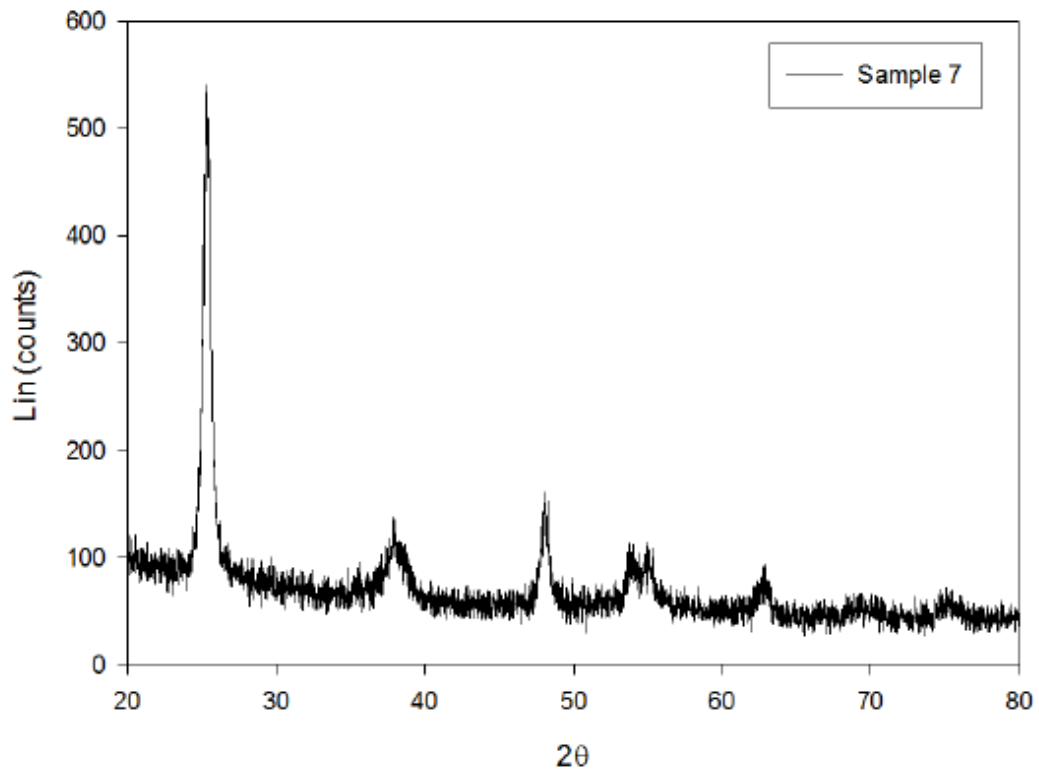


Appendix 6 – XRD calculations and plots

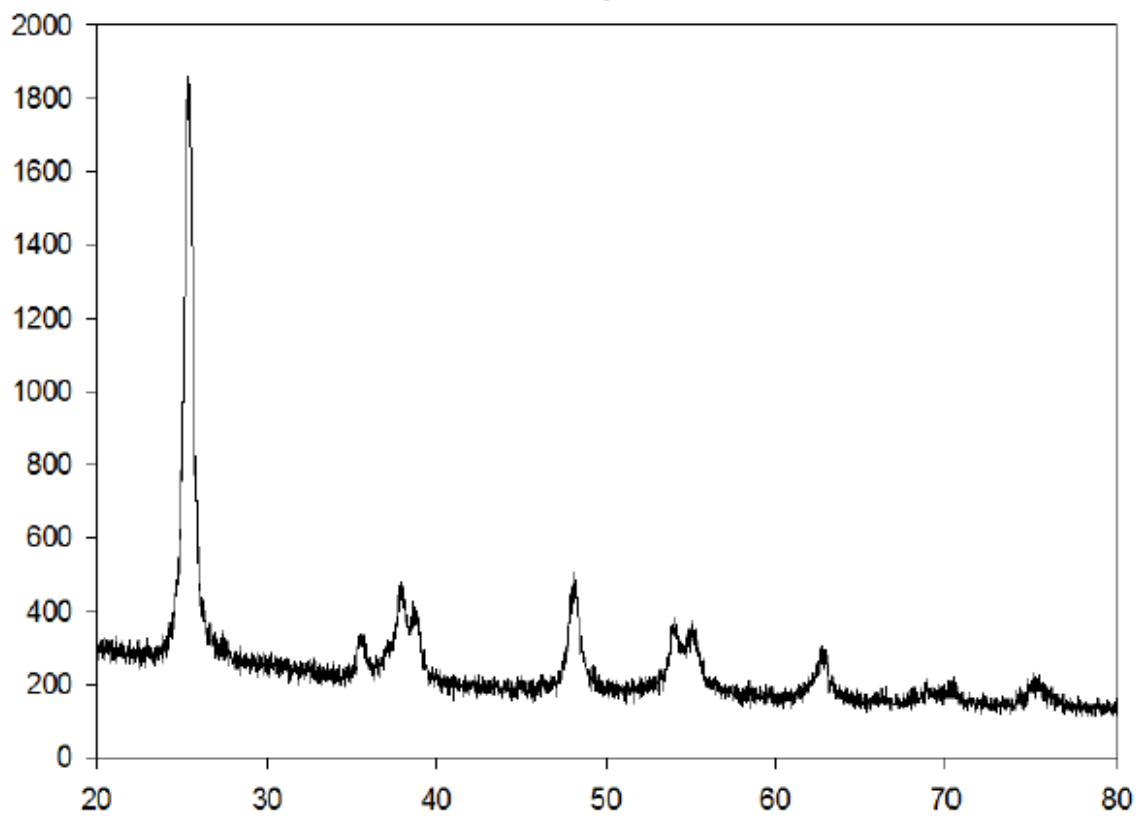
Sample 5



Appendix 6 - XRD calculations and plots

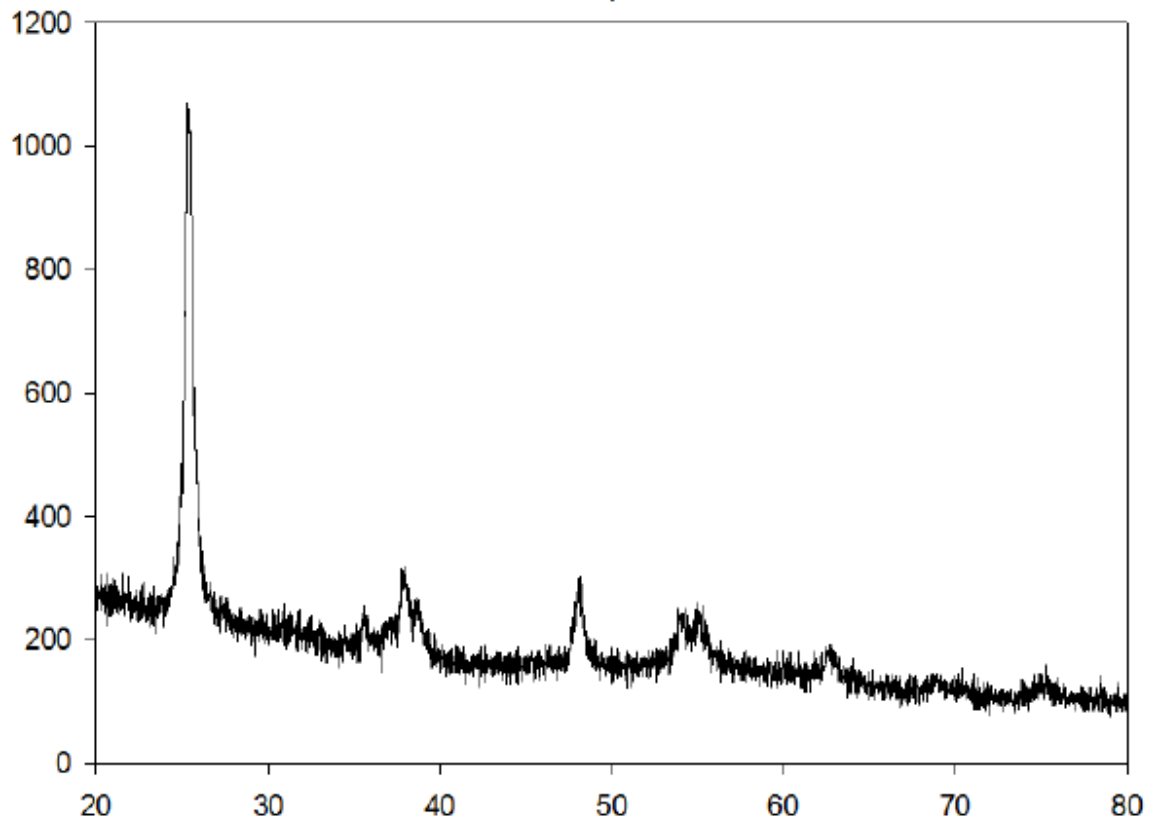


Sample 8

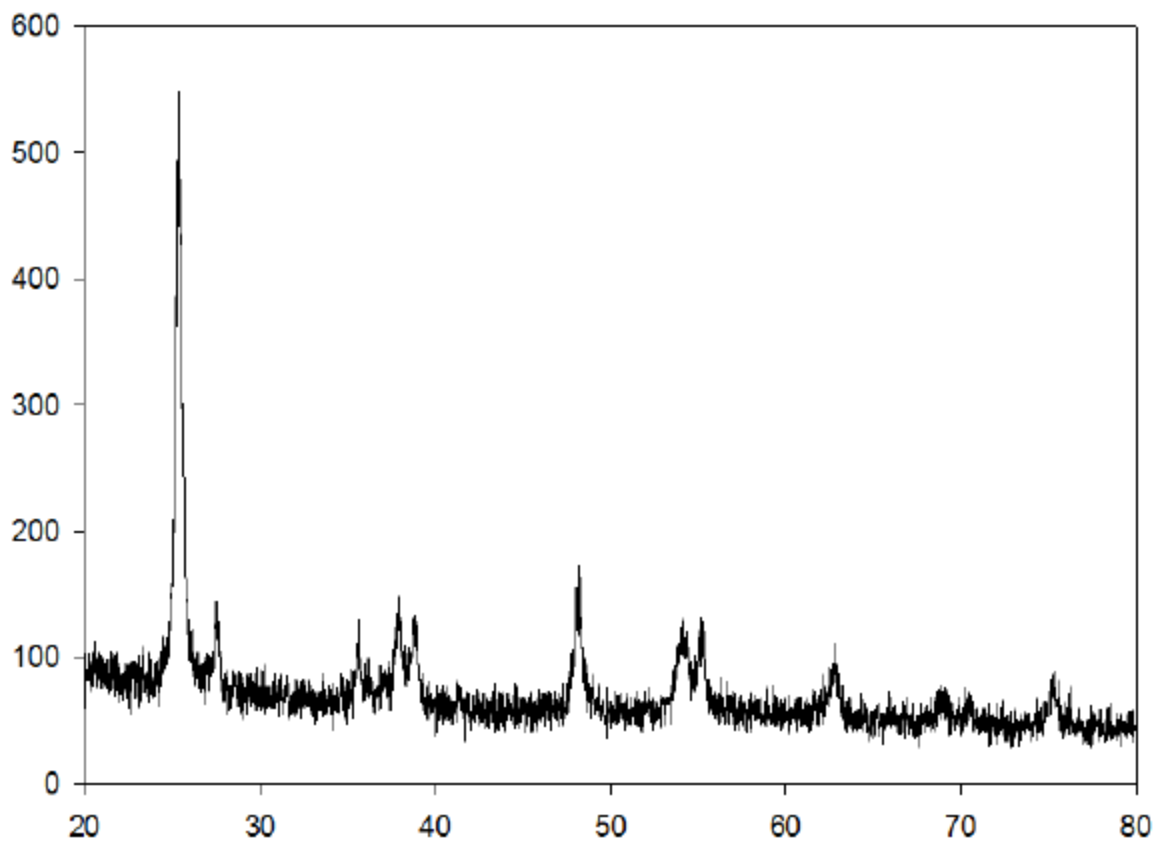


Appendix 6 – XRD calculations and plots

Sample 9



Sample 10



Appendix 7 – MS calibration

MS calibration:

The gas flow was first calibrated with a bubble gas flow meter. The MS was then calibrated using argon gas and ethylene gas. The MS signal was then noted for different argon concentrations and plotted against the concentration. The resulting plot gave a linear equation which could be used to calculate the argon concentration, and then again calculate the hydrogen evolution from photoreforming experiments. The MS signal during calibration is shown in figure 1, and the plot with MS intensity and concentration is shown in figure 2.

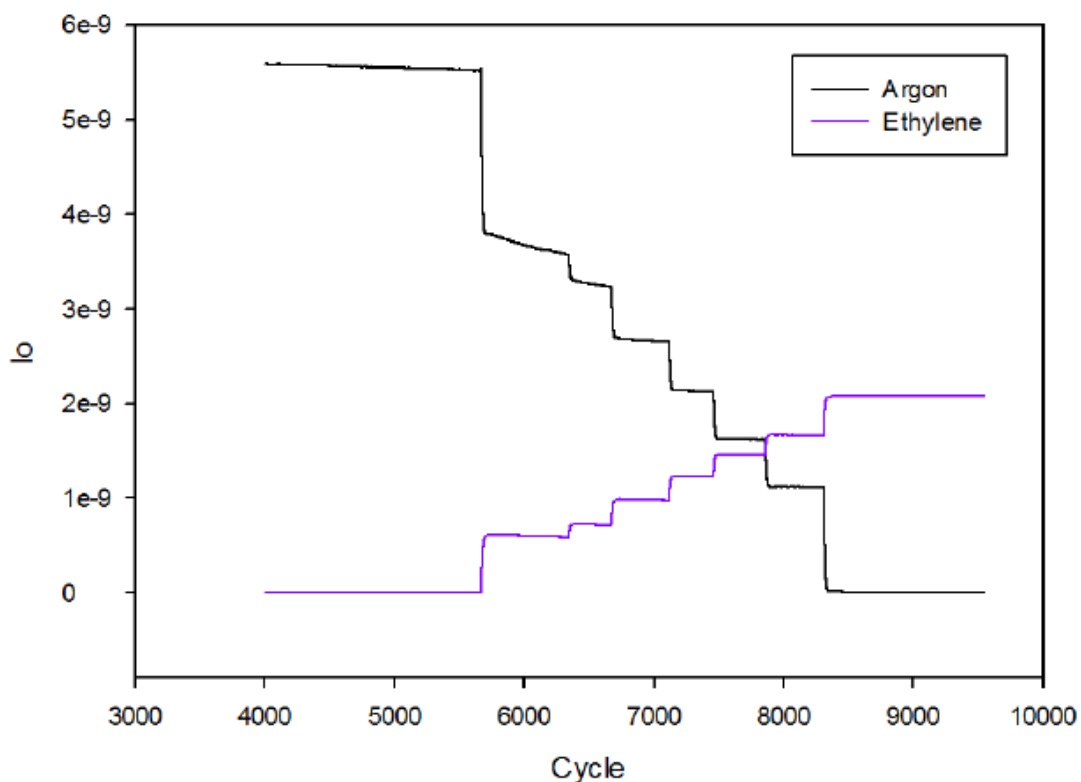
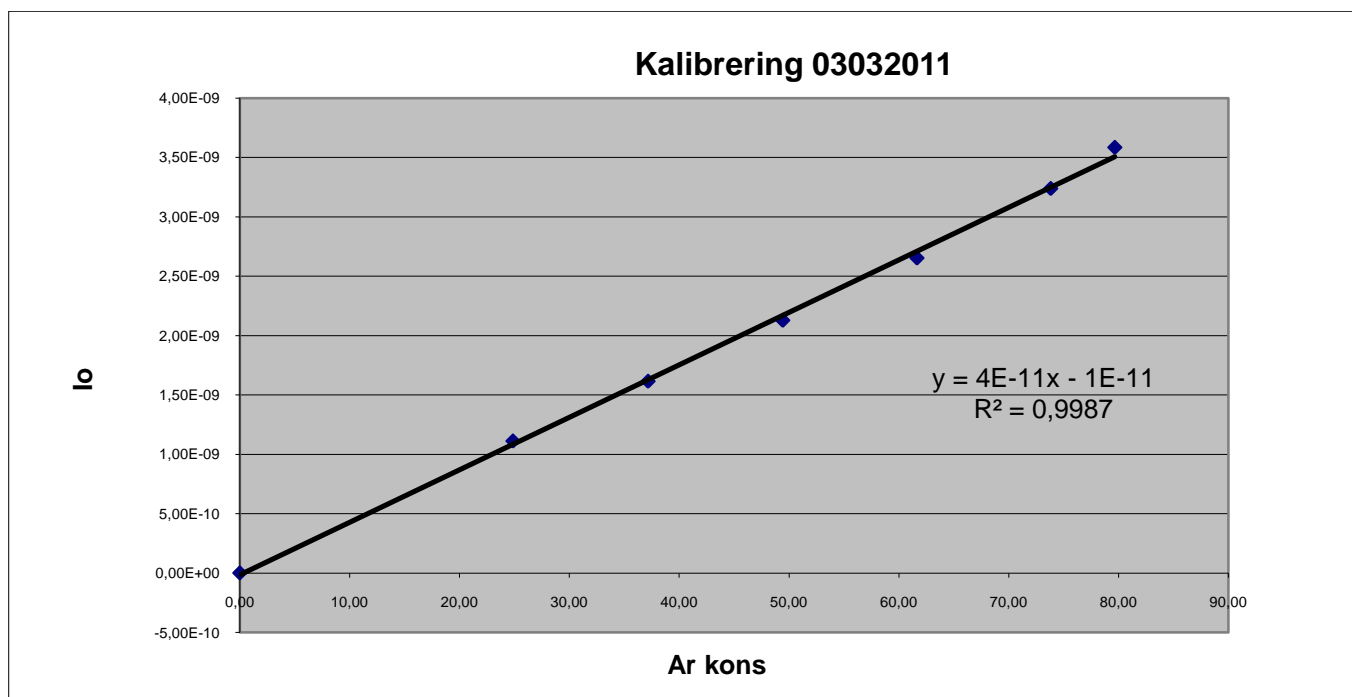


Figure 1. The MS signal for argon and ethylene during calibration

The table shows the argon flow and calculations and MS signal intensity.

Appendix 7 – MS calibration

Ar open	Et open	Ar flow	Et flow	Ar mol flow	Et mol flow	c Ar	c Et	Time	Io m/Z 40	Io m/z 26	Cycle
24,97	0,00	0,68	0,00E+00	3,01E-05	0,00E+00	100,00	0,00	1100	5,52E-09	5,69E-13	5600
20,03	2,01	0,54	1,38E-01	2,42E-05	6,17E-06	79,65	20,35	1110	3,58E-09	5,68E-10	6280
18,74	2,61	0,51	1,80E-01	2,26E-05	8,02E-06	73,82	26,18	1116	3,24E-09	6,91E-10	6600
15,62	3,82	0,42	2,63E-01	1,89E-05	1,17E-05	61,64	38,36	1123	2,65E-09	9,46E-10	7050
12,50	5,03	0,34	3,46E-01	1,51E-05	1,54E-05	49,43	50,57	1130	2,13E-09	1,19E-09	7426
9,39	6,23	0,25	4,29E-01	1,13E-05	1,91E-05	37,17	62,83	1135	1,62E-09	1,42E-09	7823
6,27	7,44	0,17	5,12E-01	7,57E-06	2,29E-05	24,87	75,13	1143	1,11E-09	1,64E-09	8310
0,00	9,86	0,00	6,78E-01	0,00E+00	3,03E-05	0,00	100,00	1203	2,78E-12	2,06E-09	9500



Figur 2. MS intensity plotted against argon concentration

Appendix 8 – Chemisorption calculations and plots

Chemisorption calculations

The dispersion was calculated from the N₂O adsorption from the following equations:

$$m_{desO} = m_{sample} - m_{red}$$

$$n_{desO} = \frac{m_{desO}}{1000mg / g \times M_O}$$

$$n_{CuTot} = n_{desO}$$

$$x_{Cu} = n_{CuTot} \times N_A$$

$$x_{CuSurface} = \frac{m_{CO_2ads} \times N_A}{1000mg / g \times M_O}$$

$$x_{CuSurface} = \frac{m_{N_2Oads} \times N_A \times 2molCu / molO}{1000mg / g \times M_O}$$

$$D = \frac{x_{CuSurface} \times 100\%}{x_{Cu}}$$

m_{desO} = mass desorbed oxygen [mg],

n_{desO} = mol desorbed oxygen,

n_{CuTot} = Total mol Cu on sample,

x_{Cu} = number of Cu atoms,

N_A = Avogadro's number, 6.022142×10^{23} molecules/mol,

$x_{CuSurface}$ = number of surface Cu atoms,

m_{CO_2ads} = mass of adsorbed CO₂ [mg]

m_{N_2Oads} = mass of adsorbed N₂O [mg],

D = dispersion [%]

Example:

Sample 4:

$$m_{desO} = 66.11mg - 64.05mg = 2.06mg$$

$$n_{desO} = \frac{2.06mg}{1000mg / g \times 16g / mol} = 1.29 \times 10^{-4} mol$$

$$n_{CuTot} = n_{desO} = 1.29 \times 10^{-4} mol$$

$$x_{Cu} = 1.29 \times 10^{-4} mol \times 6.022142 \times 10^{23} molecules / mol = 7.75 \times 10^{19} molecules$$

$$x_{CuSurface} = \frac{0.12mg \times 6.022142 \times 10^{23} molecules / mol}{1000mg / g \times 16g / mol} = 4.52 \times 10^{18} molecules$$

$$x_{CuSurface} = \frac{0.03mg \times 6.022142 \times 10^{23} molecules / mol \times 2}{1000mg / g \times 16g / mol} = 2.26 \times 10^{18} molecules$$

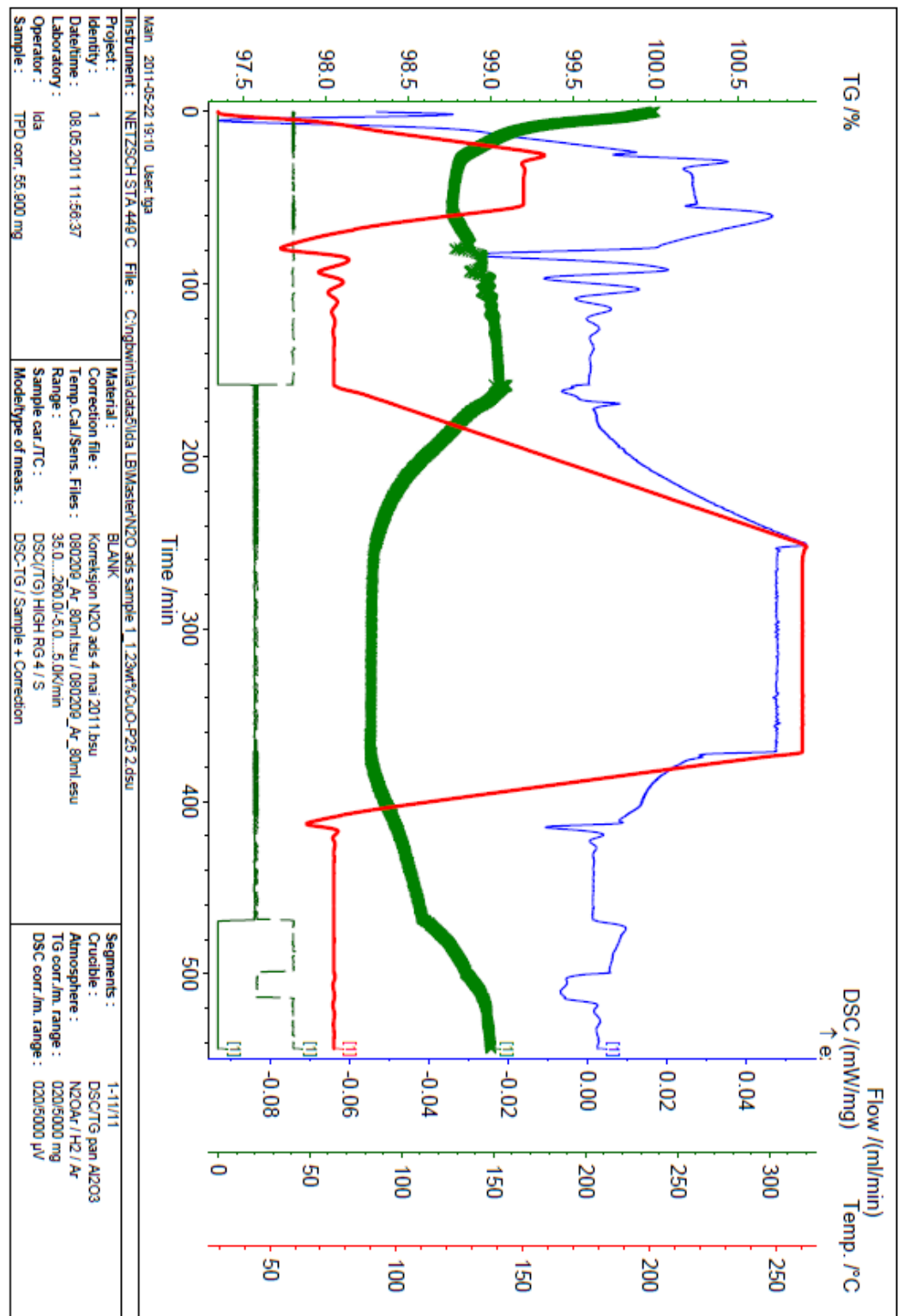
$$D = \frac{(4.52 \times 10^{18} molecules + 2.26 \times 10^{18} molecules) \times 100\%}{7.75 \times 10^{19} molecules} = 9\%$$

$$D = \frac{2.26 \times 10^{18} molecules \times 100\%}{7.75 \times 10^{19} molecules} = 3\%$$

Appendix 8 – Chemisorption calculations and plots

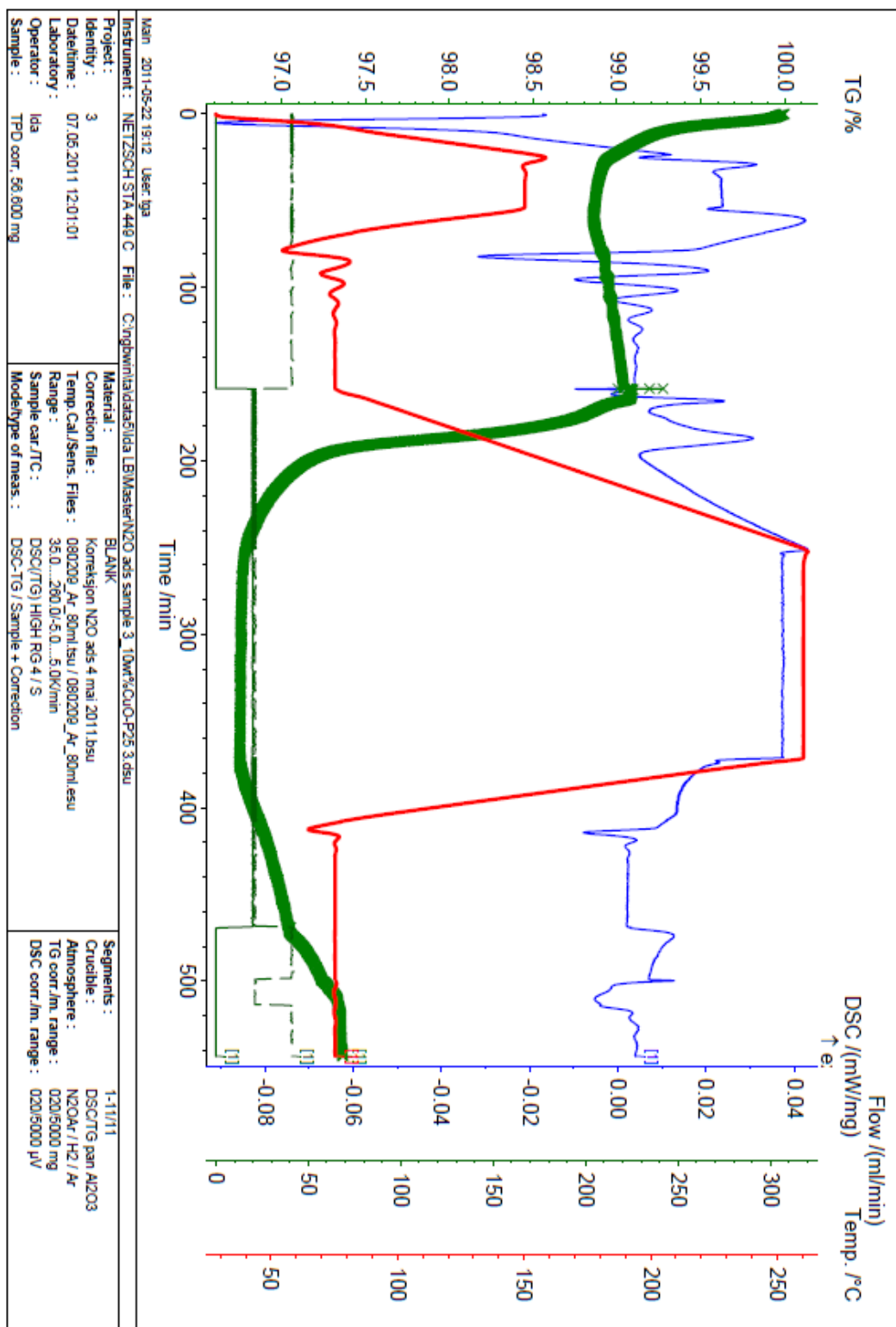
If the weight gain before the N₂O step in the program is assumed to be CO₂ chemisorption on the surface and this is taken in to account on the dispersion measurement the dispersion becomes 9%. If only the N₂O chemisorption is calculated the dispersion becomes 3%. Assume the CO₂ oxidation is bulk oxidation and Cu(0) → CuO, and use only the N₂O adsorption to calculate dispersion.

Sample 1:



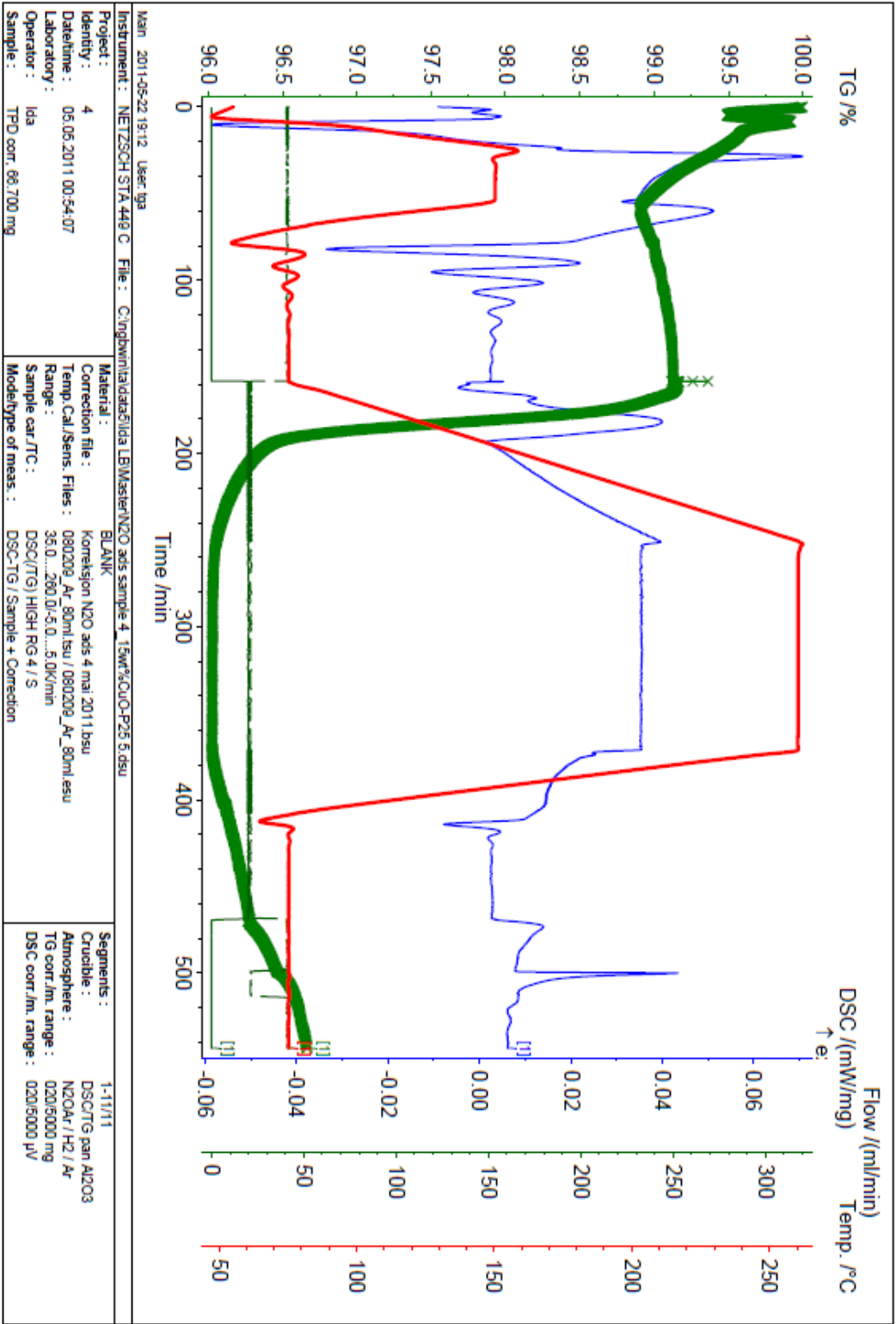
Appendix 8 – Chemisorption calculations and plots

Sample 3:



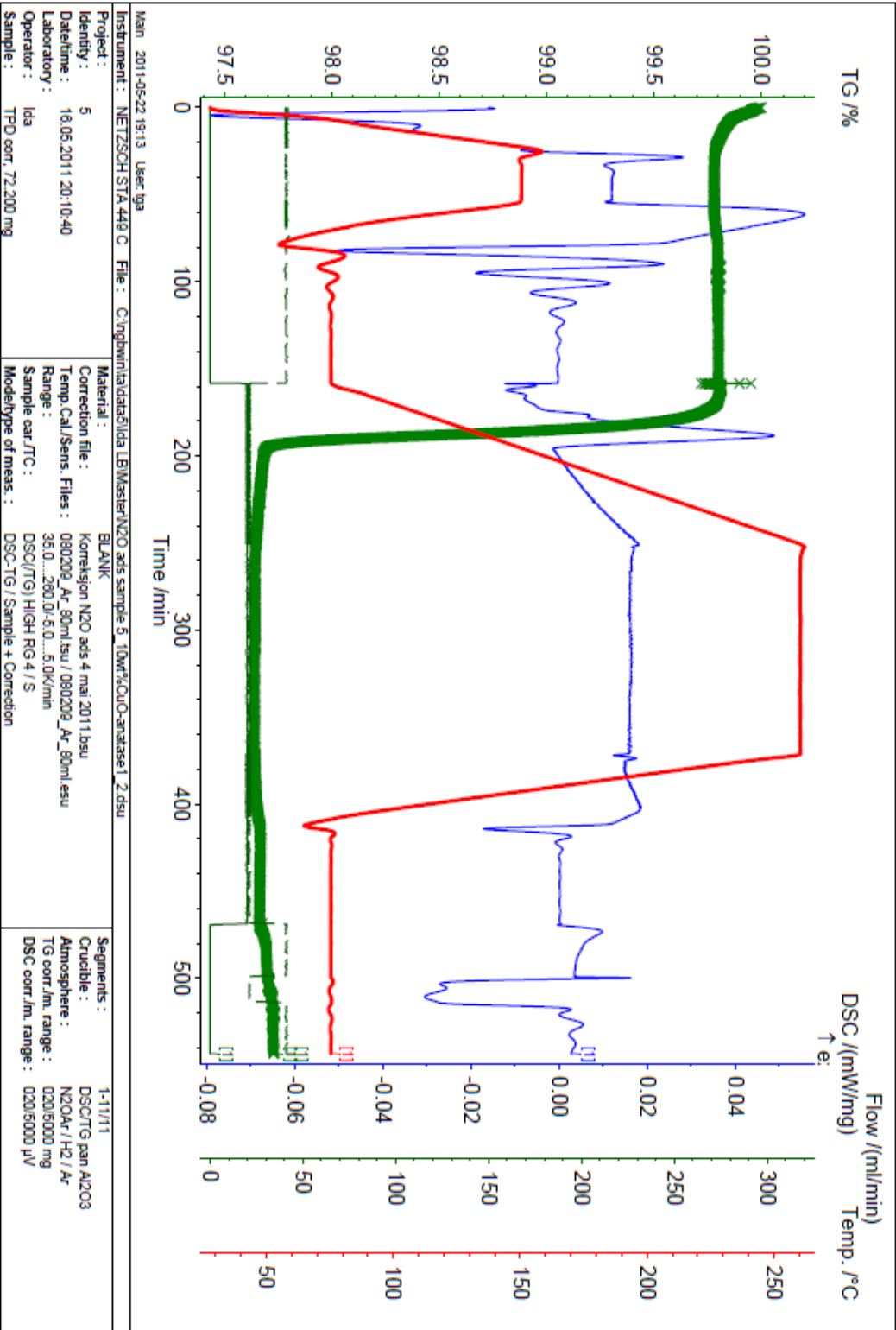
Appendix 8 – Chemisorption calculations and plots

Sample 4:



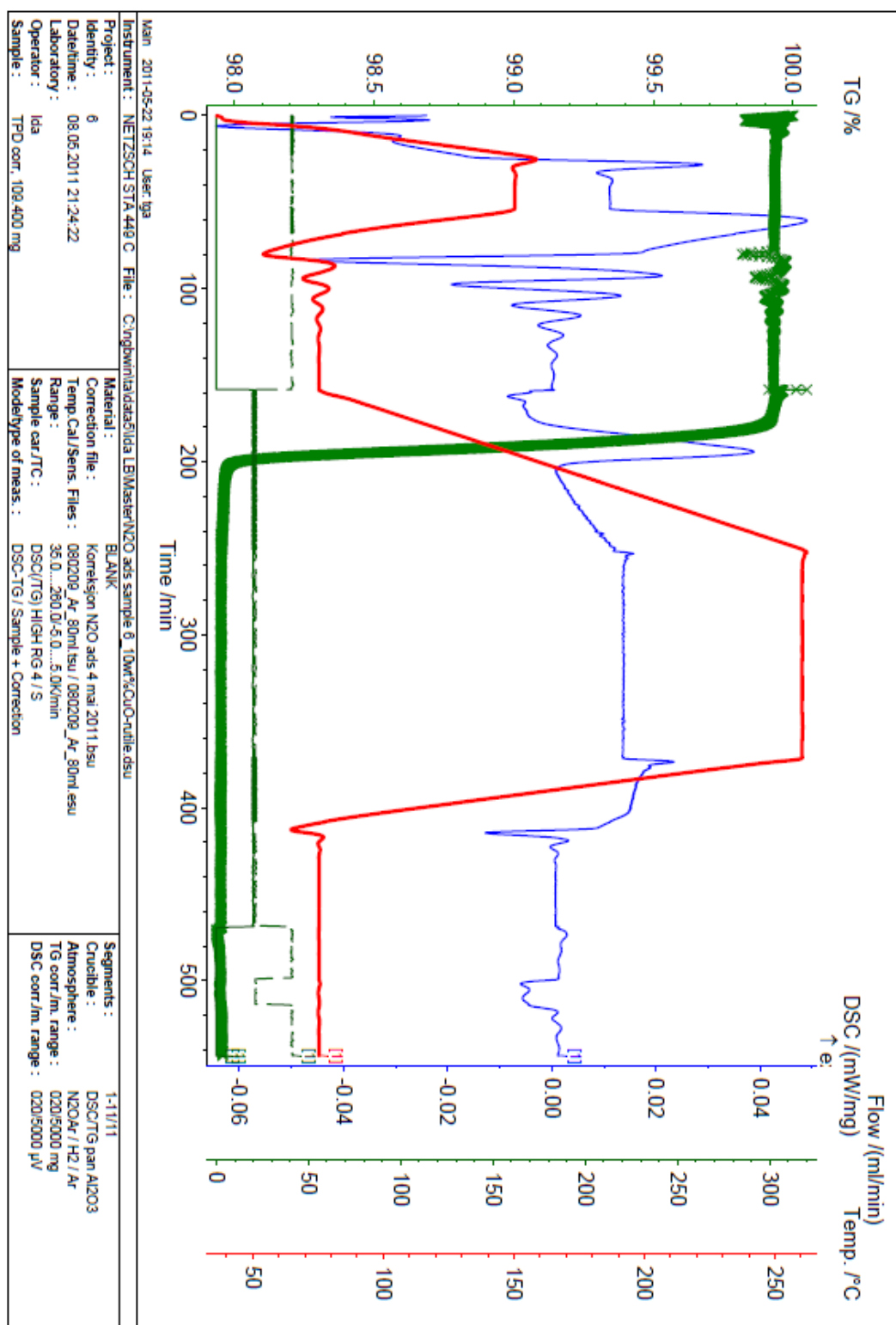
Appendix 8 – Chemisorption calculations and plots

Sample 5:



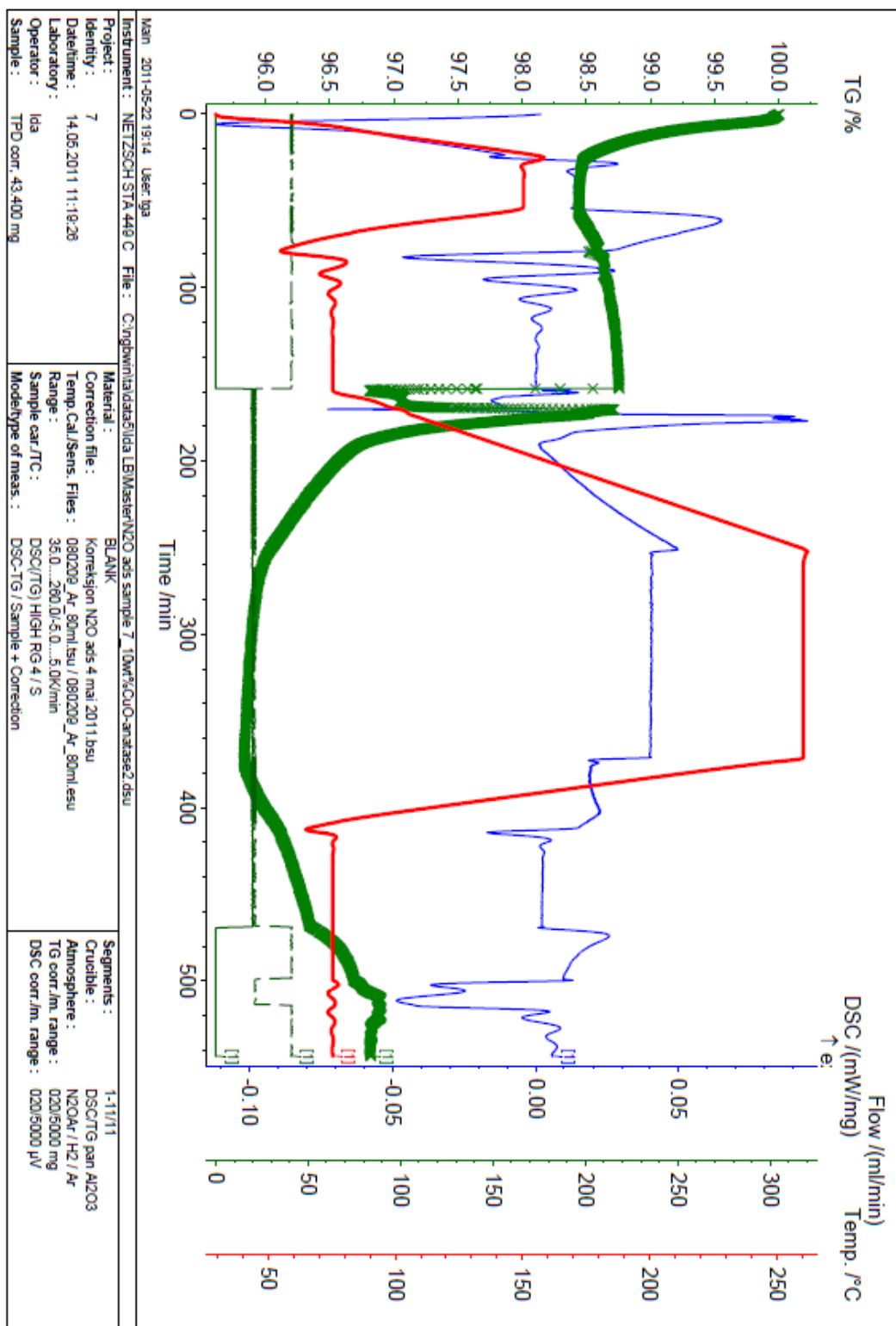
Appendix 8 – Chemisorption calculations and plots

Sample 6:



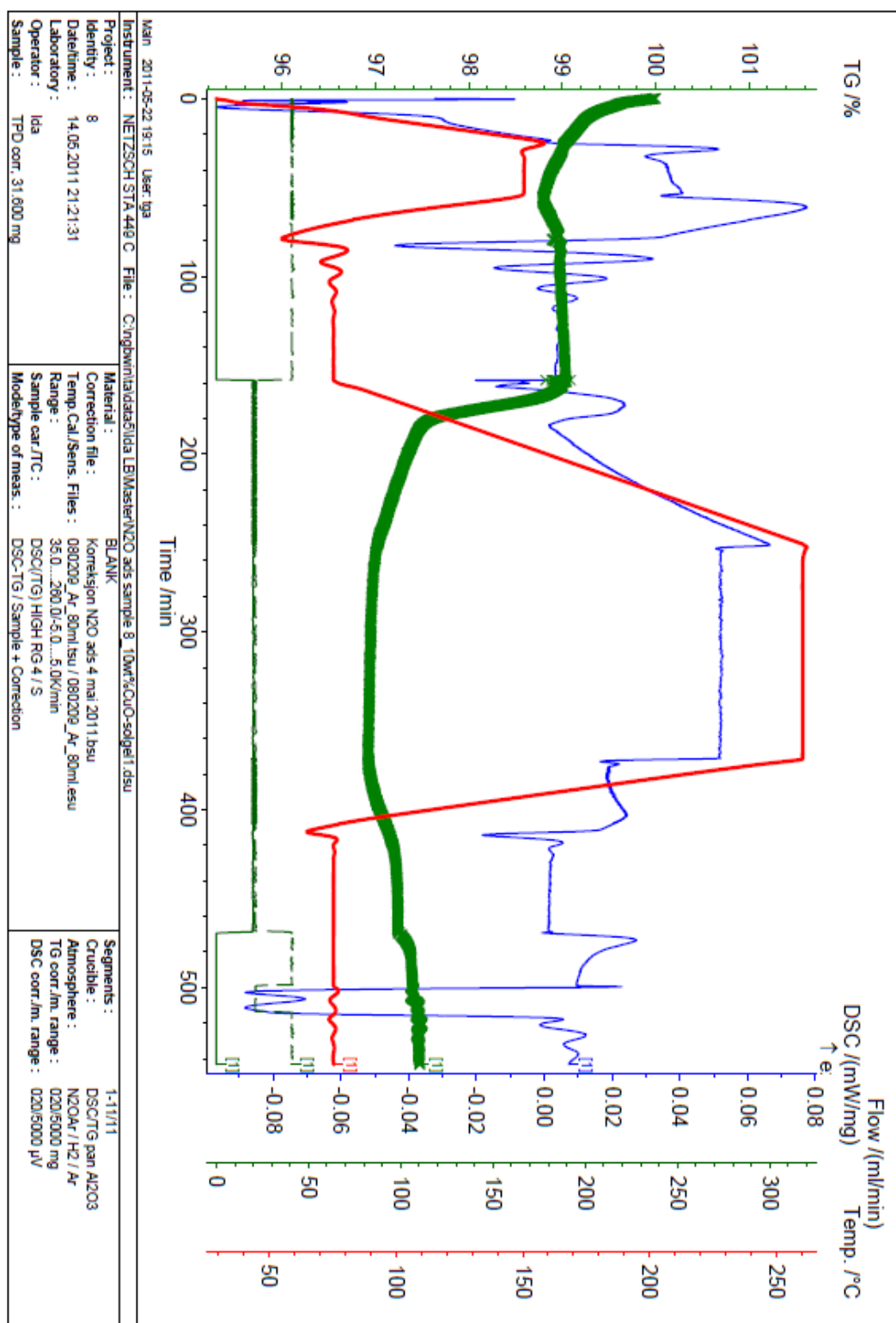
Appendix 8 – Chemisorption calculations and plots

Sample 7:



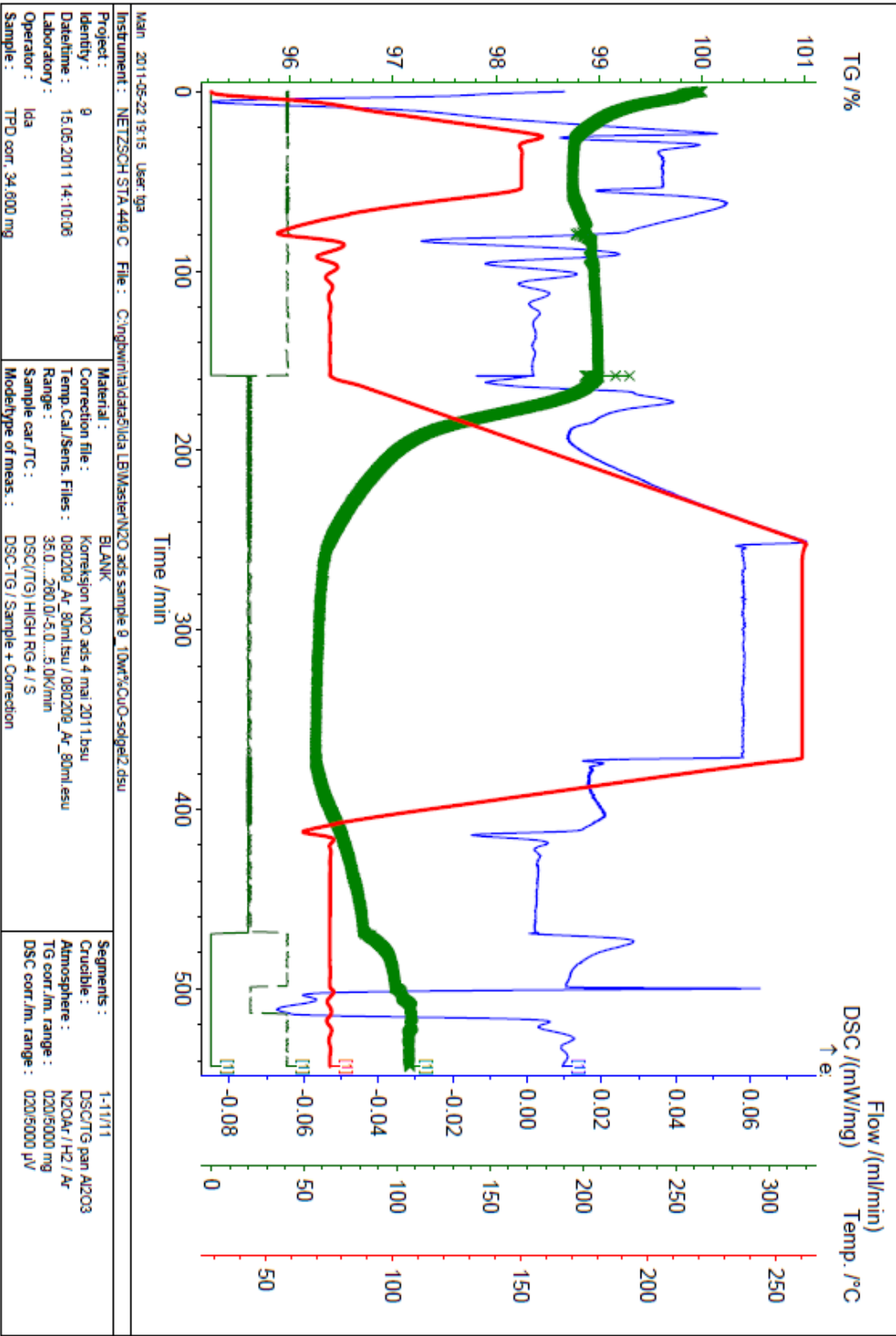
Appendix 8 – Chemisorption calculations and plots

Sample 8:



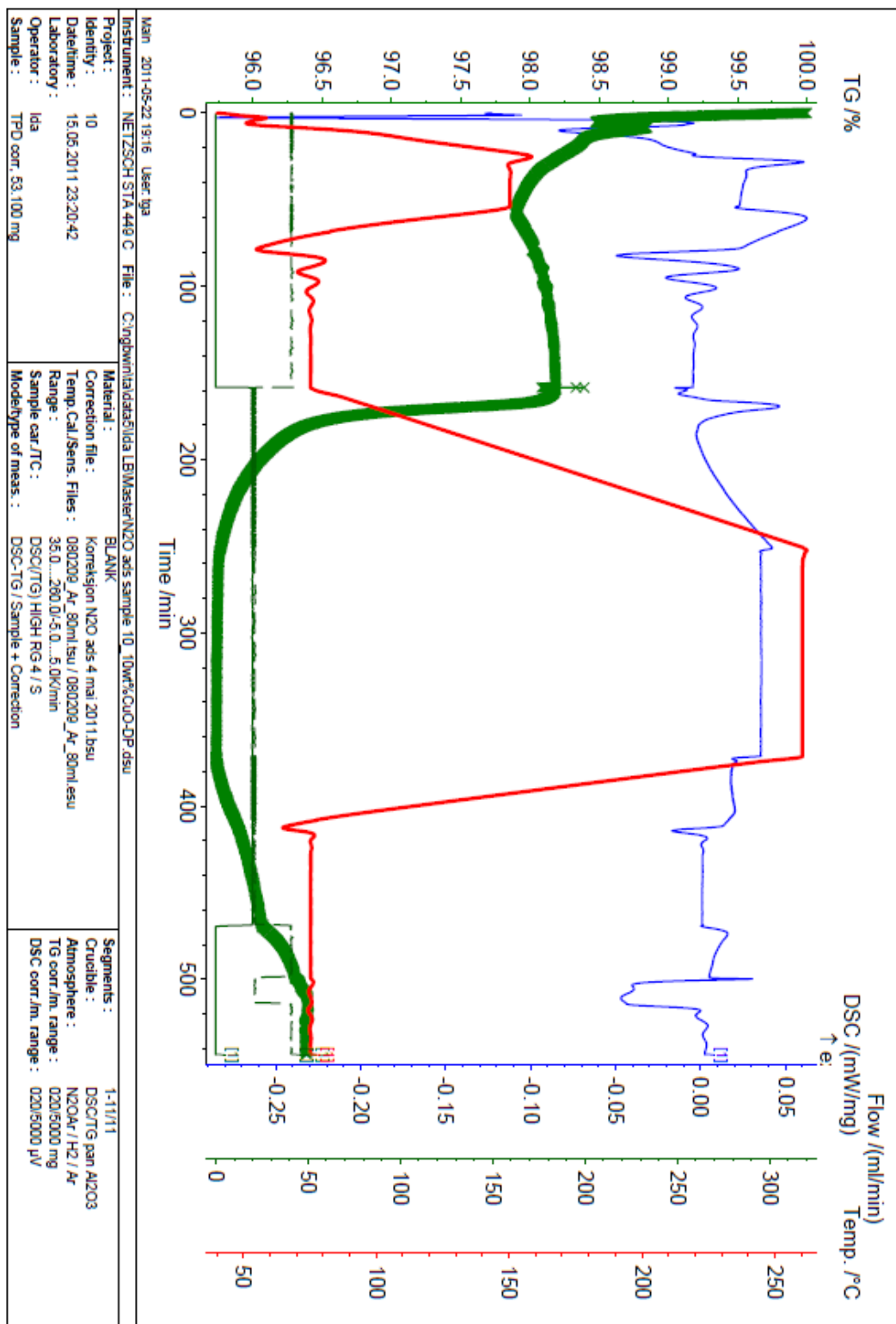
Appendix 8 - Chemisorption calculations and plots

Sample 9:



Appendix 8 – Chemisorption calculations and plots

Sample 10:



Appendix 9 – Dispersion comparison calculations

Comparison between XRD dispersion and chemisorption dispersion

CuO unit cell:

$$a=4,68375, b=3,42265, c=5,12886$$

$$\alpha=90^\circ, \beta=99,54^\circ, \gamma=90^\circ$$

$$V_{unit\ cell} = abc\sqrt{(1 - \cos^2\alpha - \cos^2\beta - \cos^2\gamma + 2\cos\alpha\cos\beta\cos\gamma)}$$

$$V_{unit\ cell\ CuO} = 4,68375 \times 3,42265 \times 5,12886 \times \\ \sqrt{(1 - \cos^2 90 - \cos^2 99,54 - \cos^2 90 + 2\cos 90\cos 90\cos 90)}$$

$$V_{unit\ cell\ CuO} = 81,08\text{\AA}^3$$

Z=4 Cu atoms/unit cell

$$V_{CuO} = \frac{V_{unit\ cell\ CuO}}{Z} = \frac{81,08\text{\AA}^3}{4} = 20,3\text{\AA}^3 / Cu$$

Cu unit cell:

$$a=3,61$$

$$\alpha = \beta = \gamma = 90^\circ$$

$$V_{unit\ cell} = abc\sqrt{(1 - \cos^2\alpha - \cos^2\beta - \cos^2\gamma + 2\cos\alpha\cos\beta\cos\gamma)}$$

$$V_{unit\ cell} = 3,61 \times 3,61 \times 3,61 = 47,05\text{\AA}^3$$

Z=4 Cu atoms/unit cell

$$V_{Cu} = \frac{V_{unit\ cell\ Cu}}{Z} = \frac{47,05\text{\AA}^3}{4} = 11,8\text{\AA}^3 / Cu$$

Assume spherical Cu particles:

$$V_{sphere} = \frac{\pi d^3}{6}$$

Appendix 9 – Dispersion comparison calculations

Relationship between CuO size and Cu size:

$$\frac{d_{CuO}}{d_{Cu}} = \frac{\left(\frac{6V_{CuO}}{\pi}\right)^{1/3}}{\left(\frac{6V_{Cu}}{\pi}\right)^{1/3}} = 1,198$$

Cu dispersion from XRD results:

$$D_{Cu} = \frac{1,1 \times 1,198 \times 100\%}{d_{CuO}}$$

XRD dispersion:

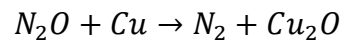
Sample	CuO crystallite size [nm]	CuO dispersion (XRD)[%]	Cu dispersion (XRD) [%]	Cu dispersion (chemisorption) [%]
1	1	110	132,2	32
2	26	4	5,0	3
3	23	5	5,7	9
4	26	4	5,0	11
5	24	5	5,5	1
6	24	5	5,5	0
7	12	9	10,8	9
8	23	5	5,6	6
9	30	4	4,4	8
10	27	4	4,9	6

Appendix 10 – Calculations of heat of reactions

Calculation of heat of reaction is done by Hess' law, shown in the following equation:

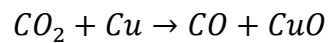
$$\Delta H_{rx} = \sum \Delta H_{product} - \sum \Delta H_{reactants}$$

Heat of reaction N₂O decomposition on Cu(0):



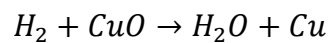
$$\Delta H_{rx} = \frac{(0 + (-168))kJ}{mol} - \frac{(0 + 82)kJ}{mol} = -250kJ/mol$$

Heat of reaction bulk oxidation of Cu(0):





$$\Delta H_{rx} = \frac{((-111) + (-157))kJ}{mol} - \frac{(0 + (-394))kJ}{mol} = 126kJ/mol$$

Heat of reaction reduction of CuO:



$$\Delta H_{rx} = \frac{(0 + (-242))kJ}{mol} - \frac{(0 + (-157))kJ}{mol} = -85kJ/mol$$

NTNU	Appendix 11 - Hazardous activity identification process	Prepared by	Number	Date	
		HSE section	HMSRV-26/01	01.12.2006	
HSE		Approved by	Page	Replaces	
		The Rector	1 out of 1	15.12.2003	



Unit: **IKP** **Date:** **14.03.2011**

Participants in the identification process (including their function):

Ida Lien Bjørnstad (student), Magnus Rønning (supervisor), Nina Hammer (co-supervisor)

Short description of the main activity/main process: Synthesis of photocatalysts

ID no.	Activity/process	Responsible person	Laws, regulations etc.	Existing documentation	Existing safety measures	Comment
S1	HNO ₃ handling	Magnus Rønning	AML §4-5, HMSRV-12/13, HMSR-39, HMSR-40, Kjemikalieforskriften	Material safety data sheet	Closed fume hood	Safety goggles, gloves, lab coat
S2	Ammonia handling	Magnus Rønning	AML §4-5, HMSRV-12/13, HMSR-39, HMSR-40, Kjemikalieforskriften	Material safety data sheet	Closed fume hood	Safety goggles, gloves, lab coat
S3	Titanium isopropoxide handling	Magnus Rønning	AML §4-5, HMSRV-12/13, HMSR-39, HMSR-40, Kjemikalieforskriften	Material safety data sheet	Closed fume hood	Safety goggles, gloves, lab coat
S4	Urea handling	Magnus Rønning	AML §4-5, HMSRV-12/13, HMSR-39, HMSR-40, Kjemikalieforskriften	Material safety data sheet	Closed fume hood	Safety goggles, gloves, lab coat
S5	Calcination	Magnus Rønning	AML §4-5, HMSRV-12/13, HMSR-39, HMSR-40, Kjemikalieforskriften, HMSR-29	Manualer	Spot extract	Safety goggles, gloves, lab coat, check the spot extract, let the apparatus cool down before sample removal

NTNU	Appendix 11 - Hazardous activity identification process	Prepared by	Number	Date	
		HSE section	HMSRV-26/01	01.12.2006	
HSE		Approved by	Page	Replaces	
		The Rector	1 out of 1	15.12.2003	

Unit: IKP

Date: 14.03.2011

Participants in the identification process (including their function):

Ida Lien Bjørnstad (student), Magnus Rønning (supervisor), Nina Hammer (co-supervisor)

Short description of the main activity/main process: Photoreforming of methanol

ID no.	Activity/process	Responsible person	Laws, regulations etc.	Existing documentation	Existing safety measures	Comment
P1	Activity measurements with UV lamp	M. Rønning	HMSR-32, strålevernloven, strålevernforskriften, manuals, procedures	Material safety data sheets, manuals		By UV protection goggles
P2	Methanol handling	M. Rønning	AML §4-5, HMSRV-12/13, HMSR-39, HMSR-40, Kjemikalieforskriften	Material safety data sheets	Fume hood	Gloves, safety goggles, lab coat
P3	Calibration of the MS with argon and ethylene	M. Rønning	AML §4-5, HMSRV-12/13, HMSR-39, HMSR-40, Kjemikalieforskriften	Material safety data sheets		Portable gas detector, leakage testing with inert gas before startup

NTNU	Appendix 12 - Risk assessment	Prepared by	Number	Date	
		HSE section	HMSRV-26/03	01.12.2006	
HSE/KS		Approved by	Page	Replaces	
		The Rector	1 out of 2	15.12.2003	

Unit: **IKP**

Date: **14.03.2011**

Line manager:

Participants in the risk assessment (including their function):

Ida Lien Bjørnstad (student), Magnus Rønning (supervisor), Nina Hammer (co-supervisor)

ID no.	Activity from the identification process form	Potential undesirable incident/strain	Likelihood: Consequence:			Risk value	Comments/status Suggested measures
			Likelihood (1-4)	Human (1-4)	Environment (1-4)		
P1	Activity measurements with UV lamp	Exposure of UV radiation	2	C			2C Use UV protection goggles
P2	Methanol handling	Methanol spill/splash	4	B			4B Use gloves, safety goggles, lab coat
P3	Calibration of the MS with argon and ethylene	Gas leakage	2	B			2B Shut the gas bottle when it's not in use
S1	HNO ₃ handling	Spill/splash, inhalation	2	D			2D Use gloves, safety goggles, lab coat
S2	Ammonia handling	Spill/splash, inhalation	2	D			2D Use gloves, safety goggles, lab coat
S3	Titanium isopropoxide handling	Spill/splash	2	B			2B Use gloves, safety goggles, lab coat
S4	Urea handling	Spill/splash, inhalation	2	C			2C Use gloves, safety goggles, lab coat
S5	Calcination	Heat exposure, gas leakage	2	B			2B Remember to check the spot extract, wait with the dismantle of the apparatus until it's cooled

Likelihood, e.g.:

1. Minimal
2. Low
3. High
4. Very high

Consequence, e.g.:



1. Relatively safe
2. Dangerous
3. Critical
4. Very critical

Risk value (each one to be estimated separately):

Human = Likelihood x Human Consequence

Environmental = Likelihood x Environmental consequence

Financial/material = Likelihood x Consequence for Economy/materiel

NTNU	Appendix 12 - Risk assessment	Prepared by	Number	Date	
		HSE section	HMSRV-26/03	01.12.2006	
HSE/KS		Approved by	Page	Replaces	
		The Rector	2 out of 2	15.12.2003	

Potential undesirable incident/strain

Identify possible incidents and conditions that may lead to situations that pose a hazard to people, the environment and any materiel/equipment involved.

Criteria for the assessment of likelihood and consequence in relation to fieldwork

Each activity is assessed according to a worst-case scenario. Likelihood and consequence are to be assessed separately for each potential undesirable incident. Before starting on the quantification, the participants should agree what they understand by the assessment criteria:

<p>The likelihood of something going wrong is to be assessed according to the following criteria:</p> <ol style="list-style-type: none"> 1 Minimal Once every 10 years or less 2 Low Once a year 3 High Once a month 4 Very high Once a week or more often 	<p>Human consequence is to be assessed according to the following criteria:</p> <ol style="list-style-type: none"> 1 Relatively safe Injury that does not involve absence from work; insignificant health risk 2 Dangerous Injury that involves absence from work; may produce acute sickness 3 Critical Permanent injury; may produce serious health damage/sickness 4 Very critical Injury that may produce fatality/ies 	<p>Environmental consequences are assessed according to the following criteria:</p> <ol style="list-style-type: none"> 1 Relatively safe Insignificant impact on the environment 2 Dangerous Possibility of undesirable long term effects; some cleanup is to be expected 3 Critical Undesirable long term effects; cleanup to be expected 4 Very critical Damaging to living organisms; irreversible impact on the environment; cleanup must be undertaken
--	--	--



The unit makes its own decision as to whether opting to fill in or not consequences for economy/materiel, for example if the unit is going to use particularly valuable equipment. It is up to the individual unit to choose the assessment criteria for this column.

Risk = Likelihood x Consequence

Please calculate the risk value for "Human", "Environment" and, if chosen, "Economy/materiel", separately. For activities with a risk value of 16 or 12, or a single value of 4, safety measures (designed to both reduce the likelihood and to limit the consequences) must be documented with descriptions of measures and allocation of responsibility.

About the column "Comments/status, suggested preventative and corrective measures":

Measures can impact on both likelihood and consequences. Prioritise measures that can prevent the incident from occurring; in other words, likelihood-reducing measures are to be prioritised above greater emergency preparedness, i.e. consequence-reducing measures.

NTNU	Appendix 13 - HSE action plan	Prepared by	Number	Date	
		The HSE section	HMSRV-12/24	01.12.2006	
HSE		Approved by	Page	Replaces	
		The Rector	1 of 1	20.08.1999	

Unit: _____ IKP _____

ID no.	Measure	Responsible	By date	Completed/ controlled, date
F1	Buy UV protection goggles	Nina Hammer	20.02	02.03 Magnus Rønning
F2	Use gloves, safety goggles and lab coat	Ida Lien Bjørnstad	20.02	02.03 Magnus Rønning
F3	Portable gas detector, leakage testing with inert gas before startup	Nina Hammer	20.02	02.03 Magnus Rønning
S1	Use gloves, safety goggles and lab coat	Ida Lien Bjørnstad	15.01	16.01 Magnus Rønning
S2	Use gloves, safety goggles and lab coat	Ida Lien Bjørnstad	15.01	16.01 Magnus Rønning
S3	Use gloves, safety goggles and lab coat	Ida Lien Bjørnstad	15.01	16.01 Magnus Rønning
S4	Use gloves, safety goggles and lab coat	Ida Lien Bjørnstad	15.01	16.01 Magnus Rønning
S5	Use gloves, safety goggles and lab coat, check spot extract, let the apparatus cool down before dismantling	Ida Lien Bjørnstad	15.01	16.01 Magnus Rønning

Appendix 14 - Material safety data sheets

Material Safety Data Sheet

Copper (II) Nitrate Hemipentahydrate

ACC# 05646

Section 1 - Chemical Product and Company Identification

MSDS Name: Copper (II) Nitrate Hemipentahydrate

Catalog Numbers: C467-500

Synonyms: Cupric Nitrate Hemipentahydrate; Copper Dinitrate Hemipentahydrate; Nitric Acid Copper Salt Hemipentahydrate.

Company Identification:

Fisher Scientific
1 Reagent Lane
Fair Lawn, NJ 07410

For information, call: 201-796-7100

Emergency Number: 201-796-7100

For CHEMTREC assistance, call: 800-424-9300

For International CHEMTREC assistance, call: 703-527-3887

Section 2 - Composition, Information on Ingredients

CAS#	Chemical Name	Percent	EINECS/ELINCS
19004-19-4	Copper (II) Nitrate, Hemipentahydrate	>98	unlisted

Section 3 - Hazards Identification

EMERGENCY OVERVIEW

Appearance: blue solid.

Danger! Strong oxidizer. Contact with other material may cause a fire. Causes digestive and respiratory tract irritation with possible burns. May cause allergic skin reaction. May cause severe eye and skin irritation with possible burns. May cause liver and kidney damage.

Target Organs: Kidneys, liver.

Potential Health Effects

Eye: Contact with eyes may cause severe irritation, and possible eye burns. Contact may cause ulceration of the conjunctiva and cornea. May cause conjunctivitis. May cause permanent corneal opacification.

Skin: May cause severe irritation and possible burns. May cause dermatitis. May cause skin discoloration.

Ingestion: May cause severe gastrointestinal tract irritation with nausea, vomiting and possible burns. May cause liver and kidney damage. May cause hemorrhaging of the digestive tract. Methemoglobinemia is characterized by dizziness, drowsiness, headache, shortness of breath, cyanosis (bluish discoloration of skin due to deficient oxygenation of the blood), rapid heart rate and chocolate-brown colored blood. May cause nausea, vomiting, and diarrhea, possibly with blood.

Inhalation: May cause methemoglobinemia, cyanosis (bluish discoloration of skin due to

Appendix 14 - Material safety data sheets

deficient oxygenation of the blood), convulsions, tachycardia, dyspnea (labored breathing), and death. May cause ulceration and perforation of the nasal septum if inhaled in excessive quantities. May cause severe irritation of the upper respiratory tract with pain, burns, and inflammation. May cause acute pulmonary edema, asphyxia, chemical pneumonitis, and upper airway obstruction caused by edema.

Chronic: Chronic inhalation and ingestion may cause effects similar to those of acute inhalation and ingestion. May cause liver and kidney damage. May cause methemoglobinemia, which is characterized by chocolate-brown colored blood, headache, weakness, dizziness, breath shortness, cyanosis (bluish skin due to deficient oxygenation of blood), rapid heart rate, unconsciousness and possible death. Individuals with Wilson's disease are unable to metabolize copper. Thus, copper accumulates in various tissues and may result in liver, kidney, and brain damage.

Section 4 - First Aid Measures

Eyes: Immediately flush eyes with plenty of water for at least 15 minutes, occasionally lifting the upper and lower eyelids. Get medical aid.

Skin: Get medical aid. Immediately flush skin with plenty of water for at least 15 minutes while removing contaminated clothing and shoes. Wash clothing before reuse.

Ingestion: Do not induce vomiting. If victim is conscious and alert, give 2-4 cupfuls of milk or water. Get medical aid immediately.

Inhalation: Get medical aid immediately. Remove from exposure and move to fresh air immediately. If breathing is difficult, give oxygen. Do NOT use mouth-to-mouth resuscitation. If breathing has ceased apply artificial respiration using oxygen and a suitable mechanical device such as a bag and a mask.

Notes to Physician: For methemoglobinemia, administer oxygen alone or with Methylene Blue depending on the methemoglobin concentration in the blood.

Antidote: The use of d-Penicillamine as a chelating agent should be determined by qualified medical personnel. Methylene blue, alone or in combination with oxygen is indicated as a treatment in nitrite induced methemoglobinemia.

Section 5 - Fire Fighting Measures

General Information: As in any fire, wear a self-contained breathing apparatus in pressure-demand, MSHA/NIOSH (approved or equivalent), and full protective gear. Strong oxidizer. Contact with other material may cause fire. During a fire, irritating and highly toxic gases may be generated by thermal decomposition or combustion. Wear appropriate protective clothing to prevent contact with skin and eyes. Wear a self-contained breathing apparatus (SCBA) to prevent contact with thermal decomposition products. Use water with caution and in flooding amounts.

Extinguishing Media: Use extinguishing media most appropriate for the surrounding fire. Contact professional fire-fighters immediately.

Flash Point: Not available.

Autoignition Temperature: Not available.

Explosion Limits, Lower: Not available.

Upper: Not available.

NFPA Rating: (estimated) Health: 2; Flammability: 0; Instability: 1; Special Hazard: OX

Section 6 - Accidental Release Measures

Appendix 14 - Material safety data sheets

General Information: Use proper personal protective equipment as indicated in Section 8.

Spills/Leaks: Vacuum or sweep up material and place into a suitable disposal container. Avoid runoff into storm sewers and ditches which lead to waterways. Clean up spills immediately, observing precautions in the Protective Equipment section. Avoid generating dusty conditions. Remove all sources of ignition. Do not use combustible materials such as paper towels to clean up spill.

Section 7 - Handling and Storage

Handling: Wash thoroughly after handling. Use with adequate ventilation. Minimize dust generation and accumulation. Contents may develop pressure upon prolonged storage. Keep away from heat, sparks and flame. Avoid contact with clothing and other combustible materials. Do not get on skin or in eyes. Avoid ingestion and inhalation.

Storage: Keep away from heat, sparks, and flame. Do not store near combustible materials. Store in a tightly closed container. Store in a cool, dry, well-ventilated area away from incompatible substances.

Section 8 - Exposure Controls, Personal Protection

Engineering Controls: Facilities storing or utilizing this material should be equipped with an eyewash facility and a safety shower. Use adequate ventilation to keep airborne concentrations low.

Exposure Limits

Chemical Name	ACGIH	NIOSH	OSHA - Final PELs
Copper (II) Nitrate, Hemipentahydrate	none listed	1 mg/m ³ TWA (dust and mist, as Cu, except copper fume) (listed under Copper compounds, n.o.s.).100 mg/m ³ IDLH (dust and mist, as Cu) (listed under Copper compounds, n.o.s.).	none listed

OSHA Vacated PELs: Copper (II) Nitrate, Hemipentahydrate: No OSHA Vacated PELs are listed for this chemical.

Personal Protective Equipment

Eyes: Wear appropriate protective eyeglasses or chemical safety goggles as described by OSHA's eye and face protection regulations in 29 CFR 1910.133 or European Standard EN166.

Skin: Wear appropriate gloves to prevent skin exposure. Wear impervious gloves.

Clothing: Wear a chemical apron. Wear appropriate clothing to prevent skin exposure.

Respirators: Wear a NIOSH/MSHA or European Standard EN 149 approved full-facepiece airline respirator in the positive pressure mode with emergency escape provisions.

Section 9 - Physical and Chemical Properties

Physical State: Solid

Appearance: blue

Appendix 14 - Material safety data sheets

Odor: odorless

pH: Not available.

Vapor Pressure: Not available.

Vapor Density: Not available.

Evaporation Rate: Not available.

Viscosity: Not available.

Boiling Point: Not available.

Freezing/Melting Point: 255 deg C

Decomposition Temperature: Not available.

Solubility: Soluble in water.

Specific Gravity/Density: >1.0

Molecular Formula: CuN₂O₆·2.5H₂O

Molecular Weight: 224.5896

Section 10 - Stability and Reactivity

Chemical Stability: Stable at room temperature in closed containers under normal storage and handling conditions.

Conditions to Avoid: Incompatible materials, ignition sources, dust generation, combustible materials, reducing agents, organic matter.

Incompatibilities with Other Materials: Reducing agents.

Hazardous Decomposition Products: Oxides of nitrogen, oxides of nitrogen, copper fumes.

Hazardous Polymerization: Has not been reported.

Section 11 - Toxicological Information

RTECS#:

CAS# 19004-19-4 unlisted.

LD50/LC50:

Not available.

Carcinogenicity:

CAS# 19004-19-4: Not listed by ACGIH, IARC, NTP, or CA Prop 65.

Epidemiology: No information found

Teratogenicity: No information found

Reproductive Effects: No information found

Mutagenicity: No information found

Neurotoxicity: No information found

Other Studies:

Section 12 - Ecological Information

No information available.

Section 13 - Disposal Considerations

Chemical waste generators must determine whether a discarded chemical is classified as a hazardous waste. US EPA guidelines for the classification determination are listed in 40 CFR Parts 261.3. Additionally, waste generators must consult state and local hazardous

Appendix 14 - Material safety data sheets

waste regulations to ensure complete and accurate classification.

RCRA P-Series: None listed.

RCRA U-Series: None listed.

Section 14 - Transport Information

	US DOT	Canada TDG
Shipping Name:	NITRATES, INORGANIC, N.O.S.	No information available.
Hazard Class:	5.1	
UN Number:	UN1477	
Packing Group:	II	

Section 15 - Regulatory Information

US FEDERAL

TSCA

CAS# 19004-19-4 is not on the TSCA Inventory because it is a hydrate. It is considered to be listed if the CAS number for the anhydrous form is on the inventory (40CFR720.3(u)(2)).

Health & Safety Reporting List

None of the chemicals are on the Health & Safety Reporting List.

Chemical Test Rules

None of the chemicals in this product are under a Chemical Test Rule.

Section 12b

None of the chemicals are listed under TSCA Section 12b.

TSCA Significant New Use Rule

None of the chemicals in this material have a SNUR under TSCA.

CERCLA Hazardous Substances and corresponding RQs

None of the chemicals in this material have an RQ.

SARA Section 302 Extremely Hazardous Substances

None of the chemicals in this product have a TPQ.

SARA Codes

CAS # 19004-19-4: immediate, delayed, fire.

Section 313

This material contains Copper (II) Nitrate, Hemipentahydrate (listed as Copper compounds, n.o.s.), >98%, (CAS# 19004-19-4) which is subject to the reporting requirements of Section 313 of SARA Title III and 40 CFR Part 373.

Clean Air Act:

This material does not contain any hazardous air pollutants.

This material does not contain any Class 1 Ozone depleters.

This material does not contain any Class 2 Ozone depleters.

Clean Water Act:

None of the chemicals in this product are listed as Hazardous Substances under the CWA.

None of the chemicals in this product are listed as Priority Pollutants under the CWA. CAS# 19004-19-4 is listed as a Toxic Pollutant under the Clean Water Act.

OSHA:

None of the chemicals in this product are considered highly hazardous by OSHA.

STATE

CAS# 19004-19-4 can be found on the following state right to know lists: California, (listed as Copper compounds, n.o.s.), New Jersey, (listed as Copper compounds, n.o.s.), Pennsylvania, (listed as Copper compounds, n.o.s.).

Appendix 14 - Material safety data sheets

California Prop 65

California No Significant Risk Level: None of the chemicals in this product are listed.

European/International Regulations

European Labeling in Accordance with EC Directives

Hazard Symbols:

○

Risk Phrases:

R 8 Contact with combustible material may cause fire.

Safety Phrases:

WGK (Water Danger/Protection)

CAS# 19004-19-4: No information available.

Canada - DSL/NDSL

None of the chemicals in this product are listed on the DSL or NDSL list.

Canada - WHMIS

This product has a WHMIS classification of C, D2B.

This product has been classified in accordance with the hazard criteria of the Controlled Products Regulations and the MSDS contains all of the information required by those regulations.

Canadian Ingredient Disclosure List

CAS# 19004-19-4 (listed as Copper compounds, n.o.s.) is listed on the Canadian Ingredient Disclosure List.

Section 16 - Additional Information

MSDS Creation Date: 9/02/1997

Revision #6 Date: 10/28/2008

SAFETY DATA SHEET

Aceton

1. Identification of the substance/preparation and of the company/undertaking

Date issued	06.12.2005
Revision date	17.11.2009
Product name	Aceton
CAS no.	67-64-1
EC no.	200-662-2
Formula	C ₃ H ₆ O
Use of the substance/preparation	Laboratory chemical
Company name	Halliburton AS
Postal address	Eldfiskvegen 1
Postcode	NO-4065
Place name	Stavanger
Country	Norway
Tel	+47 51837000
Fax	+47 51838383
E-mail	AnneKristin.Haugan@Halliburton.com
Website	http://www.Halliburton.com
Name of contact	Anne Kristin Haugan
Prepared by	National Institute of Technology as, Norway v/ Knut Finsveen
Emergency telephone	Giftinformasjonen:22 59 13 00

2. Hazards identification

Classification according to 67/548/EEC or 1999/45/EC	F; R11 Xi; R36 R66,R67
Description of hazard	Health: Irritating to eyes. Repeated exposure may cause skin dryness or cracking. Vapours may cause drowsiness and dizziness. Fire and explosion: Highly flammable. Environment: The product is not classified as harmful to the environment.

3. Composition/information on ingredients

Component name	Identification	Classification	Contents
Acetone	CAS no.: 67-64-1 EC no.: 200-662-2	Xi, F; R11, R36, R66, R67	100 %
Column headings	CAS no. = Chemical Abstracts Service; EU (Einecs or Elincs number) = European inventory of Existing Commercial Chemical Substances; Ingredient name = Name as specified in the substance list (substances that are not included in the substance list must be translated, if possible). Contents given in; %, %wt/wt, %vol/wt, %vol/vol, mg/m ³ , ppb, ppm, weight%, vol%		
HH/HF/HE	T+ = Very toxic, T = Toxic, C = Corrosive, Xn = Harmful, Xi = Irritating, E = Explosive, O = Oxidizing, F+ = Extremely flammable, F = Very flammable, N = Environmental hazard		
Component comments	See section 16 for explanation of Risk-phrases listed above.		

4. First-aid measures

General	If in doubt, get medical advice.
Inhalation	Fresh air and rest. Get medical attention if any discomfort continues.
Skin contact	Remove contaminated clothing. Wash the skin immediately with soap and water. Get medical attention if any discomfort continues.
Eye contact	Immediately flush with plenty of water for up to 15 minutes. Remove any contact lenses and open eyes wide apart. By prolonged rinsing, use lukewarm water to avoid damage to the eye. Contact physician if irritation persists.
Ingestion	Rinse mouth thoroughly. Drink a few glasses of water or milk. Do not induce vomiting. Get medical attention. Never give liquid to an unconscious person.

5. Fire-fighting measures

Suitable extinguishing media	Dry-powder, carbon dioxide (CO ₂), water mist, foam.
Improper extinguishing media	Do not use water jet.
Fire and explosion hazards	Highly flammable. Vapours may form explosive air mixtures even at room temperature. Hazardous combustion products: Carbon dioxide (CO ₂). Carbon monoxide (CO).
Personal protective equipment	Use fresh air equipment when the product is involved in fire. In case of evacuation, an approved protection mask should be used. See also sect. 8.
Other Information	Containers close to fire should be removed immediately or cooled with water.

6. Accidental release measures

Personal precautions	Use protective equipment as referred to in section 8.
Environmental precautions	Do not allow to enter into sewer, water system or soil.
Methods for cleaning	Absorb in vermiculite, dry sand or earth and place into containers. Collect in suitable containers and deliver as hazardous waste according to section 13.

7. Handling and storage

Handling	Use protective equipment as referred to in section 8. Provide good ventilation. Avoid inhalation of vapours. Avoid contact with skin and eyes. Keep away from sources of ignition - No smoking. Ground container and transfer equipment to eliminate static electric sparks.
Storage	Store in a tightly closed container in a cool, well-ventilated place, protected from heat source. Store in accordance with regulations for flammable goods. To be stored at temperatures between 8 and 15 °C.
Special risks and properties	The vapours may form explosive mixtures with air. The vapours are heavier than air and will spread along the floor.

8. Exposure controls/personal protection

Exposure limit values

Component name	Identification	Value	Year
Acetone	CAS no.: 67-64-1	8 h.: 125 ppm	2007
	EC no.: 200-662-2	8 h.: 295 mg/m ³	

Exposure controls

Occupational exposure controls	Provide adequate ventilation. Do not eat, drink or smoke during work. Personal protection equipment should be chosen according to the CEN standards and in discussion with the supplier of the personal protective equipment
Respiratory protection	Not normally required. If ventilation is insufficient, use a respirator with Ax filter against solvent vapours.

Hand protection	Use protective gloves made of: Butyl rubber. P.T.F.E (Teflon). Penetration time > 8 hours.
Eye protection	If risk of splashing, wear safety goggles or face shield.
Skin protection (other than of the hands)	Wear appropriate protective clothing to protect against skin contact.
Other Information	Eye wash facilities and emergency shower must be available when handling this product. The listed protective equipment is a suggestion. A risk assessment (of actual risk) may lead to other requirements.

9. Physical and chemical properties

Physical state	Fluid
Odour	Acetone, ketone.
Colour	Colourless
Solubility in water	Miscible.
Specific gravity	Value: 0,79 g/cm ³ @ 20 °C
Melting point/melting range	Value: -95 °C
Boiling point	Value: 55 °C
Flash point	Value: -19 °C
Spontaneous combustability	Value: 540 °C
Vapour pressure	Value: 580 hPa
Vapour density	Value: 2 Reference gas: Luft
Decomposition temperature	Value: 236 °C
Solvent content	Value: 100 %

10. Stability and reactivity

Conditions to avoid	Strong heat may lead to decomposition. Avoid heat, flames and other sources of ignition.
Materials to avoid	Strong oxidising substances.
Hazardous decomposition products	Fire or high temperatures create: Carbon dioxide (CO ₂). Carbon monoxide (CO).
Stability	Stable under normal temperature conditions and recommended use.

11. Toxicological information

Other information regarding health hazards

Inhalation	Solvent vapours are hazardous and may cause nausea, sickness and headaches.
Skin contact	Defatting, drying and cracking of skin.
Eye contact	Irritant to eyes.
Ingestion	May irritate and cause stomach pain, vomiting and diarrhoea.
Chronic effects	Repeated inhalation of vapours from organic solvents for longer time may cause permanent brain damage.

12. Ecological information

Other ecological information

Ecotoxicity	The product is not classified as dangerous for the environment.
Mobility	Soluble in water. Mobile.
Persistence and degradability	The product is potentially degradable.
Bioaccumulative potential	Contains components which have bioaccumulative potential.

13. Disposal considerations

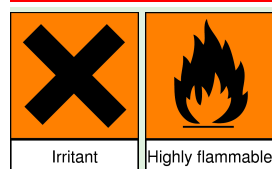
EWC waste code	EWC: 14 06 03 other solvents and solvent mixtures
NORSAS	7042 Organiske løsemidler uten halogen
Product classified as hazardous waste	Yes
Specify the appropriate methods of disposal	Disposed of as hazardous waste by approved contractor. The code for hazardous waste (EWC code) is indicative. The user must be able to set the correct EWC code on the intended use differs.

14. Transport information

Product name (national)	ACETONE
Dangerous goods ADR	UN no.: 1090 Class: 3 Hazard no.: 33 Packing group: II Proper shipping name: ACETONE
Dangerous goods RID	UN no.: 1090 Class: 3 Packing group: II Proper shipping name: ACETONE
Dangerous goods IMDG	UN no.: 1090 Class: 3 Packing group: II EmS: F-E, S-D Proper shipping name: ACETONE
Dangerous goods ICAO/IATA	UN no.: 1090 Class: 3 Packing group: II Proper shipping name: ACETONE

15. Regulatory information

Hazard symbol



EC no.	200-662-2
EC lable	Yes
R phrases	R11 Highly flammable. R36 Irritating to eyes. R66 Repeated exposure may cause skin dryness or cracking. R67 Vapours may cause drowsiness and dizziness.
S phrases	S9 Keep container in a well-ventilated place. S16 Keep away from sources of ignition - No smoking. S26 In case of contact with eyes, rinse immediately with plenty of water and seek medical advice.
References (laws/regulations)	Norwegian regulation on classification and labelling of dangerous chemicals. Valid from April 22, 2009. Directive (EC) No 1907/2006 (REACH) Annex II: Safety data sheets. Administrative norms for pollution of the atmosphere , from Norwegian labour inspection authority. The Hazardous Waste Regulations Dangerous Goods regulations The Safety Data Sheet is based on information provided by the producer.

16. Other information

List of relevant R phrases (under headings 2 and 3).	R11 Highly flammable. R36 Irritating to eyes. R66 Repeated exposure may cause skin dryness or cracking. R67 Vapours may cause drowsiness and dizziness.
Information which has been added, deleted or revised	Layout changed.
Supplier's notes	The information contained in this SDS must be made available to all those who handle the product.
Checking quality of information	This SDS is quality controlled by National Institute of Technology in Norway, certified according to the Quality Management System requirements specified in NS-EN ISO 9001:2000.
Responsible for safety data sheet	Halliburton AS

4. FIRST AID MEASURES

- Skin: • Wash material off the skin with soap and water. Seek medical attention if irritation occurs.
- Eyes: • Flush with copious amounts of water. Seek medical attention if irritation occurs.
- Ingestion: • Give one or two glasses of water to drink. Seek medical attention if gastrointestinal symptoms develop.
- Inhalation: • Remove to fresh air. Seek medical attention if cough or respiratory symptoms develop.

5. FIRE FIGHTING MEASURES

- Flashpoint • Not Applicable.
- Non-flammable • OSHA Method 16CFR1500.44 (Incorporated by reference in 29CFR1910.1200).
- Self-heating substance • May self heat. UN Manual of Tests and Criteria, Test N.3.
- Flammability Limits in Air • LFL and UFL Not Applicable.

GENERAL HAZARD:

Activated carbon is difficult to ignite and tends to burn slowly (smolder) without producing smoke or flame. Toxic gas may form upon combustion. Chemically activated carbons can self-heat under certain conditions.

FIRE FIGHTING INSTRUCTIONS:

If possible to do safely, move smoldering activated carbon to a non-hazardous area, preferably out of doors. Extinguish fire using water fog, fine water spray, carbon dioxide or foam. Avoid stirring up dust clouds.

FIRE FIGHTING EQUIPMENT:

Fire fighting personnel should wear full protective equipment, including self-contained breathing apparatus (SCBA) for all inside fires and large outdoor fires.

HAZARDOUS COMBUSTION PRODUCTS:

Products may include smoke and oxides of carbon (for example, carbon monoxide). Materials allowed to smolder for long periods in enclosed spaces, may produce amounts of carbon monoxide, which reach the lower explosive limit (carbon monoxide LEL = 12.5% in air). Under certain conditions, any airborne dust may be an explosion hazard. Used activated carbon may produce additional combustion products.

6. ACCIDENTAL RELEASE MEASURES

IF A SPILL OR LEAK OCCURS:

Clean up spills in a manner that does not disperse dust into the air. Handle in accordance with good industrial hygiene and safety practices. These practices include avoiding unnecessary exposure, and removal of material from eyes, skin, and clothing.

DISPOSAL METHOD:

Dispose of virgin (unused) carbon (waste or spillage) in a facility permitted for non-hazardous wastes. Spent (used) carbon should be disposed of in accordance with applicable laws.

CONTAINER DISPOSAL:

Do not reuse empty bags. Dispose of used bags in facility permitted for non-hazardous wastes.

7. HANDLING AND STORAGE

IF A SPILL OR LEAK OCCURS:

Clean up spills in a manner that does not disperse dust into the air. Handle in accordance with good industrial hygiene and safety practices. These practices include avoiding unnecessary exposure, and removal of material from eyes, skin, and clothing.

DISPOSAL METHOD:

Dispose of virgin (unused) carbon (waste or spillage) in a facility permitted for non-hazardous wastes. Spent (used) carbon should be disposed of in accordance with applicable laws.

CONTAINER DISPOSAL:

Do not reuse empty bags. Dispose of used bags in facility permitted for non-hazardous wastes.

8. EXPOSURE CONTROLS / PERSONAL PROTECTION

- Engineering Controls:
- Use local exhaust ventilation to control emissions near the source. Ventilation systems should be sized and configured to prevent exceedence of recommended or regulated exposure limits (for example, OSHA PELs).
- Eye Protection:
- Safety glasses with side shields are recommended for any type of handling. Where eye contact or dusty conditions may be likely, dust tight goggles are recommended. Have eye-flushing equipment available.
- Skin Protection:
- Avoid skin contact with this product. Wear appropriate dust resistant clothing. Wash contaminated clothing and clean protective equipment before reuse. Wash skin thoroughly after handling.
- Respiratory Protection:
- Keep dust exposure to a minimum with engineering and administrative controls. Use appropriate NIOSH/MSHA approved particulate respirators if necessary. Observe respirator use limitations specified by NIOSH/MSHA or the manufacturer.

Airborne Exposure Guidelines:

Recommended Exposure Limits 8-hr TWA	Activated Carbons
Total Dust	10 mg/m ³ *
Respirable Fraction	3 mg/m ³ *

*OSHA and ACGIH have not established specific exposure limits for this material. The recommended exposure limits for these activated carbon products are base on the Threshold Limit Values adopted by ACGIH for Particulates (insoluble) Not Otherwise Classified. The OSHA PEL for Nuisance Dust is 15 mg/m³ (5 mg/m³ respirable fraction).

9. PHYSICAL AND CHEMICAL PROPERTIES

Boiling Point, C:	• NA	Freezing Point, C:	• NA
Bulk Density - Powder Grades	• 12-30 lbs/ft ³	% Volatiles	• NA
Vapor Pressure	• NA	Solubility in Water	• Insoluble
Vapor Density	• NA	Appearance and Odor	• Black powder with no odor
Evaporation Rate	• NA		

NA - Not applicable

10. STABILITY AND REACTIVITY DATA

- Stability:
- This product is stable under the specified conditions of storage, shipment and use. Avoid storing at high temperatures or in direct sunlight.
- Incompatibility:
- Contact with strong oxidizers such as ozone, liquid oxygen, chlorine, permanganate, etc. may result in rapid combustion. Avoid contact with strong acids.
- Hazardous Decomposition Products:
- Oxides of Carbon
- Hazardous Polymerization:
- Does not occur.

11. TOXICOLOGICAL INFORMATION

This material is non-toxic. Used activated carbon may exhibit characteristics of the adsorbed material.

12. ECOLOGICAL INFORMATION

This material, in its original state, is not harmful to the environment. Used activated carbon may exhibit characteristics of the adsorbed material.

13. DISPOSAL CONSIDERATIONS

In its original state, this product is not a hazardous material or hazardous waste. Follow applicable governmental regulations for waste disposal.

Used activated carbon may become classified as a hazardous waste depending upon the application. Follow applicable regulations for disposal.

14. TRANSPORT INFORMATION

DOT (Department of Transportation)

Proper Shipping Name:	• Carbon, Activated
Hazard Class:	• 4.2
UN Number:	• 1362
Packing Group:	• III
Freight Classification:	• STCC Code - #4916185 NMFC 040560

15. REGULATORY INFORMATION

FEDERAL REGULATIONS:

OSHA Hazard Communication Standard, 29CFR1910.1200:	• See "Particulates not otherwise regulated," in Table Z-1, of 29CFR1910.1000, "Limits For Air Contaminates".
CERCLA/SUPERFUND, 40CFR117, 302:	• Notification of spills of this material is not required.
SARA/SUPERFUND:	• Section 302 – Extremely hazardous substances (40CFR355): This product is not listed as an extremely hazardous substance.
	• Section 313 – List of toxic chemicals: This product is not listed.
Toxic Substances Control Act, 40CFR710:	• This product is on the inventory list.
Resource Conservation and Recovery Act:	• This product, in its original state, does not meet the criteria of hazardous waste.

STATE REGULATIONS:

California Occupational Safety and Health	• Not listed.
Massachusetts Substance List	• Not listed.
New Jersey Right-To-Know	• Not listed.
Pennsylvania Right-To-Know	• Not listed.

16. OTHER INFORMATION

Activated carbon can be safely stored in any normal storage area, but away from sources of direct heat. **Storage at elevated temperatures or in direct sunlight may contribute to spontaneous combustion of this product.** This product is a self-heating substance (UN Manual of Tests and Criterion, Second Revised Edition. Test N.3.) Storage at high ambient temperature may exacerbate the self-heating tendency.

WARNING: Activated carbon (especially when wet) can deplete oxygen from the air, and dangerously low levels of oxygen may result. When workers enter a vessel containing activated carbon, procedures for potentially low oxygen areas should be followed.

REVISION SUMMARY:

REV 03: New format.
REV 02: Added new product, NORIT CNP SUPER, to product list in Section 1.
REV 01: Added new products, NORIT CAP SUPER, NORIT CGSP and NORIT CNSP.
REV 00: New MSDS

The information herein is given in good faith but no warranty, expressed or implied, is made.



MATERIAL SAFETY DATA SHEET

Ammonium hydroxide water solution, >14N NH₄OH (25-30% as ammonia, NH₃)

Section 1 - Chemical Product and Company Identification

MSDS Name: Ammonium hydroxide water solution, >14N NH₄OH (25-30% as ammonia, NH₃)

Catalog Numbers: A/3222/21, A/3222/PB17, A/3240/PB15, A/3240/PB17, A/3280/21, A/3280/25, A/3280/PB15, A/3280/PB17, A/3285/PB17, A/3290/PB08, A/3290/PB15, A/3295/PB05, A/3320/PB17, A/3360/99, A/3360/PB15, A/3360/PB17, J/9015/08

Synonyms: Ammonium hydrate; Ammonia solution; Ammonia water; Aqueous ammonia; Aqua ammonia.

Company Identification: Fisher Scientific UK
Bishop Meadow Road, Loughborough
Leics. LE11 5RG

For information in Europe, call: (01509) 231166

Emergency Number, Europe: 01509 231166

Section 2 - Composition, Information on Ingredients

CAS#	Chemical Name:	%	EINECS#	Hazard Symbols:	Risk Phrases:
7664-41-7	Ammonia	25-30	231-635-3		
7732-18-5	Water	70-75	231-791-2		

Text for R-phrases: see Section 16

Hazard Symbols: C N



Risk Phrases: 34 50

Section 3 - Hazards Identification

EMERGENCY OVERVIEW

Causes burns. Very toxic to aquatic organisms.

Potential Health Effects

- Eye:** Contact with liquid or vapor causes severe burns and possible irreversible eye damage. Lachrymator (substance which increases the flow of tears).
- Skin:** Causes severe skin irritation. Causes skin burns. May cause deep, penetrating ulcers of the skin. Contact with the skin may cause staining, inflammation, and thickening of the skin.
- Ingestion:** Harmful if swallowed. May cause severe and permanent damage to the digestive tract. Causes gastrointestinal tract burns. Causes throat constriction, vomiting, convulsions, and shock.
- Inhalation:** Effects may be delayed. Causes severe irritation of upper respiratory tract with coughing, burns, breathing difficulty, and possible coma.
- Chronic:** Prolonged inhalation may cause respiratory tract inflammation and lung damage. Prolonged or repeated exposure may cause corneal damage and the development of cataracts and glaucoma.

Section 4 - First Aid Measures

Eyes:	In case of contact, immediately flush eyes with plenty of water for at least 15 minutes. Get medical aid immediately.
Skin:	In case of contact, immediately flush skin with plenty of water for at least 15 minutes while removing contaminated clothing and shoes. Get medical aid immediately. Wash clothing before reuse.
Ingestion:	If swallowed, do NOT induce vomiting. Get medical aid immediately. If victim is fully conscious, give a cupful of water. Never give anything by mouth to an unconscious person.
Inhalation:	If inhaled, remove to fresh air. If not breathing, give artificial respiration. If breathing is difficult, give oxygen. Get medical aid.
Notes to Physician:	After inhalation exposure, observe for 24 to 72 hours as pulmonary edema may be delayed.

Section 5 - Fire Fighting Measures

General Information:	As in any fire, wear a self-contained breathing apparatus in pressure-demand, MSHA/NIOSH (approved or equivalent), and full protective gear. During a fire, irritating and highly toxic gases may be generated by thermal decomposition or combustion. Use water spray to keep fire-exposed containers cool. Contact with metals may evolve flammable hydrogen gas. Containers may explode when heated. Approach fire from upwind to avoid hazardous vapors and toxic decomposition products. Ammonium hydroxide itself is non-combustible. However concentrated ammonia solutions may give off ammonia vapours. Ammonia gas is generally not considered a serious fire or explosion hazard because ammonia/air mixtures are difficult to ignite. A relatively high concentration of ammonia gas must be present in order for ignition to occur. However, a large and intense energy source may cause ignition and/or explosion in a confined space.
Extinguishing Media:	Use extinguishing media most appropriate for the surrounding fire.

Section 6 - Accidental Release Measures

General Information:	Use proper personal protective equipment as indicated in Section 8.
Spills/Leaks:	Absorb spill with inert material (e.g. vermiculite, sand or earth), then place in suitable container. Neutralize spill with a weak acid such as vinegar or acetic acid. Avoid runoff into storm sewers and ditches which lead to waterways. Clean up spills immediately, observing precautions in the Protective Equipment section. Provide ventilation. Approach spill from upwind.

Section 7 - Handling and Storage

Handling:	Wash thoroughly after handling. Remove contaminated clothing and wash before reuse. Do not get in eyes, on skin, or on clothing. Keep container tightly closed. Discard contaminated shoes. Do not breathe vapor. Use only with adequate ventilation.
Storage:	Do not store in direct sunlight. Store in a tightly closed container. Store in a cool, dry, well-ventilated area away from incompatible substances. Corrosives area. Isolate from oxidizing materials and acids. Walls, floors, shelving, fittings, lighting and ventilation systems in storage area should be made from carbon steel or stainless steel which do not react with ammonium hydroxide.

Section 8 - Exposure Controls, Personal Protection

Engineering Controls:	Use process enclosure, local exhaust ventilation, or other engineering controls to control airborne levels below recommended exposure limits. Facilities storing or utilizing this material should be equipped with an eyewash facility and a safety shower.
Exposure Limits	

CAS# 1336-21-6:

CAS# 7664-41-7:

United Kingdom, WEL - TWA: 25 ppm TWA (anhydrous); 18 mg/m³ TWA (anhydrous) United Kingdom, WEL - STEL: 35 ppm STEL (anhydrous); 25 mg/m³ STEL (anhydrous)

United States OSHA: 50 ppm TWA; 35 mg/m³ TWA

Belgium - TWA: 20 ppm TWA; 14 mg/m³ TWA Belgium - STEL: 50 ppm STEL; 36 mg/m³ STEL

France - VME: 10 ppm VME (restrictive limit); 7 mg/m³ VME (restrictive limit)

France - VLE: 20 ppm VLCT (restrictive limit); 14 mg/m³ VLCT (restrictive limit)

Japan: 25 ppm OEL; 17 mg/m³ OEL

Malaysia: 25 ppm TWA; 17 mg/m³ TWA

Netherlands: 50 ppm STEL; 36 mg/m³ STEL Netherlands: 20 ppm MAC; 14 mg/m³ MAC

Spain: 20 ppm VLA-ED (indicative limit value); 14 mg/m³ VLA-ED (indicative limit value) Spain: 50 ppm VLA-EC (indicative limit value); 36 mg/m³ VLA-EC (indicative limit value)

CAS# 7732-18-5:

Personal Protective Equipment

Eyes: Wear chemical splash goggles and face shield.

Skin: Wear appropriate gloves to prevent skin exposure.

Clothing: Wear appropriate protective clothing to prevent skin exposure.

Respirators: Follow the OSHA respirator regulations found in 29 CFR 1910.134 or European Standard EN 149. Use a NIOSH/MSHA or European Standard EN 149 approved respirator if exposure limits are exceeded or if irritation or other symptoms are experienced.

Section 9 - Physical and Chemical Properties

Physical State: Liquid

Color: colorless

Odor: strong odor - ammonia-like

pH: 13.6

Vapor Pressure: 557 mm Hg @ 21 deg C

Viscosity: Not available

Boiling Point: 27 deg C (80.60°F)

Freezing/Melting Point: -69 deg C (-92.20°F)

Autoignition Temperature: Not applicable

Flash Point: Not available

Explosion Limits: Lower: Not available

Explosion Limits: Upper: Not available

Decomposition Temperature: Not available

Solubility in water: Soluble

Specific Gravity/Density: 0.89

Molecular Formula: NH₄OH

Molecular Weight: 35.04

Section 10 - Stability and Reactivity

Chemical Stability: Stable under normal temperatures and pressures. Ammonium hydroxide is

actually a solution of ammonia in water. Therefore the flammable properties of ammonia apply.

- Conditions to Avoid:** High temperatures, confined spaces, Ammonia solutions are corrosive to copper, zinc, aluminum and their alloys..
- Incompatibilities with Other Materials** Strong oxidizing agents, acids, acrolein, halogens, mercury, hypochlorite, silver nitrate, acrylic acid, dimethyl sulfate, silver oxide.
- Hazardous Decomposition Products** Nitrogen oxides (NOx) and ammonia (NH3).
- Hazardous Polymerization** Will not occur.

Section 11 - Toxicological Information

- RTECS#:** CAS# 1336-21-6: BQ9625000
CAS# 7664-41-7: BO0875000
CAS# 7732-18-5: ZC0110000
- LD50/LC50:** RTECS:
CAS# 1336-21-6: Draize test, rabbit, eye: 250 ug Severe;
Draize test, rabbit, eye: 44 ug Severe;
Oral, rat: LD50 = 350 mg/kg;
- RTECS:
CAS# 7664-41-7: Inhalation, mouse: LC50 = 4230 ppm/1H;
Inhalation, mouse: LC50 = 4600 mg/m³/2H;
Inhalation, rabbit: LC50 = 7 gm/m³/1H;
Inhalation, rat: LC50 = 2000 ppm/4H;
Inhalation, rat: LC50 = 18600 mg/m³/5M;
Inhalation, rat: LC50 = 7040 mg/m³/30M;
Skin, rat: LD50 = 112000 mg/m³/15M;
Skin, rat: LD50 = 71900 mg/m³/30M;
Skin, rat: LD50 = 4840 mg/m³/60M;
- RTECS:
CAS# 7732-18-5: Oral, rat: LD50 = >90 mL/kg;
- Carcinogenicity:** Ammonium hydroxide - Not listed as a carcinogen by ACGIH, IARC, NTP, or CA Prop 65.
Ammonia - Not listed as a carcinogen by ACGIH, IARC, NTP, or CA Prop 65.
Water - Not listed as a carcinogen by ACGIH, IARC, NTP, or CA Prop 65.
- Other:** See actual entry in RTECS for complete information.

Section 12 - Ecological Information

- Ecotoxicity:** Fish: Rainbow trout: LC50 = 0.008 mg/L; 24 Hr.; Unspecified
Fish: Fathead Minnow: LC50 = 8.2 mg/L; 96 Hr.; Unspecified
Fish: Bluegill/Sunfish: LC50 = 0.024-0.093 mg/L; 48 Hr.; Unspecified
Water flea Daphnia: EC50 = 0.66 mg/L; 48 Hr.; 22 degrees C

Section 13 - Disposal Considerations

Products considered hazardous for supply are classified as Special Waste and the disposal of such chemicals is covered by regulations which may vary according to location. Contact a specialist disposal company or the local authority or advice. Empty containers must be decontaminated before returning for recycling.

Section 14 - Transport Information

	IATA	IMO	RID/ADR
Shipping Name:	AMMONIA SOLUTION	AMMONIA SOLUTION	AMMONIA SOLUTION
Hazard Class:	8	8	8
UN Number:	2672	2672	2672
Packing Group:	III	III	III

USA RQ: CAS# 1336-21-6: 1000 lb final RQ; 454 kg final RQ

USA RQ: CAS# 7664-41-7: 100 lb final RQ; 45.4 kg final RQ

Section 15 - Regulatory Information

European/International Regulations

European Labeling in Accordance with EC Directives

Hazard Symbols: C N

Risk Phrases:

R 34 Causes burns.

R 50 Very toxic to aquatic organisms.

Safety Phrases:

S 26 In case of contact with eyes, rinse immediately with plenty of water and seek medical advice.

S 36/37/39 Wear suitable protective clothing, gloves and eye/face protection.

S 45 In case of accident or if you feel unwell, seek medical advice immediately (show the label where possible).

S 61 Avoid release to the environment. Refer to special instructions/safety data sheets.

WGK (Water Danger/Protection)

CAS# 1336-21-6: 2

CAS# 7664-41-7: 2

CAS# 7732-18-5: Not available

Canada

CAS# 1336-21-6 is listed on Canada's DSL List

CAS# 7664-41-7 is listed on Canada's DSL List

CAS# 7732-18-5 is listed on Canada's DSL List

US Federal

TSCA

CAS# 1336-21-6 is listed on the TSCA Inventory.

CAS# 7664-41-7 is listed on the TSCA Inventory.

CAS# 7732-18-5 is listed on the TSCA Inventory.

Section 16 - Other Information

Text for R-phrases from Section 2

MSDS Creation Date: 6/22/1999

Revision #16 Date 4/28/2008

The information above is believed to be accurate and represents the best information currently available to us. However, we make no warranty of merchantability or any other warranty, express or implied, with respect to such information, and we assume no liability resulting from its use. Users should make their own investigations to determine the suitability of the information for their particular purposes. In no event shall the company be liable for any claims, losses, or damages of any third party or for lost profits or any special, indirect, incidental, consequential, or exemplary damages howsoever arising, even if the company has been advised of the possibility of such damages.

SAFETY DATA SHEET

NITRIC ACID 20-70%

1. Identification of the substance/preparation and of the company/undertaking

Date issued	02.11.2005
Revision date	22.10.2007
Product name	NITRIC ACID 20-70%
Synonyms	Nitric acid 53%. Nitric acid 62%.
CAS no.	7697-37-2
EC no.	231-714-2
Index no.	007-004-00-1
Formula	HNO ₃
Use of the substance/preparation	Chemical / technical use.

Downstream user

Company name	SOLBERG INDUSTRI AS
Office address	Rosenlund Allé
Postal address	Boks 628
Postcode	1616
Place name	FREDRIKSTAD
Country	Norge
Tel	69382908
Fax	69382901
E-mail	cathrine.lillestrand@solbergindustri.no
Website	http://www.solbergindustri.no/
Name of contact	Cathrine Lillestrand
Prepared by	National Institute of Technology as, Norway v/ Monica Rustad

2. Hazards identification

Classification according to 67/548/EEC or 1999/45/EC	C; R35
Description of hazard	Health: Causes severe burns.
	Fire and explosion: The product is not classified as flammable.
	Environment: The product is not considered to be dangerous to the environment.

3. Composition/information on ingredients

Component name	Identification	Classification	Contents
Nitric acid...%	CAS no.: 7697-37-2 EC no.: 231-714-2 Index no.: 007-004-00-1	C,O; R8,R35	20 - 70 %
Water	CAS no.: 7732-18-5 EC no.: 231-791-2		30 - 80 %
Column headings	CAS no. = Chemical Abstracts Service; EU (Einecs or Elincs number) = European inventory of Existing Commercial Chemical Substances; Ingredient name = Name as specified in the substance list (substances that are not included in the substance list must be translated, if possible). Contents given in; %, %wt/wt, %vol/wt, %vol/vol, mg/m ³ , ppb, ppm, weight%, vol%		

HH/HF/HE	T+ = Very toxic, T = Toxic, C = Corrosive, Xn = Harmful, Xi = Irritating, E = Explosive, O = Oxidizing, F+ = Extremely flammable, F = Very flammable, N = Environmental hazard
Component comments	See section 16 for explanation of Risk-phrases listed above.

4. First-aid measures

General	If in doubt, get medical advice.
Inhalation	Fresh air and rest. In case of unconsciousness, loosen tight fitting clothing. If respiratory problems, provide artificial respiration or oxygen. Seek medical advice.
Skin contact	Remove contaminated clothing. Wash the skin immediately with soap and water. Continue to rinse for at least 15 minutes. Contact physician if irritation continues or sores develop.
Eye contact	Immediately flush with plenty of water for up to 15 minutes. Remove any contact lenses and open eyelids widely. If irritation persists: Continue flushing during transport to hospital. Take along these instructions.
Ingestion	Immediately give a couple of glasses of water or milk, provided the victim is fully conscious. Do not induce vomiting. Risk of perforation of esophagus and stomach. Get medical attention.
Information for health personnel	Do not neutralize with Sodium bicarbonate or Calcium carbonate if the product has been ingested perorally.

5. Fire-fighting measures

Suitable extinguishing media	Use fire-extinguishing media appropriate for surrounding materials.
Improper extinguishing media	Do not use water jet.
Fire and explosion hazards	The product is not classified as flammable. May form toxic or explosive vapours in presence of certain metals. Hydrogen gas. Fire or high temperatures create: Nitrous gases (NOx).
Personal protective equipment	Use fresh air equipment when the product is involved in fire. In case of evacuation, an approved protection mask should be used. See also sect. 8.
Other Information	Containers close to fire should be removed immediately or cooled with water.

6. Accidental release measures

Personal precautions	Use protection equipment as given in section 8. Look out! The product is corrosive. Warn everybody of potential hazards and evacuate if necessary.
Environmental precautions	Do not allow to enter into sewer, water system or soil.
Methods for cleaning	Neutralise small amounts with sodium bicarbonate or lime and flush to sewer with large amounts of water. Large Spillages: Collect with absorbent, non-combustible material into suitable containers. Collect in suitable containers and deliver as hazardous waste according to section 13.

7. Handling and storage

Handling	Use safety equipment as given in section 8. Never add water directly to this product - may cause vigorous reaction/boiling. Always dilute by carefully pouring the product into the water. Provide good ventilation. Avoid inhalation of vapours. Avoid contact with skin and eyes.
Storage	Store in original packaging. Store in a tightly closed container in a cool, well-ventilated room, protected from direct sunlight. Store separated from: Strong bases. Metals

8. Exposure controls/personal protection

Exposure limit values

Component name	Identification	Value	Year
Nitric acid...%	CAS no.: 7697-37-2 EC no.: 231-714-2 Index no.: 007-004-00-1	8 h.: 5,2 mg/m ³ 15 min.: 10 mg/m ³ 15min	

Exposure controls

Other Information about threshold limit values	The given safety equipment is a suggestion. Risk assessment (actual risk) may lead to other requirements.
Occupational exposure controls	Provide adequate ventilation. No eating, drinking or smoking while working with this material.
Respiratory protection	In case of inadequate ventilation: Use respiratory equipment with gas filter, type B. Use filtercombination B/P2 with aerosols.
Hand protection	Use gloves from resistant material, eg.: Butyl eller viton. Penetration time > 8 hours.
Eye protection	Use approved safety goggles or face shield.
Skin protection (other than of the hands)	Wear appropriate protective clothing to protect against possible skin contact.
Other Information	Eye wash facilities and emergency shower must be available when handling this product.

9. Physical and chemical properties

Physical state	Fluid
Odour	Slightly pungent odour Suffocating.
Colour	Clear. Colourless
Solubility in water	Soluble
Specific gravity	Value: 1,38 g/cm ³ Comments: (62 %)
Melting point/melting range	Value: -24-0 °C
Boiling point	Value: 0-116,4 °C
pH (aqueous solution)	Value: < 1

10. Stability and reactivity

Conditions to avoid	Do not add water directly to the product. It may cause a violent reaction. In contact with metals generates hydrogen gas, which together with air can form explosive mixtures. Heating.
Materials to avoid	Amines. Strong oxidising substances. Strong bases. Alcohols. Aniline. Toluene. Acetone. Carbides. Hydrogen sulphides. Nitrobenzene. Acetic acid. Metals.
Hazardous decomposition products	Nitrous gases (NO _x). Hydrogen.
Stability	Stable under normal temperature conditions and recommended use.

11. Toxicological information

Other information regarding health hazards

General	In industrial use, the corrosive properties represents the highest level of danger.
Inhalation	Irritating to respiratory system. May cause damage to mucous membranes in nose, throat, lungs and bronchial system.
Skin contact	Causes burns.
Eye contact	Strongly corrosive. Causes severe pains. Immediate first aid is imperative. Vapour or spray may cause eye damage, impaired sight or blindness.
Ingestion	Strongly corrosive. Even small amounts may cause very severe internal damage and may be fatal.
Sensitisation	Sensitizing properties are not known.
Carcinogenicity	Carcinogenic properties are not known.

Teratogenic properties	Effects on fetus development are not known.
Reproductive toxicity	Effects harmful to reproduction are not known.
Mutagenicity	Mutagenic properties are not known.

12. Ecological information

Other ecological information

Ecotoxicity	The product is not considered to be dangerous to the environment.
Mobility	Soluble in water.
Persistence and degradability	Is readily biologically degradable.
Bioaccumulative potential	Not expected to bioaccumulate.
Other adverse effects / Remarks	Acids cause decreased pH in the water, this may cause fish-kill.

13. Disposal considerations

EWC waste code	EWC: 06 01 05 nitric acid and nitrous acid
Product classified as hazardous waste	Yes
Specify the appropriate methods of disposal	Deliver as hazardous waste according to the local regulations. The hazardous waste code (EWC/ EAL)-Code) is intended as a guide. The code must be given by the user if the use differs from the one given here.

14. Transport information

Proper Shipping Name	NITRIC ACID
Product name (national)	NITRIC ACID
Dangerous goods ADR	Status: Yes UN no.: 2031 Class: 8 Hazard no.: 80 Packing group: II
Dangerous goods RID	Status: Yes UN no.: 2031 Class: 8 Packing group: II
Dangerous goods IMDG	Status: Yes UN no.: 2031 Class: 8 Packing group: II IMDG Marine pollutant: N EmS: F-A, S-B
Dangerous goods ICAO/IATA	Status: Yes UN no.: 2031 Class: 8 Packing group: II
Hazard label	8

15. Regulatory information

Hazard symbol



Corrosive

Composition on the label	Nitric acid...%: 20 - 70 %
--------------------------	----------------------------

EC no.	231-714-2
R phrases	R35 Causes severe burns.
S phrases	S1/2 Keep locked up and out of the reach of children. S23 Do not breathe vapour/spray S26 In case of contact with eyes, rinse immediately with plenty of water and seek medical advice. S36/37/39 Wear suitable protective clothing, gloves and eye/faceprotection. S38 In case of insufficient ventilation, wear suitable respiratory equipment. S45 In case of accident or if you feel unwell, seek medical advice immediately (show the label where possible).
References (laws/regulations)	CHIPS Regulation. Regulation regarding compiling of material safety data sheets Occupational Exposure Limits. EH40/2005. Regulation on Hazardous Waste. Dangerous goods regulation. The Material Safety Data Sheet is made on the basis of information given by the producer.
Declaration no.	53%: 82404. 62%: 32048.

16. Other information

List of relevant R phrases (under headings 2 and 3).	R35 Causes severe burns. R8 Contact with combustible material may cause fire.
Information which has been added, deleted or revised	Version: 1(02.11.2005). Amendment : 1-16. Responsible: ST. Version: 2(22.10.2007). Amendment : 1-16. Responsible: MR.
Supplier's notes	Information in this document is to be made available for all who handle the product.
Checking quality of information	This MSDS is quality controlled by National institute of Technology, Norway, which complies with the Quality Management System requirements specified in NS-EN ISO 9001:2000.
Responsible for safety data sheet	SOLBERG INDUSTRI AS

SAFETY DATA SHEET

Dye Marker E+

1. Identification of the substance/preparation and of the company/undertaking

Date issued	20.08.2006
Revision date	15.09.2009
Product name	Dye Marker E+
Formula	TiO ₂
Use of the substance/preparation	Pigment
Company name	Halliburton AS
Postal address	Eldfiskvegen 1
Postcode	NO-4065
Place name	Stavanger
Country	Norway
Tel	+47 51837000
Fax	+47 51838383
E-mail	AnneKristin.Haugan@Halliburton.com
Website	http://www.Halliburton.com
Name of contact	Anne Kristin Haugan
Prepared by	National Institute of Technology as, Norway v/ John-Kåre Egeland
Emergency telephone	Toxic information::22 59 13 00

2. Hazards identification

Description of hazard	Health: The product is not classified as hazardous to health. Fire and explosion: The product is not classified as flammable. Environment: The product is not classified as harmful to the environment.
Other hazards	Refer to section 5, 11 and 12 for complementary information.

3. Composition/information on ingredients

Component comments	No hazardous substances subject to listing.
--------------------	---

4. First-aid measures

General	If in doubt, get medical advice.
Inhalation	Fresh air and rest. Get medical attention if any discomfort continues.
Skin contact	Remove contaminated clothing. Wash the skin immediately with soap and water. Contact physician if symptoms appears.
Eye contact	Promptly wash eyes with plenty of water while lifting the eye lids. Continue to rinse for at least 15 minutes. Remove any contact lenses. By prolonged rinse, use lukewarm water to avoid damage to the eye. Contact physician if irritation persists.
Ingestion	Rinse mouth thoroughly. Drink a few glasses of water or milk. Do not induce vomiting. Get medical attention. Never give liquid to an unconscious person.

5. Fire-fighting measures

Suitable extinguishing media	Use fire-extinguishing media appropriate for surrounding materials.
Fire and explosion hazards	The product is not classified as flammable.
Personal protective equipment	Use fresh air equipment when the product is involved in fire. In case of

evacuation, an approved protection mask should be used. See also sect. 8.

6. Accidental release measures

Personal precautions	Use protective equipment as referred to in section 8.
Environmental precautions	Do not allow to enter into sewer, water system or soil.
Methods for cleaning	Collect powder using special dust vacuum cleaner with particle filter or carefully sweep into closed container. Collect in suitable containers and deliver as waste according to section 13.

7. Handling and storage

Handling	Use protective equipment as referred to in section 8. Provide adequate ventilation. Use work methods which minimise dust production. Avoid inhalation of dust. Avoid contact with eyes.
Storage	Keep containers tightly closed and dry.

8. Exposure controls/personal protection

Exposure limit values

Component name	Identification	Value	Year
Titanium dioxide	CAS no.: 13463-67-7 EC no.: 236-675-5	8 h.: 5 mg/m ³	2007

Exposure controls

Occupational exposure controls	Provide adequate ventilation. Do not eat, drink or smoke during work. Personal protection equipment should be chosen according to the CEN standards and in discussion with the supplier of the personal protective equipment
Respiratory protection	In case of inadequate ventilation or risk of inhalation of dust, use suitable respiratory equipment with particle filter (type P2).
Hand protection	Use gloves suitable for the work. Penetration time is not relevant, since the product is solid.
Eye protection	Use tight fitting goggles if dust is generated.
Skin protection (other than of the hands)	Wear appropriate clothing to prevent repeated or prolonged skin contact.
Other Information	Eye wash facilities should be available when handling this product. The listed protective equipment is a suggestion. A risk assessment (of actual risk) may lead to other requirements.

9. Physical and chemical properties

Physical state	Powder.
Odour	No characteristic odour.
Colour	White
Solubility in water	Insoluble.
Specific gravity	Value: 3,9 g/cm ³
Melting point/melting range	Value: > 1800 °C

10. Stability and reactivity

Conditions to avoid	Reacts with metals at high temperatures.
Hazardous decomposition products	None under normal conditions.
Stability	Stable under normal temperature conditions and recommended use.

11. Toxicological information

Other information regarding health hazards

Inhalation	Dust may irritate respiratory system or lungs.
Skin contact	Prolonged and repeated contact can cause drying of the skin.
Eye contact	Dust may irritate eyes mechanically.
Ingestion	May irritate and cause stomach pain, vomiting and diarrhoea.

12. Ecological information

Other ecological information

Ecotoxicity	The product is not classified as dangerous for the environment.
Mobility	Insoluble in water.
Persistence and degradability	The product is not readily biodegradable.
Bioaccumulative potential	Will not bio-accumulate.

13. Disposal considerations

EWC waste code	EWC: 08 03 13 waste ink other than those mentioned in 08 03 12
Product classified as hazardous waste	No
Specify the appropriate methods of disposal	Deliver to approved depot. The waste code (EWC-Code) is intended as a guide. The code must be chosen by the user, if the use differs from the one mentioned above.

14. Transport information

Other applicable information.	Not considered as dangerous goods under UN, IMO, ADR/RID or IATA/ICAO regulations.
-------------------------------	--

15. Regulatory information

S phrases	S22 Do not breathe dust.
References (laws/regulations)	Norwegian regulation on classification and labelling of dangerous chemicals. Valid from April 22, 2009. Directive (EC) nr 1907/2006 (REACH) Annex II: Safety data sheets. Administrative norms for pollution of the atmosphere, from Norwegian labour inspection authority. Regulation on Hazardous Waste. Dangerous goods regulation.
	The Safety Data Sheet is based on information provided by the producer.

16. Other information

Information which has been added, deleted or revised	Layout changed.
Supplier's notes	The information contained in this SDS must be made available to all those who handle the product.
Checking quality of information	This SDS is quality controlled by National institute of Technology in Norway, certified according to the Quality Management System requirements specified in NS-EN ISO 9001:2000.
Responsible for safety data sheet	Halliburton AS

MATERIAL SAFETY DATA SHEET

Date Printed: 02/28/2007

Date Updated: 02/08/2007

Version 1.5

Section 1 - Product and Company Information

Product Name TITANIUM(IV) ISOPROPOXIDE, 97%
Product Number 205273
Brand ALDRICH

Company Sigma-Aldrich
Address 3050 Spruce Street
SAINT LOUIS MO 63103 US

Technical Phone: 800-325-5832
Fax: 800-325-5052
Emergency Phone: 314-776-6555

Section 2 - Composition/Information on Ingredient

Substance Name	CAS #	SARA 313
TETRA-ISO-PROPYL ORTHOTITANATE	546-68-9	No

Formula $Ti[OCH(CH_3)_2]_4$
Synonyms Isopropyl orthotitanate * Isopropyl titanate(IV)
* Tetraisopropoxide titanium *
Tetraisopropoxytitanium * Tetraisopropyl
orthotitanate * Tetraisopropyl titanate *
Tetrakis(isopropoxy)titanium * Titanium(4+)
isopropoxide * Titanium isopropylate * Titanium
tetraisopropoxide * Titanium tetraisopropylate *
Titanium tetra-n-propoxide * Tyzor TPt

RTECS Number: NT8060000

Section 3 - Hazards Identification

EMERGENCY OVERVIEW

Flammable. Irritant.
Irritating to eyes.

HMIS RATING

HEALTH: 1
FLAMMABILITY: 3
REACTIVITY: 1

NFPA RATING

HEALTH: 1
FLAMMABILITY: 3
REACTIVITY: 1

For additional information on toxicity, please refer to Section 11.

Section 4 - First Aid Measures

ORAL EXPOSURE

If swallowed, wash out mouth with water provided person is
conscious. Call a physician.

INHALATION EXPOSURE

If inhaled, remove to fresh air. If not breathing give artificial respiration. If breathing is difficult, give oxygen.

DERMAL EXPOSURE

In case of contact, immediately wash skin with soap and copious amounts of water.

EYE EXPOSURE

In case of contact, immediately flush eyes with copious amounts of water for at least 15 minutes.

Section 5 - Fire Fighting Measures

FLAMMABLE HAZARDS

Flammable Hazards: Yes

EXPLOSION HAZARDS

Vapor may travel considerable distance to source of ignition and flash back. Container explosion may occur under fire conditions.

FLASH POINT

113 °F 45 °C Method: closed cup

AUTOIGNITION TEMP

N/A

FLAMMABILITY

N/A

EXTINGUISHING MEDIA

Suitable: For small (incipient) fires, use media such as "alcohol" foam, dry chemical, or carbon dioxide. For large fires, apply water from as far as possible. Use very large quantities (flooding) of water applied as a mist or spray; solid streams of water may be ineffective. Cool all affected containers with flooding quantities of water.

FIREFIGHTING

Protective Equipment: Wear self-contained breathing apparatus and protective clothing to prevent contact with skin and eyes.
Specific Hazard(s): Flammable liquid. Emits toxic fumes under fire conditions.

Section 6 - Accidental Release Measures

PROCEDURE TO BE FOLLOWED IN CASE OF LEAK OR SPILL

Evacuate area. Shut off all sources of ignition.

PROCEDURE(S) OF PERSONAL PRECAUTION(S)

Wear respirator, chemical safety goggles, rubber boots, and heavy rubber gloves.

METHODS FOR CLEANING UP

Cover with dry-lime, sand, or soda ash. Place in covered containers using non-sparking tools and transport outdoors. Ventilate area and wash spill site after material pickup is complete.

Section 7 - Handling and Storage

HANDLING

User Exposure: Avoid breathing vapor. Avoid contact with eyes, skin, and clothing. Avoid prolonged or repeated exposure.

STORAGE

Suitable: Keep tightly closed. Keep away from heat, sparks, and open flame. Handle and store under nitrogen.

SPECIAL REQUIREMENTS

Readily hydrolyzed.

Section 8 - Exposure Controls / PPE

ENGINEERING CONTROLS

Safety shower and eye bath. Use nonsparking tools. Mechanical exhaust required.

PERSONAL PROTECTIVE EQUIPMENT

Respiratory: Use respirators and components tested and approved under appropriate government standards such as NIOSH (US) or CEN (EU). Where risk assessment shows air-purifying respirators are appropriate use a full-face respirator with multi-purpose combination (US) or type ABEK (EN 14387) respirator cartridges as a backup to engineering controls. If the respirator is the sole means of protection, use a full-face supplied air respirator.

Hand: Compatible chemical-resistant gloves.

Eye: Chemical safety goggles.

GENERAL HYGIENE MEASURES

Wash thoroughly after handling. Wash contaminated clothing before reuse.

Section 9 - Physical/Chemical Properties

Appearance	Physical State: Clear liquid Color: Very faintly yellow	
Property	Value	At Temperature or Pressure
Molecular Weight	284.26 AMU	
pH	N/A	
BP/BP Range	104 °C	10 mmHg
MP/MP Range	14 °C	
Freezing Point	N/A	
Vapor Pressure	N/A	
Vapor Density	N/A	
Saturated Vapor Conc.	N/A	
SG/Density	0.97 g/cm ³	
Bulk Density	N/A	
Odor Threshold	N/A	
Volatile%	N/A	
VOC Content	N/A	
Water Content	N/A	
Solvent Content	N/A	
Evaporation Rate	N/A	
Viscosity	N/A	
Surface Tension	N/A	
Partition Coefficient	N/A	
Decomposition Temp.	N/A	
Flash Point	113 °F 45 °C	Method: closed cup
Explosion Limits	N/A	
Flammability	N/A	
Autoignition Temp	N/A	

Refractive Index 1.466
Optical Rotation N/A
Miscellaneous Data N/A
Solubility N/A

N/A = not available

Section 10 - Stability and Reactivity

STABILITY

Conditions of Instability: May decompose on exposure to moist air or water.

Materials to Avoid: Strong oxidizing agents, Strong acids.

HAZARDOUS DECOMPOSITION PRODUCTS

Hazardous Decomposition Products: Carbon monoxide, Carbon dioxide, Titanium/titanium oxides.

HAZARDOUS POLYMERIZATION

Hazardous Polymerization: Will not occur

Section 11 - Toxicological Information

ROUTE OF EXPOSURE

Skin Contact: May cause skin irritation.

Skin Absorption: May be harmful if absorbed through the skin.

Eye Contact: Causes eye irritation.

Inhalation: May be harmful if inhaled. Material is irritating to mucous membranes and upper respiratory tract.

Ingestion: May be harmful if swallowed.

SIGNS AND SYMPTOMS OF EXPOSURE

To the best of our knowledge, the chemical, physical, and toxicological properties have not been thoroughly investigated.

TOXICITY DATA

Oral
Rat
7460 UL/KG
LD50

Skin
Rabbit
>16 ML/KG
LD50

IRRITATION DATA

Skin
Rabbit
500 mg
24H
Remarks: Mild irritation effect

Eyes
Rabbit
20 mg
24H
Remarks: Moderate irritation effect

Section 12 - Ecological Information

No data available.

Section 13 - Disposal Considerations

APPROPRIATE METHOD OF DISPOSAL OF SUBSTANCE OR PREPARATION

Contact a licensed professional waste disposal service to dispose of this material. Burn in a chemical incinerator equipped with an afterburner and scrubber but exert extra care in igniting as this material is highly flammable. Observe all federal, state, and local environmental regulations.

Section 14 - Transport Information

DOT

Proper Shipping Name: Flammable liquids, n.o.s.
UN#: 1993
Class: 3
Packing Group: Packing Group II
Hazard Label: Flammable liquid
PIH: Not PIH

IATA

Proper Shipping Name: Flammable liquid, n.o.s.
IATA UN Number: 1993
Hazard Class: 3
Packing Group: II

Section 15 - Regulatory Information

EU ADDITIONAL CLASSIFICATION

Symbol of Danger: Xi
Indication of Danger: Irritant.
R: 10-36
Risk Statements: Flammable. Irritating to eyes.
S: 16-26-36/37/39
Safety Statements: Keep away from sources of ignition - no smoking. In case of contact with eyes, rinse immediately with plenty of water and seek medical advice. Wear suitable protective clothing, gloves, and eye/face protection.

US CLASSIFICATION AND LABEL TEXT

Indication of Danger: Flammable. Irritant.
Risk Statements: Irritating to eyes.
Safety Statements: Keep away from sources of ignition - no smoking. In case of contact with eyes, rinse immediately with plenty of water and seek medical advice. Wear suitable protective clothing, gloves, and eye/face protection.

UNITED STATES REGULATORY INFORMATION

SARA LISTED: No
TSCA INVENTORY ITEM: Yes

CANADA REGULATORY INFORMATION

WHMIS Classification: This product has been classified in accordance with the hazard criteria of the CPR, and the MSDS contains all the information required by the CPR.
DSL: Yes
NDSL: No

Section 16 - Other Information

DISCLAIMER

For R&D use only. Not for drug, household or other uses.

WARRANTY

The above information is believed to be correct but does not purport to be all inclusive and shall be used only as a guide. The information in this document is based on the present state of our knowledge and is applicable to the product with regard to appropriate safety precautions. It does not represent any guarantee of the properties of the product. Sigma-Aldrich Inc., shall not be held liable for any damage resulting from handling or from contact with the above product. See reverse side of invoice or packing slip for additional terms and conditions of sale. Copyright 2007 Sigma-Aldrich Co. License granted to make unlimited paper copies for internal use only.